Monte Carlo simulations of physics beyond the standard model

Martyn Anthony Gigg

Monte Carlo Simulations of Physics Beyond the Standard Model

A thesis presented for the degree of
Doctor of Philosophy
by

Martyn Anthony Gigg

July 2008

Institute for Particle Physics Phenomenology
Durham University

Durham University

Abstract

The Large Hadron Collider, currently under construction at CERN, will give direct access to physics at the TeV scale for the first time. The lack of certainty over the type of physics that will be revealed has produced a wealth of ideas for so-called Beyond the Standard Model physics, all with the aim of solving the problems possessed by the Standard Model. The oldest and most well studied is supersymmetry but new ideas based on extra dimensions and collective symmetry breaking have been proposed more recently. In order to study these models most effectively, we argue that they must be implemented within the framework of a Monte Carlo event generator so that their signals can be studied in a real world setting.

In this thesis we develop a general approach for the simulation of new physics models with the aim of reducing the effort in implementing a new model into the Herwig++ event generator. The approach is based upon the external spin structures of production and decay matrix elements so that the amount of information required to input a new model is simply a set of Feynman rules and mass spectrum. The first method uses an on-shell approximation throughout but this is later refined to include the effects of finite widths, as these are found to be important when processes occur close to threshold.

In all of the discussions regarding our new approach we make specific reference to two models of new physics, the Minimal Supersymmetric Standard Model and the Minimal Universal Extra Dimensions model. Our general matrix elements and approach to finite widths are all demonstrated and tested using examples from these two models. The concluding discussion makes use of a third model, the Littlest Higgs model with T-parity, such that signals from the three models are compared and contrasted using the general framework developed here.

For my Dad,
with love and admiration.

Declaration

I declare that this thesis is a result of my own work, except where reference is made to external material, and has not been submitted for any other degree at this or any other university.

This research was carried out in collaboration with Dr. Peter Richardson and the Herwig++ collaboration. Chapters 3 and 4 are based on the work in the following publications:

- M. Gigg and P. Richardson, *Simulation of Beyond Standard Model Physics in Herwig++*, *Eur. Phys. J.* **C51** (2007) 989–1008, hep-ph/0703199,
- M. A. Gigg and P. Richardson, *Simulation of Finite Width Effects in Physics Beyond the Standard Model*, arXiv:0805.3037.

While Appendix C is based upon work in

- M. Bahr *et. al.*, *Herwig++ Physics and Manual*, arXiv:0803.0883.

Acknowledgements

First and foremost I would like to thank my Mum, Dad and my sister Kate for their unwavering love and support over the years. Thanks for lots of great memories, whether it be in a caravan in the rain or in a hotel in New York, its always been fun. In particular to my Dad, even though you will never read this, I thank you for your many words of wisdom and I miss you very much.

When I came to Durham four years ago, I was very lucky to meet some great people: James, John, Kemal, Sarah, Simon and Wendy. We spent many a great evening throwing some arrows at one of many darts matches or just dancing the night away. After the first year in college, James, John, Kemal and Simon became my housemates and I would like to thank them in particular, along with Liz for the last year, for many great memories. Whether it be physics discussions, a pint (or two) in the pub or scratching our heads over a polygon, its been awesome.

In my work life, my first thanks must go to my supervisor Peter who has always been very helpful and quite prepared to answer whatever silly questions that I might have. Also I would like to thank him for taking the time to read through this thesis, offering both helpful advice and correcting my bad grammar! To my office mates, Ciaran, Gareth, Karina, Kemal and Stefan, I would like to thank you for making each day that little bit more interesting. In the same vain thank you to all the other members of the IPPP who make it an environment that is a pleasure to work in.

I also thank the Herwig++ collaboration for many interesting meetings and in particular to David for setting me straight on many a C++ issue. In regards to funding I thank STFC for the studentship that made this research possible and also the extra money that was available to attend conferences and meetings.

Last, but by no means least, I want to say thank you to the smallest and newest member of our family, my niece Olivia, who helps me keep smiling.

Contents

List of Figures

List of Tables

'In the beginning the Universe was created. This had made a lot of people very angry and been widely regarded as a bad move.'

— Douglas Adams, 'The Restaurant at the End of the Universe'

Chapter 1

Introduction

Attempting to understand the world around us in terms of fundamental building blocks began with the ancient philosophies, where "elements" were used to explain the observed patterns in nature. While by modern-day standards the idea that these elements are entities such as fire or water is known to be untrue, our basic approach to understanding the universe remains the same.

The current theory of fundamental interactions, the Standard Model, has performed extremely well when compared to data from many experiments over the past thirty years and only a single particle remains undiscovered, namely the Higgs boson. However, despite its successes the theory is known to possess problems, most notably the fine-tuning problem. Here, radiative corrections introduce quadratic divergences in the Higgs boson mass squared so that large cancellations are required to keep the known gauge boson masses at the measured scale. If, however, new physics enters at a different scale, this can serve to alleviate these problems. In this thesis, Monte Carlo simulations of several new physics scenarios are developed and used to study the phenomenological consequences of these models. This chapter reviews the Standard Model and introduces three models

of new physics that will be explored. Chapter 2 reviews Monte Carlo techniques used in particle physics simulations. Chapter 3 describes a general method for the simulation of new physics models and Chapter 4 extends the basic method to include the effects of finite widths. In Chapter 5 comparisons of the three models of new physics are presented, including work done with detector simulations and finally Chapter 6 provides a summary and conclusions.

1.1 Standard Model

The Standard Model of particle physics has its roots in the theory of Quantum Electrodynamics (QED), which is based up on the principle of local gauge invariance[1]. The Lagrangian possesses a space-time dependent symmetry and invariance under this symmetry requires the introduction of a new field, the gauge field. In QED this field is identified with the photon and the requirement of invariance under a local $U(1)$ transformation, the gauge group, leads to a Lagrangian[2]

$$\mathcal{L} = \underbrace{i\bar{\psi}\gamma^{\mu}\partial_{\mu}\psi - \frac{1}{4}F^{\mu\nu}F_{\mu\nu}}_{\text{kinetic}} - \underbrace{e\bar{\psi}\gamma^{\mu}\psi A_{\mu}}_{\text{interaction}} - \underbrace{m\bar{\psi}\psi}_{\text{mass}}, \tag{1.1}$$

where ψ is the electron field, A_{μ} is the photon field and $F^{\mu\nu}$ is the electromagnetic field strength tensor, that possesses an interaction term of the desired form. Also, it is known that the photon is massless and the requirement of local gauge invariance actually forbids a mass term for the photon field. In fact, generally, massless gauge fields are a consequence of the invariance of a Lagrangian under any local gauge transformation. While this is acceptable, and indeed required, for QED, extending

[1] Although originally QED was not understood in the context of a gauge symmetry, it was later realised that the theory could be formulated in such a way.

[2] A good discussion of this topic can be found in [1].

these ideas to the weak interactions, governed by the $W^{\pm}$ and Z^0 bosons, would not seem viable as the gauge particles need to be massive.

In 1964 the Higgs mechanism [2–5] was proposed as a method of both retaining local gauge invariance and giving masses to the gauge bosons by breaking the gauge symmetry in the ground state alone, a method known as spontaneous symmetry breaking. Building on previous work done by Glashow, the symmetry group of QED was extended to include the weak interactions and the proposed Higgs mechanism, for which Glashow, Weinberg and Salam shared the 1979 Nobel Prize [6–8].

1.1.1 Glashow-Salam-Weinberg Model of Electroweak Physics

Experiments at the Brookhaven National Laboratory in 1957 established that neutrinos (anti-neutrinos) were left-handed (right-handed)[3], leading to the conclusion that the weak interaction must be a chiral theory and distinguish between helicity states. As a result the theory acts differently upon the left- and right-handed parts of a Dirac fermion, through the use of the projection operators defined as

$$P_{L,R} = \frac{1}{2}(1 \mp \gamma_5)\,. \tag{1.2}$$

Given this requirement the enlarged gauge group of the electroweak model is given by $SU(2)_L \times U(1)_Y$, where the L denotes a left-handed doublet with *weak isospin* T and Y is not the electromagnetic charge but a related quantity known as *hypercharge*. A fermion, for example the electron, is composed of a left-handed $SU(2)$ doublet field that transforms under both isospin and hypercharge transformations

[3]This lead to the belief that neutrinos were massless fermions, although this has now been disproved. However, compared to the scales we are considering in this thesis, their masses are negligible and will not play a role.

and a right-handed singlet field which is charged under $U(1)_Y$ alone. The complete field is the sum of the two pieces, $\psi_e = \psi_{eL} + \psi_{eR}$.

The gauge sector of the theory lives in the adjoint representation of the group given above. The $SU(2)_L$ gauge bosons are denoted $W_\mu^{1,2,3}$ and the $U(1)_Y$ gauge boson as B_μ. As discussed above, the symmetry must be spontaneously broken for them to acquire a mass. Introducing a single complex doublet ϕ, the Higgs field, with a potential, see for example Ref. [9],

$$V(\phi) = \lambda \left(\phi^\dagger \phi\right)^2 - \mu^2 \phi^\dagger \phi, \tag{1.3}$$

where $\lambda, \mu^2 > 0$ gives a minimum at

$$|\phi| = \sqrt{\frac{\mu^2}{2\lambda}} = \frac{v}{\sqrt{2}}, \tag{1.4}$$

where v is the vacuum expectation value of the Higgs field. Analysing perturbations around this minimum and making a choice of gauge, here and throughout we will use a unitary gauge[4], leads to three degrees of freedom of the original Higgs field appearing as the longitudinal components of the, now massive, gauge bosons. The remaining component is a massive scalar field, the Higgs boson h^0. Looking at the mass terms for the gauge fields

$$\mathcal{L} = \frac{v^2}{8}\left[\left(gW_\mu^3 - g'B_\mu\right)\left(gW^{3\mu} - g'B^\mu\right) + 2g^2 W^- W^+\right], \tag{1.5}$$

where g is the $SU(2)$ coupling, g' is the $U(1)_Y$ coupling and $W^\pm = (W^1 \mp iW^2)/\sqrt{2}$,

[4]In other gauges, for example t'Hooft gauge, the gauge bosons remain massless and instead, the three components of the Higgs field appear explicitly in the interaction Lagrangian and have to be taken into account when performing calculations.

the $W^{\pm}$ boson now has a mass

$$M_W = \frac{1}{2}gv. \tag{1.6}$$

However, the W^3_μ and B_μ mass terms are no longer diagonal and to obtain physically independent states the fields are redefined such that

$$\begin{pmatrix} W^3_\mu \\ B_\mu \end{pmatrix} = \begin{pmatrix} \cos\theta_W & \sin\theta_W \\ -\sin\theta_W & \cos\theta_W \end{pmatrix} \begin{pmatrix} Z_\mu \\ A_\mu \end{pmatrix}, \tag{1.7}$$

where

$$\sin\theta_W = \frac{g'}{\sqrt{g^2 + g'^2}}. \tag{1.8}$$

The mass eigenstates are now the Z^0 boson with a mass

$$M_Z = \frac{1}{2}v\sqrt{g^2 + g'^2}, \tag{1.9}$$

and the photon A_μ, which remains massless as required[5]. In comparison with Eqn. (1.1) the introduction of local gauge invariance gives rise to interactions between the fermions and gauge bosons. Since the coupling between the photon and the electron fields is a measured quantity, the electric charge e, we can relate the above gauge couplings through

$$e = \frac{g'g}{\sqrt{g^2 + g'^2}}, \qquad g = g_W = \frac{e}{\sin\theta_W}. \tag{1.10}$$

As discussed at the beginning of this section, the electroweak model is a chiral theory with the left- and right-handed components of the fermion fields transform-

[5]The photon does not acquire a mass because its symmetry generator is now $T^3 + Y/2$, which still leaves the ground state invariant.

Fermion field	$SU(2)_L \times U(1)_Y$ charge
$\begin{pmatrix} \nu_i \\ l_i \end{pmatrix}_L$	$(\mathbf{2}; -1)$
l_{Ri}	$(\mathbf{1}; -2)$
$\begin{pmatrix} u_i \\ d_i \end{pmatrix}_L$	$(\mathbf{2}; +1/3)$
u_{Ri}	$(\mathbf{1}; +4/3)$
d_{Ri}	$(\mathbf{1}; -2/3)$

Table 1.1: The Standard Model fermion fields with their associated quantum numbers under the $SU(2)_L \times U(1)_Y$ gauge group. The $\{L,R\}$ sub-scripts denote the left- and right-handed components respectively and $i = \{1, 2, 3\}$.

ing differently under a gauge transformation, requiring us to place the components in different representations of the gauge group. Table 1.1 gives the field content and charges under $SU(2)_L \times U(1)_Y$. A mass term for each fermion is also required and it should have the same form as the electron mass term in Eqn. (1.1). However, the left- and right-handed components of the fermion transform differently under a gauge transformation, therefore the term is written as

$$m\bar{\psi}\psi = m\left(\bar{\psi}P_R + \bar{\psi}P_L\right)\left(P_L\psi + P_R\psi\right), \tag{1.11}$$

which cannot be made locally gauge invariant. The remedy is, again, to use spontaneous symmetry breaking by coupling each of the fermions to the Higgs field. When the Higgs field acquires a non-zero vacuum expectation value, a mass term is induced for each fermion with the value $g_f v/\sqrt{2}$. The constant g_f is known as a Yukawa coupling and it must be different for each fermion and proportional to its mass. While this is a necessary procedure because we know that the fermions are massive particles, it is entirely *ad-hoc* and the couplings are not predicted by the model.

1.1.2 Strong Interactions

The final ingredient of the Standard Model is the theory governing the strong interaction, namely Quantum Chromodynamics (QCD), a good introduction for which can be found, for example, in Ref. [9]. Its fundamental constituents are the quarks, which were introduced after a plethora of low-mass hadronic states were discovered in early cosmic ray and collider experiments and there was a need to classify them in some way. The quark model provided an elegant framework by which this abundance of states could be built from a small set of fundamental objects, namely the quarks. However, it was soon realised that there was a problem with this model and some of the observed baryons, for example the Δ^{++} which is composed of three u-type quarks. Given that the quarks are fermions[6] their overall wave function has to be antisymmetric but with only spatial, spin and flavour degrees-of-freedom, these types of baryon have symmetric wave functions. The resolution of the problem came with the introduction of another quantum number known as *colour*, where each quark would carry an extra index and the wave function would always be antisymmetric in this new index and hence antisymmetric overall. Also, as this new colour charge was not directly observed in experiment it was proposed that only states of neutral colour could be observed.

From these requirements and the demand for a gauge theory of the strong interaction, QCD was born. The theory places the quarks in the fundamental representation of $SU(3)$

$$q_\alpha = \begin{pmatrix} q_r \\ q_g \\ q_b \end{pmatrix}, \tag{1.12}$$

[6]The quarks have to be fermions to explain the spin of the lower mass hadrons.

where r, g, b are their colour indices. Requiring local gauge invariance of the Lagrangian introduces eight massless gauge bosons, the gluons, each carrying a colour charge of their own and transforming under the adjoint representation of $SU(3)$. Unlike the electroweak case, we do not spontaneously break the $SU(3)$ symmetry as massive gluons have not been observed.

As discussed above, the gluons carry colour charge and therefore interact with each other. This is encoded in the form of the field strength tensor for a gluon field G^A_μ,

$$F^A_{\mu\nu} = \partial_\mu G^A_\nu - \partial_\nu G^A_\mu - g_s f^{ABC} G^B_\mu G^C_\nu, \tag{1.13}$$

where $A = 1 \ldots 8$, f^{ABC} are the $SU(3)$ structure constants and g_s is the coupling strength for a coloured field. The additional term over the familiar form of the electromagnetic field strength tensor makes QCD a non-abelian gauge theory and hence self interacting. The structure constants f^{ABC} are related to the generators in the fundamental representation of $SU(3)$ t^A by

$$\left[t^A, t^B\right] = i f^{ABC} t^C, \tag{1.14}$$

a representation for which is provided by the eight Gell-Mann matrices λ^A, which are shown, for example, in Ref. [9].

1.1.3 Standard Model Lagrangian

As briefly reviewed above, the electroweak model and QCD provide elegant descriptions of the currently known fundamental constituents of matter and their interactions. Combining these theories gives the Standard Model as it currently stands, a spontaneously broken gauge theory under the $SU(3)_C \times SU(2)_L \times U(1)_Y$

Sector	Physical states
Scalar	h^0
Gauge boson	g, γ, $W^{\pm}$, Z^0
Quark	d, u, s, c, b, t
Lepton	ν_e, e^-, ν_μ, μ^-, ν_τ, τ^-

Table 1.2: The particle spectrum of the Standard Model. The Higgs boson h^0 is the only undiscovered particle.

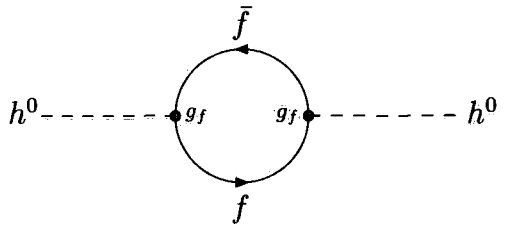

Figure 1.1: A self-energy diagram for the Higgs boson with a fermion running in the loop, where g_f is the Higgs-fermion coupling and for all SM fermions except the top quark it is much less than 1. In the Standard Model there are also contributions from gauge bosons and the Higgs boson itself running in the loop.

gauge group. The full Lagrangian is given by combining each of the sectors

$$\mathcal{L}_{\text{SM}} = \mathcal{L}_{\text{gauge}} + \sum_{i=1}^{3} \mathcal{L}^i_{\text{fermion}} + \mathcal{L}_{\text{Higgs}}, \tag{1.15}$$

with the particle content given in Table 1.2.

As has been discussed previously, the Standard Model is an extremely well tested model and agrees with many tests to a high degree of precision. However, despite its many successes there is a fundamental problem with the scalar sector of the theory, namely the *hierarchy problem*. If we consider one-loop corrections to the tree-level Higgs boson mass, there will be contributions from diagrams such as that shown in Fig. 1.1[7]. Computing the loop integral gives a correction to the

[7]In the Standard Model there are also contributions from $W^{\pm}$ and Z^0 bosons and the Higgs boson running in the loop.

Higgs boson mass of

$$\Delta m_h^2 = -\frac{|g_f|^2}{8\pi^2}\left[\Lambda_{UV}^2 + 4m_f^2 \log(\Lambda_{UV}/m_f)\right], \tag{1.16}$$

where g_f is the coupling of a fermion to the Higgs field, Λ_{UV} is the cut-off scale of the loop integral and we have neglected terms finite in the $\Lambda_{UV} \to \infty$ limit [10]. If the Standard Model is to be considered as valid up to a high scale, *e.g.* the Planck scale $\mathcal{O}(10^{19}\,\text{GeV})$, the Higgs boson mass would naturally prefer to live at this high scale rather than at around a few hundred GeV where electroweak precision data suggests it is. This would mean that in order for the physical mass to have this value a large cancellation, or fine-tuning, between the tree-level mass parameter and the one-loop correction has to occur. This is the hierarchy problem, the natural scale of the Higgs boson mass is the highest scale in the theory and not the electroweak scale as one would expect it to be.

The above calculation assumes that the Standard Model is valid over seventeen orders of magnitude. Given this range it would seem naïve to assume this is the case and that there is no new physics until the Planck scale. In the next section three models of new physics are presented, each of which attempts to solve the hierarchy problem in a different fashion.

1.2 Beyond the Standard Model

There are many open questions concerning the Standard Model, for example why are there three fermion generations, why are the Yukawa couplings for the fermions all, with the exception of the top quark, much less than 1. The models described and discussed in this thesis do not address any of these issues as it is expected that a unified theory, possibly a quantum theory of gravity, would provide answers to

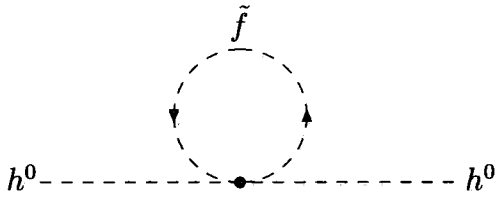

Figure 1.2: A self-energy diagram for the Higgs boson with a heavy scalar particle running in the loop.

such questions. The models introduced below all seek to remedy the more technical problems with the Standard Model such as the hierarchy problem described in the previous section.

1.2.1 Supersymmetry

The hierarchy problem illustrated in Section 1.1.3 can be remedied if one simply supposes that additional fields exist and also contribute to the self-energy of the Higgs boson. For example, if there exists a heavy complex scalar field S which couples to the Higgs field with a term such as $-\lambda_s|\phi|^2|S|^2$, a loop of the form shown in Fig. 1.2 will give a contribution to the Higgs boson mass of

$$\Delta m_h^2 = \frac{\lambda_S}{16\pi^2}\left[\Lambda_{UV}^2 - 2m_S^2 \log(\Lambda_{UV}/m_S)\right], \tag{1.17}$$

where again we have neglected terms finite in the $\Lambda_{UV} \to \infty$. Referring back to the correction obtained for the fermion loop in Eqn. (1.16), one can see that if two of these scalar fields exist then the piece that is quadratically divergent would cancel exactly if $\lambda_S = |g_f|^2$ and only a mild logarithmic divergence would remain. In supersymmetry (SUSY) this is precisely what occurs, for each Standard Model fermion there are two corresponding scalar particles and if supersymmetry is unbroken they have the required couplings.

In order to have this correspondence between the fermionic and bosonic degrees of freedom, some type of symmetry transformation Q is required that turns a bosonic field into a fermionic field and vice versa, *i.e.*

$$Q\,|\text{boson}\rangle = |\text{fermion}\rangle\,, \quad Q\,|\text{fermion}\rangle = |\text{boson}\rangle\,. \tag{1.18}$$

As this transformation involves changing the spin of the original state, the generator Q carries a spin quantum number and hence is also a space-time symmetry. The fact that this generator is a spinor object is important in evading the so called "no-go" theorems, such as the Coleman-Mandula theorem, which states that *the only consistent symmetries of the S-matrix are a direct product of the Poincaré group and internal symmetry groups* [11]. The realisation that if the generator was a spinor then this theorem does not apply was found by Gol'fand and Lihktman [12] in 1971.

The algebra which Q and $Q^\dagger$ follow in order to extend the Poincaré group, generated by P^μ and $M^{\mu\nu}$, is as follows

$$[Q_\alpha, P_\mu] = [\bar{Q}_{\dot{\beta}}, P_\mu] = 0, \tag{1.19a}$$

$$[Q_\alpha, M^{\mu\nu}] = i(\sigma^{\mu\nu})^\beta_\alpha Q_\beta, \tag{1.19b}$$

$$\{Q_\alpha, Q_\beta\} = \{\bar{Q}_{\dot{\alpha}}, \bar{Q}_{\dot{\beta}}\} = 0, \tag{1.19c}$$

$$\{Q_\alpha, Q_{\dot{\alpha}}\} = 2(\sigma^\mu)_{\alpha\dot{\alpha}} P_\mu, \tag{1.19d}$$

where

$$\sigma^\mu = (1, \boldsymbol{\sigma}), \tag{1.20a}$$

$$\bar{\sigma}^\mu = (1, -\boldsymbol{\sigma}), \tag{1.20b}$$

$$\sigma^{\mu\nu} = \frac{1}{4}(\sigma^\mu\bar{\sigma}^\nu - \sigma^\nu\bar{\sigma}^\mu)\,. \tag{1.20c}$$

Therefore, if there exists a fermionic state $|f\rangle$ with mass m, acting upon such a state with Q,

$$P^2 |b\rangle = P^2 Q_\alpha |f\rangle = Q_\alpha P^2 |f\rangle = Q_\alpha m^2 |f\rangle = m^2 |b\rangle , \tag{1.21}$$

produces a bosonic state with equal mass. Therefore, if one were to extend the symmetries of the Standard Model to include supersymmetric generators, we should find counterpart states differing in spin by half a unit but that are degenerate in mass. Since there is no evidence for the existence of these particles, we must conclude that if supersymmetry is realised in nature it is a broken symmetry.

In a phenomenologically viable model we require that supersymmetry is broken in the ground state but only in a way that does not spoil the cancellation of the quadratic divergences in the Higgs boson mass for which we introduced the symmetry originally. When we added the additional scalar field to cancel the ultraviolet divergence we stated that a relationship between the dimensionless couplings g_f and λ_S was required, *i.e.* $\lambda_S = |g_f|^2$, for the cancellation to occur. We therefore require this coupling relation to hold in the broken theory so that the fine-tuning problem is not reintroduced. This type of symmetry breaking is known as soft-symmetry breaking, where we write the Lagrangian for the broken supersymmetric theory as

$$\mathcal{L} = \mathcal{L}_{\text{SUSY}} + \mathcal{L}_{\text{soft}}, \tag{1.22}$$

where $\mathcal{L}_{\text{SUSY}}$ contains all supersymmetry preserving terms and $\mathcal{L}_{\text{soft}}$ contains the soft-breaking terms. These soft terms also contribute to the Higgs boson mass correction with an associated scale m_{soft}, so that Δm_h^2 is proportional to this scale and vanishes as required in the SUSY preserving limit.

Supermultiplets

In the Standard Model Lagrangian, the matter fields are grouped into multiplets according to their transformations under the gauge groups, *e.g.* the $SU(2)_L$ quark doublet. If we are to include supersymmetric counterparts into the Lagrangian, we need to find irreducible representations of the supersymmetry algebra to hold the single particle states, namely supermultiplets. The two simplest multiplets which are required to build a supersymmetric version of the Standard Model are known as chiral and vector supermultiplets. A chiral supermultiplet holds a massless Weyl fermion and an associated complex scalar, while a vector supermultiplet contains a massless spin-1 gauge boson and its partner, a massless Weyl fermion known as a *gaugino*.

In Section 1.1.1 it was demonstrated that the left- and right-handed components of the fermion fields in the Standard Model transform differently under a gauge transformation. As a result, $SU(2)$ doublet and singlet fermions have to be placed in different chiral supermultiplets so that for each Standard Model fermion there exists two complex scalar fields known as *sfermions*. In order to distinguish the two fields and identify the corresponding fermion, each scalar is labelled with the helicity of its Standard Model counterpart, for example the scalar partner of the $SU(2)$ doublet electron field is denoted by $\tilde{e}_L$.

So far the chiral and vector supermultiplets all contain massless particles, therefore the Higgs mechanism is needed to break the electroweak symmetry of the ground state. However, unlike the Standard Model, two Higgs fields H_u and H_d are required to give masses to the up- and down-type fermions respectively[8]. Following a similar procedure to the Standard Model Higgs mechanism the fields can

[8]One reason for this is that two doublets of opposite hypercharge are needed for the cancellation of gauge anomalies [10].

be written in component form as

$$H_u = \begin{pmatrix} \phi_u^+ \\ \\ \phi_u^0 \end{pmatrix}, \quad H_d = \begin{pmatrix} \phi_d^0 \\ \\ \phi_d^- \end{pmatrix}, \tag{1.23}$$

where a total of eight degrees of freedom exist prior to electroweak symmetry breaking. Upon the introduction of a vacuum expectation value for each of the neutral Higgs fields, v_u and v_d, three components give masses to the $SU(2)$ gauge bosons and the remaining five degrees of freedom are seen as physical Higgs bosons. The mass eigenstates are the CP-odd A^0, the charged scalars $H^\pm$ and the CP-even h^0 and H^0 which are mixtures of the two neutral states.

In the gauge sector we have vector supermultiplets containing the Standard Model gauge bosons $W^{1,2,3}$ and B^0 and their SUSY counterparts the winos $\tilde{W}^{1,2,3}$ and the bino $\tilde{B}$. After electroweak symmetry breaking we obtain the familiar $W^\pm$ boson, Z^0 boson and photon and the corresponding SUSY fields, the charged winos $\tilde{W}^\pm$, the zino $\tilde{Z}$ and the photino $\tilde{\gamma}$. There is also a supermultiplet containing the Standard Model gluon with its supersymmetric counterpart the gluino $\tilde{g}$ which is unaffected by electroweak symmetry breaking as it does not couple to the Higgs field.

In the exact supersymmetric limit, as discussed so far in this section, the Standard Model and SUSY particles are degenerate in mass, see Eqn. (1.21). Adding soft SUSY breaking terms into the Lagrangian lifts this degeneracy and introduces a mass splitting between the Standard Model particles and their SUSY partners.

Minimal Supersymmetric Standard Model

The states described in the previous section constitute the minimal set required to form a phenomenologically viable supersymmetric version of the Standard Model, the Minimal Supersymmetric Standard Model (MSSM). However, the discussion is not complete as the mass eigenstates of the MSSM are not those discussed above as we have yet to take into account supersymmetry breaking.

As discussed previously, the supersymmetric Lagrangian needs to be supplemented with terms that break supersymmetry but only such that the cancellation of quadratic divergences in the Higgs boson mass are not spoilt [13]. Unfortunately, as supersymmetry remains undiscovered, we are completely ignorant of how it is broken. Thus we are required to add the most general parameterisation of all soft SUSY-breaking terms into the Lagrangian, thereby adding 105 new masses, mixing matrix parameters and couplings into the MSSM framework.

After the introduction of these soft terms, together with electroweak symmetry breaking, there is a mixing of states so that the mass eigenstates are no longer the same as the interaction eigenstates. For example, the mass terms for the neutral gauginos $\tilde{B}$ and $\tilde{W}^0$ are given by components of the soft SUSY-breaking terms

$$-\frac{1}{2}M_1\tilde{B}\cdot\tilde{B}-\frac{1}{2}M_2\tilde{W}^0\cdot\tilde{W}^0+\text{h.c.}, \tag{1.24}$$

where M_1 and M_2 are the so-called soft masses. After the neutral scalar Higgs fields acquire vacuum expectation values, mixing terms between $(\tilde{B},\tilde{W}^0)$ and $(\tilde{H}_u^0,\tilde{H}_d^0)$ are induced and the mass matrix is no longer diagonal. In a basis defined by $\tilde{G}^0=(\tilde{B},\tilde{W}^0,\tilde{H}_d^0,\tilde{H}_u^0)^{\mathrm{T}}$, the mass terms can be written as

$$-\frac{1}{2}\tilde{G}^{0\mathrm{T}}\boldsymbol{M}_{\tilde{\boldsymbol{G}}^{\mathbf{0}}}\tilde{G}^0+\text{h.c.}, \tag{1.25}$$

with

$$M_{\tilde{G}^0} = \begin{pmatrix} M_1 & 0 & -c_\beta s_W M_Z & s_\beta s_W M_Z \\ 0 & M_2 & c_\beta c_W M_Z & -s_\beta c_W M_Z \\ -c_\beta s_W M_Z & c_\beta c_W M_z & 0 & -\mu \\ s_\beta s_W M_z & -s_\beta c_W M_Z & -\mu & 0 \end{pmatrix}, \tag{1.26}$$

where $s_\beta = \sin\beta$, $c_\beta = \cos\beta$, $s_W = \sin\theta_W$, $c_W = \cos\theta_W$, β is defined by $\tan\beta = v_u/v_d$ and μ is a parameter from the Higgs potential. After diagonalisation of the mass matrix the resulting eigenstates are known as the neutralinos denoted by $\tilde{\chi}_i^0$ where $i = 1, 2, 3, 4$. In a similar manner the charged partners $\tilde{W}^\pm$ and $\tilde{H}^\pm$ mix to form mass eigenstates called charginos $\tilde{\chi}_i^\pm$ where $i = 1, 2$.

In the sfermion sector there is also mixing of the interaction states. While in principle there can be mixing between all scalar states that carry the same electric and colour charge, this is constrained heavily by phenomenology. For example, if terms such as $(m_{\tilde{L}}^2)_{e\mu}\tilde{e}_L^\dagger\tilde{\mu}_L$ are not suppressed then contributions to the decay $\mu^- \rightarrow e^- + \gamma$ produce unacceptably large rates. This suggests that the true SUSY-breaking mechanism should naturally lead to suppression of these dangerous off-diagonal terms. In minimal SUSY-breaking scenarios, as we will consider here, the form of the parameters ensures that mixings of this type do not occur and all we must consider is mixing of the partners of the left- and right-handed fermions. In general we can write down terms that mix each of the sfermions "left" and "right" states but since the mixing is proportional to the Yukawa coupling of the Standard Model fermion, it is only considered for the 3rd generation sfermions $\tilde{t}$, $\tilde{b}$ and $\tilde{\tau}$. As in the case of $W^3 - B^0$ mixing in the electroweak model, we can parameterise the mixing by an angle θ. For example, in the stop case the interaction states $\tilde{t}_L$

Sector	Particles
squark	$\tilde{d}_L$, $\tilde{u}_L$, $\tilde{s}_L$, $\tilde{c}_L$, $\tilde{b}_1$, $\tilde{t}_1$ $\tilde{d}_R$, $\tilde{u}_R$, $\tilde{s}_R$, $\tilde{c}_R$, $\tilde{b}_2$, $\tilde{t}_2$
slepton	$\tilde{e}_L^-$, $\tilde{\nu}_e$, $\tilde{\mu}_L^-$, $\tilde{\nu}_\mu$, $\tilde{\tau}_1^-$, $\tilde{\nu}_\tau$ $\tilde{e}_R^-$, $\tilde{\mu}_R^-$, $\tilde{\tau}_2^-$
gaugino	$\tilde{\chi}_1^0$, $\tilde{\chi}_2^0$, $\tilde{\chi}_3^0$, $\tilde{\chi}_4^0$, $\tilde{\chi}_1^\pm$, $\tilde{\chi}_2^\pm$, $\tilde{g}$
Higgs	h^0, H^0, A^0, $H^\pm$

Table 1.3: The new mass eigenstates of the Minimal Supersymmetric Standard Model. The Higgs boson h^0 shown here replaces the Standard Model version denoted by the same symbol.

and $\tilde{t}_R$ mix to give the mass eigenstates $\tilde{t}_1$ and $\tilde{t}_2$ through

$$\begin{pmatrix} \tilde{t}_1 \\ \tilde{t}_2 \end{pmatrix} = \begin{pmatrix} \cos\theta_t & -\sin\theta_t \\ \sin\theta_t & \cos\theta_t \end{pmatrix} \begin{pmatrix} \tilde{t}_L \\ \tilde{t}_R \end{pmatrix}, \tag{1.27}$$

where $m_{\tilde{t}_1}^2 < m_{\tilde{t}_2}^2$. The mixing of the sbottom and stau states is of the same form, with the angles θ_b and θ_τ respectively.

Another important concept in the MSSM as it will be discussed throughout this thesis is the existence of a discrete symmetry called R-parity. This symmetry prevents any couplings that violate conservation of baryon and lepton number from entering the Lagrangian and ensures an acceptably low rate for proton decay. It is defined as $R = (-1)^{2J+B+L}$, where J is the spin angular momentum, B is baryon number and L is lepton number. Hence for any Standard Model particle $R = +1$ and for a SUSY partner $R = -1$. As a result of this assignment certain interactions are forbidden since they violate conservation of R-parity, such as the decay of the lightest supersymmetric particle (LSP), which provides an excellent dark matter candidate. A summary of the new particle spectrum of the MSSM is shown in Table 1.3.

Earlier in this section we stated that the introduction of explicit SUSY breaking terms introduces over one hundred new parameters into the MSSM Lagrangian. While this does not prohibit the use of the model, it becomes impractical since all of the parameters would have to be specified with each use. Instead we choose to work with a smaller set of parameters within a standard SUSY-breaking scenario that makes certain assumptions about the behaviour of masses and couplings at high scales, *i.e.* unification of gaugino masses at the GUT scale in supergravity models. This drastically reduces the number of parameters which need to be specified and makes the model more tractable.

1.2.2 Universal Extra Dimensions

While supersymmetry is by far the most popular and well studied candidate for physics beyond the Standard Model, it is not the only possibility proposed. In the past two decades there has been renewed interest in the ideas of extra dimensions, first proposed by Kaluza [14] and Klein [15] in the early part of the 20th century. The resurgence was initially due to the fact that string theory could not be consistently formulated in a four dimensional space-time. However, these theories took on a life of their own when the possibility of large extra dimensions[9] was proposed, the so-called ADD model [16–19]. In ADD type models, extra spatial dimensions are added and only gravity is allowed to propagate through them, leaving the Standard Model fields confined to a four-dimensional brane. This results in a lowering of the Planck scale as perceived from our point-of-view and therefore offers a possible solution to the hierarchy problem. Along similar lines Randall and Sundrum proposed that the fundamental Planck scale could be lowered by the addition of a small extra dimension that possessed a large degree of curvature,

[9] In this context, large translates to millimetre sized.

the RS model [20].

A common feature of all of the models discussed above is that the Standard Model fields are confined to our four-dimensional brane. If this restriction is relaxed and all fields are free to propagate into the extra spatial dimensions, one enters a class of theories called Universal Extra Dimensions (UED), first proposed by Appelquist, Cheng and Dobrescu [21]. Here, upon compactification of the extra dimension(s), a new spectrum of particle states arises as Kaluza-Klein excitations in the compact dimension that from our viewpoint look like massive particles. In this thesis it is this type of model that will be considered, where only a single extra dimension exists, for which some of the main motivations are [22]:

- a viable dark matter candidate;
- proton stability;
- phenomenologically similar to supersymmetry.

In order to be able to analyse the four-dimensional phenomenology of the model, we first consider compactification of the theory from its original five dimensions to our familiar four space-time dimensions.

Compactification

In a minimal type model there is one extra spatial dimension y along with the familiar four space-time dimensions x^μ. We require the final Lagrangian that will specify the low-energy interactions to be a function of x^μ only and therefore need to integrate over the extra dimension to remove these degrees of freedom, *i.e.* compactify the extra dimension. In order to do this we must specify the form of the space over which we integrate, namely the compactification scheme. The

choice in this model is to compactify on an $S_1/\mathcal{Z}_2$ orbifold such that $0 \leq y \leq \pi R$, where R is the compactification scale[10].

The five-dimensional Lagrangian is written as [21],

$$\begin{aligned}\mathcal{L}(x^\mu) &= \int \mathrm{d}y \left\{ -\sum_{i=1}^{3} \frac{1}{2\hat{g}_i^2} \mathrm{Tr}\left[F_i^{\alpha\beta}(x^\mu, y) F_{i\,\alpha\beta}(x^\mu, y)\right] + \mathcal{L}_{\text{Higgs}}(x^\mu, y) \right. \\ &\quad + i\left(\bar{\mathcal{Q}}, \bar{\mathcal{U}}, \bar{\mathcal{D}}\right)(x^\mu, y)\left(\Gamma^\mu D_\mu + \Gamma^4 D_4\right)\left(\mathcal{Q}, \mathcal{U}, \mathcal{D}\right)^T(x^\mu, y) \\ &\quad + \left[\bar{\mathcal{Q}}(x^\mu, y)\hat{\lambda}_{\mathcal{U}}\mathcal{U}(x^\mu, y) i\sigma_2 H^*(x^\mu, y)\right. \\ &\quad \left.\left. + \bar{\mathcal{Q}}(x^\mu, y)\hat{\lambda}_{\mathcal{D}}\mathcal{D}(x^\mu, y) i\sigma_2 H(x^\mu, y) + \text{h.c.}\right]\right\}, \end{aligned} \tag{1.28}$$

where $F_i^{\alpha\beta}$ are the five-dimensional field strength tensors, $D_{\mu,4} = \partial/\partial\{x^\mu, y\} - \mathcal{A}_{\mu,4}$ are the covariant derivatives for the gauge fields, $A_\alpha = -i\sum_{i=1}^{3} \hat{g}_i \mathcal{A}^r_{\alpha\, i} T_i^r$ and $\mathcal{L}_{\text{Higgs}}$ contains the kinetic and potential terms for the five-dimensional Higgs fields. The $\mathcal{Q}$, $\mathcal{U}$ and $\mathcal{D}$ fields are the five-dimensional fermion fields transforming as an $SU(2)$ doublet and two $SU(2)$ singlets respectively[11]. The gauge fields are decomposed in terms of x^μ and y as

$$\mathcal{A}_\mu(x^\mu, y) = \frac{1}{\sqrt{\pi R}}\left\{\mathcal{A}_\mu^0(x^\mu) + \sqrt{2}\sum_{j=1}\mathcal{A}_\mu^j(x^\mu)\cos\left(\frac{jy}{R}\right)\right\}, \tag{1.29a}$$

$$\mathcal{A}_4(x^\mu, y) = \sqrt{\frac{2}{\pi R}}\sum_{j=1}\mathcal{A}_4^j(x^\mu)\sin\left(\frac{jy}{R}\right), \tag{1.29b}$$

while the scalar fields are decomposed as in Eqn. (1.29a). The zeroth level is identified with the Standard Model gauge field and for $j \geq 1$ there exists a Kaluza-Klein tower of states with a mass $\mathcal{O}(j/R)$. The polarisations along the fifth dimension

[10]The orbifold construction here simply amounts to a circle S_1 where the points at θ and $-\theta$ are identified and hence the coordinate runs over only half of the circle's circumference.

[11]In five dimensions it is not possible to define a matrix that has the same properties as γ_5 in four dimensions. Therefore, the five-dimensional theory contains two fields for each Standard Model fermion so that a four-dimensional chiral fermion can be constructed from the two zeroth level states.

$\mathcal{A}_4$ have no zero mode and serve to give masses to the higher-level modes. The Standard Model fields acquire their masses through the usual Higgs mechanism where only the zeroth component of H acquires a vacuum expectation value.

For the doublet and singlet fermion fields the decomposition is as follows,

$$\begin{aligned} \mathcal{Q}(x^\mu, y) &= \frac{1}{\sqrt{\pi R}}\left\{ Q_L^0(x^\mu) + \sqrt{2}\sum_{j=1}\left[P_L \mathcal{Q}^j(x^\mu)\cos\left(\frac{jy}{R}\right)\right.\right. \\ &\qquad \left.\left. + P_R \mathcal{Q}^j(x^\mu)\sin\left(\frac{jy}{R}\right)\right]\right\}, \qquad (1.30a) \\ \mathcal{U}(x^\mu, y) &= \frac{1}{\sqrt{\pi R}}\left\{ u_R^0(x^\mu) + \sqrt{2}\sum_{j=1}\left[P_R \mathcal{U}^j(x^\mu)\cos\left(\frac{jy}{R}\right)\right.\right. \\ &\qquad \left.\left. + P_L \mathcal{U}^j(x^\mu)\sin\left(\frac{jy}{R}\right)\right]\right\}, \qquad (1.30b) \end{aligned}$$

where again the zeroth level is identified with the Standard Model field. The masses for the zeroth level fermion fields come from their Yukawa couplings to the Higgs field. For the $j \geq 1$ levels the Higgs terms on the last line of Eqn. (1.28) induce mixings between the left- and right-handed modes so that the interaction eigenstates are related to the mass eigenstates through

$$\begin{pmatrix} \mathcal{U}^j \\ \mathcal{Q}^j \end{pmatrix} = \begin{pmatrix} -\gamma_5 \cos\alpha_j & \sin\alpha_j \\ \gamma_5 \sin\alpha_j & \cos\alpha_j \end{pmatrix} \begin{pmatrix} \mathcal{U}'^j \\ \mathcal{Q}'^j \end{pmatrix}, \qquad (1.31)$$

with

$$\tan 2\alpha_j = \frac{m_f}{M_j}, \qquad (1.32)$$

where m_f is the Standard Model fermion mass and $M_j = j/R$ is the mass of higher level modes[12]. It is clear from Eqn. (1.32) that mixing effects are only phenomenologically relevant for the top quark as electroweak precision tests suggest

[12]It should be noted that this is only the case at tree level and radiative corrections will alter this value. These effects will explained in due course.

that $R^{-1} > 700\,\text{GeV}$ [23].

After compactification, it may be expected that KK-number would no longer be conserved due to the breaking of translational invariance along the fifth dimension. While this is true, there is a discrete subgroup called KK-parity that can still be preserved. KK-parity essentially conserves the "evenness" or "oddness" of an interaction and prevents some different KK-mode mixings in analogous way to that of R-parity in supersymmetry. Unfortunately, the existence of KK-parity conservation cannot be confirmed until the UV behaviour of the theory is understood and is only present if terms that explicitly violate it are not included. In our study we do not include terms that violate this parity since it provides an excellent dark matter candidate, namely the lightest KK particle (LKP).

Minimal Universal Extra Dimensions

So far all of the masses for the KK-modes have been taken as the five-dimensional momentum j/R, which leads to an enormous degeneracy in the spectrum of states. As such, all of the states are stable since they are prevented from decaying to Standard Model particles by KK-parity conservation. However, the above mass relation is only valid at tree-level and radiative corrections induce mass splittings within the spectrum. The loop corrections come in two forms, first from bulk contributions where internal propagators wind around the extra dimension and the second from boundary contributions at the orbifold fixed points $y = 0, \pi R$. The first set of corrections are well-behaved and only depend on the compactification scale, whereas the second set are divergent and require renormalisation. This introduces an explicit cut-off Λ at which the boundary terms are assumed to vanish. The details of these corrections for each field are given in Appendix A.

This completes the discussion of the new particle spectrum for the Minimal

Sector	Particles
Quark	$d_1^\bullet$, $u_1^\bullet$, $s_1^\bullet$, $c_1^\bullet$, $b_1^\bullet$, $t_1'^\bullet$ d_1°, u_1°, s_1°, c_1°, b_1°, $t_1'^\circ$
Lepton	$e_1^{\bullet -}$, $\nu_{1e}^\bullet$, $\mu_1^{\bullet -}$, $\nu_{1\mu}^\bullet$, $\tau_1^{\bullet -}$, $\nu_{1\tau}^\bullet$ $e_1^{\circ -}$, $\mu_1^{\circ -}$, $\tau_1^{\circ -}$
Gauge	γ_1, Z_1^0, $W_1^\pm$, g_1
Higgs	H_1^0, A_1^0, $H_1^\pm$

Table 1.4: The new mass eigenstates of the Minimal Universal Extra Dimensions model for $j = 1$, where $\bullet$ and $\circ$ denote a partner to an $SU(2)$ doublet and singlet fermion respectively.

Universal Extra Dimensions (MUED) model. In this thesis we only concern ourselves with the additional modes with $j = 1$, shown in Table 1.4. Phenomenologically, this is very similar to the MSSM spectrum with the exception that the new partners all carry the same spin as their counterpart Standard Model fields.

1.2.3 Little Higgs

In Section 1.1.3 it was shown that the Standard Model Higgs boson mass is quadratically divergent when radiative corrections are taken into account. One might naïvely assume that this would occur for other particles in the Standard Model. However, due to protection from various symmetries, this does not occur. For example, the Lagrangian possesses a symmetry for the electron field ψ_e in the $m_e \to 0$ limit of the form

$$\psi_e \to \mathrm{e}^{i\alpha\gamma_5}\psi_e. \tag{1.33}$$

Therefore, radiative corrections to the electron mass must be proportional to m_e and vanish when $m_e \to 0$. Dimensional analysis therefore tells us that, at most, the divergence is logarithmic in the cut-off scale Λ rather than quadratic, so that the fermion masses remain at the required scale. This type of symmetry is known as

a chiral symmetry and exists for all fermions in the Standard Model, whereas the gauge particles are protected by a different symmetry, namely gauge invariance. The problem with the Higgs boson mass is now apparent, it has no associated symmetry to protect it against large radiative corrections.

Little Higgs models introduce symmetry mechanisms to protect the Higgs mass, with original models proposed such that the Higgs boson became a pseudo-Goldstone boson of a broken symmetry. However, a scale for the symmetry breaking that gave rise to the Higgs boson was necessary, which reintroduced fine-tuning issues between the electroweak scale and the new symmetry breaking scale. More recently, ideas based on collective symmetry breaking have been introduced to try and alleviate these fine-tuning issues. The first Little Higgs models possessed a global symmetry broken at a scale f so that new particles were introduced at this scale. Unfortunately, to avoid constraints from electroweak precision data, f had to be increased such that fine-tuning issues were again reintroduced.

The conflict with electroweak precision tests came mostly from mixing between the new heavier mass spectrum and lighter Standard Model particles. It was realised that a new discrete symmetry, analogous to R-parity in SUSY and KK-parity in UED, would prevent this type of mixing and give a spectrum that was phenomenologically viable, including a dark matter candidate [24–26]. The new symmetry, known as T-parity, gave rise to a minimal Little Higgs model known as the Littlest Higgs model with T-parity (LHT) and it is this model that we will consider here.

Collective Symmetry Breaking

The Littlest Higgs model begins with an $SU(5)$ global symmetry, which contains an $[SU(2) \times U(1)]^2$ subgroup identified as the gauge group. At a scale f both the

global and local symmetry groups are broken down to $SO(5)$ and $SU(2) \times U(1)$ respectively. From the point-of-view of the global symmetry breaking mechanism, there are now ten unbroken generators[13] so that a total of fourteen massless Goldstone bosons are present. Coupled with spontaneous breaking of the local symmetry, a set of heavy gauge particles is introduced with masses characterised by the global symmetry breaking scale f, the partners of the Standard Model gauge bosons. The longitudinal components of these heavy gauge bosons are formed from four of the Goldstone bosons of the global symmetry breaking mechanism.

Perturbations around the direction of the vacuum expectation value of the $SU(5)$ field,

$$\Pi = \begin{pmatrix} 0 & H/\sqrt{2} & \Phi \\ H^\dagger/\sqrt{2} & 0 & H^T/\sqrt{2} \\ \Phi^\dagger & H^*/\sqrt{2} & 0 \end{pmatrix}, \tag{1.34}$$

where $H = (h^+, h^0)^T$ and

$$\Phi = \begin{pmatrix} -i\phi^{++} & -i\phi^+/\sqrt{2} \\ -i\phi^+/\sqrt{2} & -i(\phi^0 + i\phi^P)/\sqrt{2} \end{pmatrix}, \tag{1.35}$$

parameterise the remaining ten Goldstone bosons. After electroweak symmetry is broken at a scale $v_{\rm SM}$ the $W^\pm$ and Z^0 bosons acquire a mass by eating three of the components of the Higgs doublet H, leaving seven physical Higgs bosons h^0, ϕ^0, ϕ^P, $\phi^\pm$ and $\phi^{\pm\pm}$.

We now discuss the action of T-parity upon the different sectors. A T-parity transformation exchanges the fields charged under the $[SU(2) \times U(1)]_{1,2}$ gauge groups. The physical states are combinations of the fields which are either even or

[13] $SU(N)$ has $N^2 - 1$ generators, while $SO(N)$ has $N(N-1)/2$.

Sector	Particle content
Quark	d_-, u_-, s_-, c_-, b_-, t_-, T_+, T_-
Lepton	e_-^-, ν_{e-}, μ_-^-, $\nu_{\mu-}$, τ_-^-, $\nu_{\tau-}$
Gauge	A_H, Z_H, $W_H^\pm$
Higgs	h^0, ϕ^0, ϕ^P, $\phi^\pm$, $\phi^{\pm\pm}$

Table 1.5: The additional particle spectrum in the Littlest Higgs model with T-parity. For the fermion fields, the subscript denotes the action under T-parity and all other fields, with the exception of the Higgs boson h^0, are odd under a T-parity transformation.

odd under the action of T-parity, *e.g.* the T-even $SU(2)_L$ gauge boson is given by $(W_{1\mu}^\pm + W_{2\mu}^\pm)/\sqrt{2}$ and is identified as the Standard Model $W^\pm$ boson. All Standard Model fields are even under the action of T-parity and the new spectrum of "heavy" states are odd under T-parity. In the fermion sector this also leads to a spectrum of heavy T-odd fermions, one for each Standard Model fermion. However, in contrast to the MSSM and MUED model, there is only one partner for each of the fermions, with the exception of the top quark. In addition to the T-odd partner of the SM top quark there are two additional T-even and T-odd combinations of new singlet fields that are required to avoid quadratic divergences in the Higgs boson mass, since the SM top quark has a large Yukawa coupling. Table 1.5 gives the new particle spectrum of the Littlest Higgs model with T-parity, where a subscript denotes whether they are odd or even under the action of the T-parity. Again, in contrast to supersymmetry, the additional particles have the same spin as their Standard Model counterparts.

1.3 Summary

A common feature of the new physics models described above is the addition of a new spectrum of heavy particles. Assuming these particles have masses around

the TeV-scale, which is required so that the problems with the Higgs boson mass are avoided, they will be detectable at the collider currently under construction at CERN, the Large Hadron Collider (LHC). It is crucial, therefore, that we are able to accurately predict the signals that both the Standard Model and any new physics model will produce. To achieve this we use so-called Monte Carlo event generators to compare theory and data. The next chapter will introduce the basic methods of Monte Carlo simulations with focus on their uses in high-energy physics.

Chapter 2

Monte Carlo Simulations

'All exact science is dominated by the idea of approximation.'

— Bertrand Russell

Theoretical predictions must be compared to experimental data in order to confirm the validity of any model. This requires the calculation of numerical values for observable quantities so that a direct comparison with experiment can be made. For real-world problems these calculations are generally not exactly solvable and one must use numerical techniques to arrive at the required answers. The Monte Carlo method is one such way of obtaining numerical results when an exact analytic answer is not possible. Throughout this thesis we will refer to Monte Carlo techniques as a method for solving complex integrals, although they are by no means limited to such applications.

The Monte Carlo method treats an integral as an average over a set of values. For example, the integral I of a function $g(x)$, which exists between the limits

$\{x_1, x_2\}$, can written as

$$I = \int_{x_1}^{x_2} g(x)\,\mathrm{d}x = \int_{x_1}^{x_2} \frac{g(x)}{f_X(x)} f_X(x)\,\mathrm{d}x = (x_2 - x_1)E[g(X)], \tag{2.1}$$

where X is distributed according to the probability density function $f_X(x)$ with

$$f_X(x) = \begin{cases} \dfrac{1}{x_2 - x_1}, & \text{if } x_1 < x < x_2, \\ 0, & \text{otherwise.} \end{cases} \tag{2.2}$$

The average value of the continuous distribution $E[g(X)]$ is estimated from a discrete sampling of $g(X)$ using N random selected points such that

$$I \approx I_N = (x_2 - x_1)\frac{1}{N}\sum_{i=1}^{N} g(X_i). \tag{2.3}$$

The error on the estimated distribution I_N is given by the central limit theorem as the standard deviation of $g(x)$

$$I = I_N \pm \sqrt{\frac{\sigma^2}{N}}, \tag{2.4}$$

where

$$\sigma^2 = (x_2 - x_1)\int_{x_1}^{x_2} g^2(x)\,\mathrm{d}x - \left[\int_{x_1}^{x_2} g(x)\,\mathrm{d}x\right]^2. \tag{2.5}$$

Equation (2.4) shows that the convergence rate for a one-dimensional integral computed using the Monte Carlo method is $1/\sqrt{N}$. For a simple example such as this it would be more efficient to use either the trapezium or Simpson's rule where the convergence is $1/N^2$ and $1/N^4$, respectively. However, the convergence of these methods becomes less rapid for higher dimensional integrals, whereas the error for Monte Carlo method stays as $1/\sqrt{N}$[1].

[1]The accuracy of any Monte Carlo is also dependent on the availability of a good quality random number generator which can produce sequences of uncorrelated numbers with very large

2.1 Event Generation

In particle physics, the comparison of theoretical predictions with experimental data is a complicated task. This is mostly due to fundamental barriers in our observing powers. For example, consider the process $u\bar{u} \rightarrow Z^0 \rightarrow d\bar{d}$, which has a differential cross section given by

$$\frac{\mathrm{d}\sigma}{\mathrm{d}\Omega} = \frac{1}{64\pi^2}\frac{1}{s}|\mathcal{M}(u\bar{u} \rightarrow Z^0 \rightarrow d\bar{d})|^2, \tag{2.6}$$

where $\sqrt{s}$ is the centre-of-mass energy, $\mathcal{M}$ is the matrix element and $\mathrm{d}\Omega = \mathrm{d}\cos\theta\mathrm{d}\phi$ forms the two-dimensional phase space where θ and ϕ are the polar and azimuthal angles respectively. In a theoretical prediction a value for the total cross section is found by integrating over the phase space. However, in an experimental setting single quarks cannot be isolated since they are always bound into colour singlets. Therefore, the colliding particles are composite objects, *e.g.* protons and antiprotons, while the observed final-state particles are a colour singlet combination of the quark-anti-quark pair. In order to give an accurate description of real data, all of this information must be folded into the theoretical calculation.

The aim of general purpose Monte Carlo event generators [28–33] is to implement theoretical models and produce events that are distributed as they would be prior to interacting with a detector. This type of generator is generally based upon simple initial processes but has the advantage that the output can be directly compared with data. They will be described in more detail in this chapter. Another type of generator, known as a matrix-element generator [34–39], calculates the full $2 \rightarrow n$ matrix element for a given process but the output must still be interfaced to a general-purpose generator to be able to compare it directly with

periods. For more information see, for example, the discussion in Ref. [27].

data. The author of this thesis is also an author of the Herwig++ [28] program and as such the descriptions that follow relate directly to this program, unless otherwise stated.

A general-purpose event generator, such as Herwig++, produces events in well-defined stages:

Hard subprocess The momentum of the primary outgoing partons are generated from the initial state, which can be a parton extracted from a composite object or an elementary particle such as an electron.

Parton shower QCD radiation from coloured objects in the initial and/or final state evolves the scale of the reaction from the perturbative scale of the hard scattering down to the non-perturbative hadronization scale $\backsimeq \Lambda_{QCD}$.

Perturbative decays In BSM physics models, top quark, $W^{\pm}$, Z^0 and Higgs production, the hard subprocess contains heavy states that will subsequently decay, perturbatively, to lighter objects. If the initial and/or final states of the decay contain coloured particles, parton showers will also be initiated from these states.

Multiple scattering In hadron-hadron reactions, the primary subprocess involves only one parton extracted from each incoming state. However, the remaining parts of the hadrons, the remnants, can also interact and produce other partonic processes. The additional processes take place in the perturbative regime and therefore also initiate parton showers.

Hadronization At scales below the hadronization cut-off, the coloured objects formed as result of the previous stages combine to form colour singlets, called clusters. This is an entirely non-perturbative effect and is governed by phenomenological models, such as the cluster model in HERWIG [29]

and Herwig++ [28]. Other programs use different models such as the string model in PYTHIA [31].

Hadron decays Finally, the unstable hadrons produced by the cluster model or in the decay of other hadrons undergo non-perturbative decays to form the observed hadrons.

The elementary particles and hadrons produced by the simulation are the states that exist prior to their interaction with the detector in an experiment. In order to study these effects, the output from the event generator is passed to a detector simulation package which models the interaction of the particles with the detector. Packages such as GEANT [40] provide detailed modelling of the interactions between the particles with matter in the detector. Whereas other packages, such as AcerDet [41] or PGS [42], provide a simple model based on smearing of the position and momenta of the particles. The model in these simpler packages is usually based on a parameterisation of results from the GEANT simulation and they are useful for phenomenological studies.

In the new physics scenarios under discussion in this thesis, the important stages of the event generation are the hard subprocess and perturbative decays. This is because the new particles will all decay into the lightest new particle state and a Standard Model particle. As such, the remaining stages can be handled, essentially, without regard for the type of new physics in question[2]. As a result we limit our discussion to the initial hard scattering and subsequent decays.

[2]This statement is not true in general as there are possible SUSY scenarios where, for example, coloured sparticles can hadronize to form R-hadrons [43].

2.1.1 Hard Process

In a general purpose event generator the initial hard subprocess is typically a tree-level $2 \rightarrow 2$ scattering, such as the example given in the introduction to this section. To produce real events, the first step is to assign a momentum to each of the outgoing particles. This is achieved by using the Monte Carlo procedure to estimate the cross-section integral for the selected process. In a hadron-hadron initiated hard process, the cross-section integral is given by

$$\sigma = \int \mathrm{d}x_1 \mathrm{d}x_2 \sum_{i,j} \hat{\sigma}_{ij}(\hat{s}, \mu^2) f_i(x_1, \mu^2) f_j(x_2, \mu^2), \tag{2.7}$$

where $f_i(x, \mu^2)$ is the *parton distribution function* for the ith parton with a fraction x of the incoming hadrons momentum at factorisation scale μ[3]. The partonic cross section $\hat{\sigma}_{ij}$ can be rewritten in terms of the differential cross section through

$$\hat{\sigma}_{ij}(\hat{s}, \mu^2) = \int_{-1}^{1} \mathrm{d}\cos\theta \int_0^{2\pi} \mathrm{d}\phi \, \frac{\mathrm{d}\sigma_{ij}}{d\Omega}(\hat{s}, \theta, \phi, \mu^2), \tag{2.8}$$

where $\hat{s} = (p_1 + p_2)^2 = x_1 x_2 s$, θ is the polar angle of parton three with respect to the beam axis in the centre-of-mass frame and ϕ is the azimuthal angle. During the estimation of the cross section, random values for the angles $(\theta\,, \phi)$ are generated, where ϕ is generated isotropically and θ is sampled from the $\mathrm{d}\sigma_{ij}/\mathrm{d}\Omega$ distribution for the process being generated. These values are used to calculate the momenta of the outgoing particles using

$$p_{3,4} = \left(\sqrt{q^2 + m_{3,4}^2}, \pm p_t \sin\phi, \pm p_t \cos\phi, \pm q \cos\theta\right), \tag{2.9}$$

[3]The cross section should not depend on the factorisation scale μ but since the perturbative expansion is finite, a residual dependence remains.

where $p_t = q \sin\theta$ and

$$q = \frac{1}{2\hat{s}} \left[\left(\hat{s} - (m_3 + m_4)^2 \right) \left(\hat{s} - (m_3 - m_4)^2 \right) \right]^{1/2}. \tag{2.10}$$

2.1.2 Perturbative Decays

In both the Standard Model and new physics scenarios, the unstable particles produced by the hard scattering process will undergo perturbative decays. Ideally, the full matrix element for the $2 \to n$ process, including both production and decay, would be used [34–39], however, in reality there are a number of issues:

- the time to compute the full matrix element, even if only the resonant diagrams are included, grows with the number of final-state particles. This is particularly problematic for the types of model considered here, which can contain long decay chains;
- most new physics models introduce a large number of new states, which lead to many possible production and decay mechanisms. If the full calculation is used in all cases then the number of processes required becomes prohibitively large;
- any new coloured states will emit QCD radiation in their production and decay which must be simulated using the parton shower approximation.

Given these issues, for the foreseeable future, we will need to use general purpose event generators [28,31,33] that treat the production and decay of heavy particles in a factorised approximation, namely the *narrow width approximation*. We start by considering the form of the propagator for an unstable particle.

In scattering processes unstable states reveal themselves as resonances, where the mass of the unstable particle is defined as the position of the resonance. The form of the peak is known as a Breit-Wigner and is given by

$$\sigma \propto \left| \frac{1}{p^2 - m^2 + im\Gamma} \right|^2, \tag{2.11}$$

where p is the four-momentum of the unstable particle, m is position of the resonance and Γ is the decay rate of the unstable particle, known as the width. In a field theory the tree-level propagator $(p^2 - m^2)^{-1}$ receives corrections from all orders in perturbation theory and the exact propagator can be represented as a geometric series,

$$\frac{1}{D} = \frac{i}{p^2 - m_0^2} + \frac{i}{p^2 - m_0^2}(-iM^2)\frac{i}{p^2 - m_0^2} + \ldots, \tag{2.12a}$$

$$= \sum_{k=0}^{\infty} \frac{i}{p^2 - m_0^2} \left[(-iM^2)\frac{i}{p^2 - m_0^2} \right]^k, \tag{2.12b}$$

$$= \frac{i}{p^2 - m_0^2 - M^2(p^2)}, \tag{2.12c}$$

where m_0 is the mass parameter found in the Lagrangian, p is the four-momentum and $M^2(p^2)$ is the sum of all amputated diagrams for $1 \to 1$ scattering and for an unstable particle is complex valued. Defining the particle's rest mass m by

$$m^2 - m_0^2 - \operatorname{Re} M^2(m^2) = 0, \tag{2.13}$$

displaces the pole in the propagator such that

$$\frac{1}{D} \sim \frac{iZ}{p^2 - m^2 - iZ \operatorname{Im} M^2(p^2)}, \tag{2.14}$$

where Z is defined by the Lehmann-Symanzik-Zimmermann (LSZ) reduction formula [44] as

$$\mathcal{M}(p \to p) = -ZM^2(p^2). \tag{2.15}$$

The optical theorem, a good discussion of which can be found in Ref. [45], relates the imaginary part of the forward scattering amplitude $\mathcal{M}(p \to p)$ to the sum of contributions from all possible intermediate states such that

$$Z \operatorname{Im} M^2(p^2) = -\operatorname{Im} \mathcal{M}(p \to p) = -\frac{1}{2} \sum_f \int \mathrm{d}\Pi_f |\mathcal{M}(p \to f)|^2, \tag{2.16}$$

where $\mathrm{d}\Pi_f$ is the phase space for all possible final states f. The decay rate Γ for a particle of mass m is given by

$$\Gamma = \frac{1}{2m} \sum_f \int \mathrm{d}\Pi_f |\mathcal{M}(p \to f)|^2, \tag{2.17}$$

so that the propagator for an unstable particle can be written as

$$\frac{1}{D} \sim \frac{1}{p^2 - m^2 + im\Gamma}, \tag{2.18}$$

where it is assumed that the resonance is narrow so that Γ has a fixed value over the resonance. If this is not the case, the tails of the distribution will deviate from the form given in Eqn. (2.11).

We can separate the production and decay by integrating out the propagators connecting each step,

$$\int_{-\infty}^{\infty} \mathrm{d}q^2 \left| \frac{1}{(q^2 - M^2) + iM\Gamma} \right|^2 = \frac{\pi}{M\Gamma}, \tag{2.19}$$

so that the cross section integral becomes an on-shell production step followed by a series of cascade decays. By using this approximation we are assuming:

1. the resonance has a small width Γ compared with its pole mass M, $\Gamma \ll M$;
2. we are far from threshold, $\sqrt{s} - M \gg \Gamma$, where $\sqrt{s}$ denotes the centre-of-mass energy;
3. the propagator is separable;
4. the mass of the parent is much greater than the mass of the decay products;
5. there are no significant non-resonant contributions.

If these assumptions are valid, one obtains an estimate of the cross section with an error of $O(\Gamma/M)$. In this and the subsequent chapter we will assume that the narrow width approximation described above is valid and we will work in the limit where all external states are on mass shell. In Chapter 4 we will consider the effects of finite widths and present a method to include them into our Monte Carlo approximation.

2.2 Spin Correlations

The decay of a heavy resonance can be performed either via phase space, using an algorithm such as RAMBO [46] or MAMBO [47], or by including a matrix element to give the distribution of the decay products. In the former case all information concerning the spin structure of the event is lost since the decay is performed based entirely upon kinematics. To be able to keep so-called spin correlation information, the calculation of the outgoing momenta must be based upon a matrix element for that process so that the dynamics of the process are also included. However,

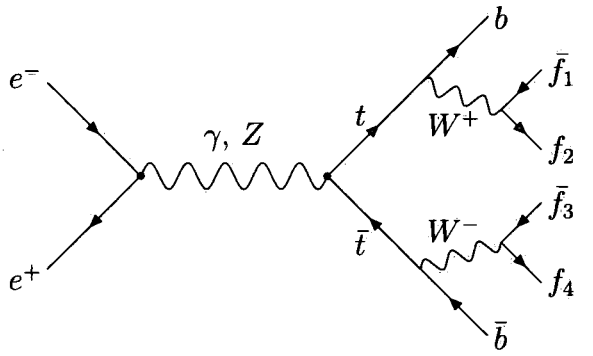

Figure 2.1: Production of a $t\bar{t}$ pair at an electron-positron collider, where the top quark subsequently decays, via a W-boson, to a b-quark and a pair of light fermions. The top quark can also decay to either a d- or a s-quark but these are heavily suppressed by CKM factors.

if the two stages are performed naïvely as isolated calculations, no information about the underlying spin structure of the physics model will be transmitted to the final state and the angular distributions will remain incorrect. This is due to the generation of the momenta in hard process and decay stages depending only on the squared matrix elements for each process, so that the polarisation vectors and spinors are summed over separately in each step. Therefore, we require a method of preserving the necessary amplitude information so that the spin correlations can be reconstructed as the simulation progresses. A general algorithm for dealing with these correlations, which is both in keeping with the step-by-step approach of event generation and also does not require larger spin density matrices for longer decay chains, is demonstrated in [48–51]. Instead of describing the algorithm in its general form, we will discuss its application to the process $e^+e^- \to t\bar{t}$ where the top quark subsequently decays, via a W-boson, to a b-quark and a pair of light fermions, as shown in Fig. 2.1.

Initially, the outgoing momenta are generated according to the usual cross-

section integral

$$\frac{(2\pi)^4}{2s}\int \frac{d^3p_t}{(2\pi)^3 2E_t}\frac{d^3p_{\bar{t}}}{(2\pi)^3 2E_{\bar{t}}}\mathcal{M}^{e^+e^-\to t\bar{t}}_{\lambda_t\lambda_{\bar{t}}}\mathcal{M}^{*e^+e^-\to t\bar{t}}_{\lambda_t\lambda_{\bar{t}}}, \tag{2.20}$$

where $\mathcal{M}^{e^+e^-\to t\bar{t}}_{\lambda_t\lambda_{\bar{t}}}$ is the matrix element for the initial hard process and $\lambda_{t,\bar{t}}$ are the helicities of the t and $\bar{t}$ respectively. One of the outgoing particles is picked at random, for instance the top and a spin density matrix calculated

$$\rho^t_{\lambda_t\lambda'_t} = \frac{1}{N}\mathcal{M}^{e^+e^-\to t\bar{t}}_{\lambda_t\lambda_{\bar{t}}}\mathcal{M}^{*e^+e^-\to t\bar{t}}_{\lambda'_t\lambda_{\bar{t}}}, \tag{2.21}$$

with N defined such that $\mathrm{Tr}\,\rho = 1$.

The top is decayed and the momenta of the decay products distributed according to

$$\frac{(2\pi)^4}{2m_t}\int \frac{d^3p_b}{(2\pi)^3 2E_b}\frac{d^3p_{W^+}}{(2\pi)^3 2E_{W^+}}\rho^t_{\lambda_t\lambda'_t}\mathcal{M}^{t\to bW^+}_{\lambda_t\lambda_{W^+}}\mathcal{M}^{*t\to bW^+}_{\lambda'_t\lambda_{W^+}}, \tag{2.22}$$

where the inclusion of the spin density matrix ensures the correct correlation between the top decay products and the beam.

A spin density matrix for the W^+ is calculated, because the b is stable[4],

$$\rho^{W^+}_{\lambda_{W^+}\lambda'_{W^+}} = \frac{1}{N}\rho^t_{\lambda_t\lambda'_t}\mathcal{M}^{t\to bW^+}_{\lambda_t\lambda_{W^+}}\mathcal{M}^{*t\to bW^+}_{\lambda'_t\lambda'_{W^+}}, \tag{2.23}$$

and the W decayed in the same manner as the top with the inclusion of the spin density matrix here ensuring the correct correlations between the W decay products, the beam and the bottom quark.

The decay products of the W are stable fermions so the decay chain terminates

[4]While the b-quark does decay semi-leptonically, in the perturbative regime that we are considering here it is a good approximation to say that it is stable.

here and a decay matrix for the W

$$D^{W^+}_{\lambda_{W^+}\lambda'_{W^+}} = \frac{1}{N}\mathcal{M}^{W^+\to f\bar{f}'}_{\lambda_{W^+}}\mathcal{M}^{*W^+\to f\bar{f}'}_{\lambda'_{W^+}}, \tag{2.24}$$

is calculated. Moving back up the chain a decay matrix for the top quark is calculated using the decay matrix of the W,

$$D^{t}_{\lambda_t\lambda'_t} = \frac{1}{N}\mathcal{M}^{t\to bW^+}_{\lambda_t\lambda_{W^+}}\mathcal{M}^{*t\to bW^+}_{\lambda'_t\lambda'_{W^+}}D^{W^+}_{\lambda_{W^+}\lambda'_{W^+}}. \tag{2.25}$$

Since the top came from the hard process we must now deal with the $\bar{t}$ in a similar manner. However, instead of using $\delta_{\lambda_{\bar{t}}\lambda_{\bar{t}'}}$ when calculating the initial spin density matrix, as in Eqn. (2.21), the decay matrix of the top is used such that

$$\rho^{\bar{t}}_{\lambda_{\bar{t}}\lambda'_{\bar{t}}} = \frac{1}{N}\mathcal{M}^{e^+e^-\to t\bar{t}}_{\lambda_t\lambda_{\bar{t}}}\mathcal{M}^{*e^+e^-\to t\bar{t}}_{\lambda'_t\lambda'_{\bar{t}}}D^{t}_{\lambda_t\lambda'_t}, \tag{2.26}$$

where again $\mathrm{Tr}\,\rho = 1$. The $\bar{t}$ decay is generated accordingly and the density matrices pass information from one decay chain to the associated chain thereby preserving the correct correlations.

The production and decay of the top, using the spin correlation algorithm, is demonstrated in Figs. 2.2–2.4 and compared to the full matrix element calculation. The separate plots illustrate the different stages of the algorithm at work. Figure 2.2 gives the angle between the beam and the outgoing lepton. The results from the simulation agree well with the full matrix element calculation which demonstrates the consistency of the algorithm for the decay of the $\bar{t}$.

Figure 2.3 gives the angle between the top quark and the produced lepton. This shows the same agreement as the previous figure and demonstrates the correct implementation of the spin density matrix for the $\bar{t}$ decay. Finally, Fig. 2.4 gives

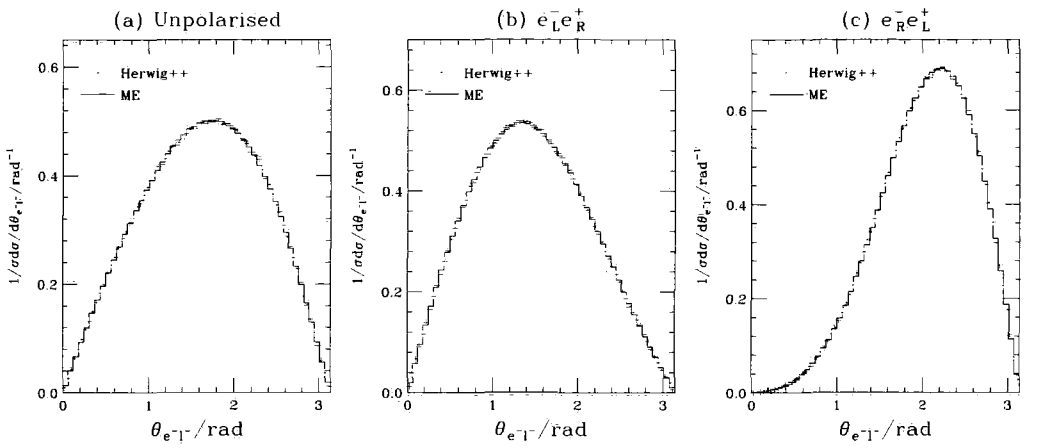

Figure 2.2: Angle between the beam and the outgoing lepton in $e^+e^- \to t\bar{t} \to b\bar{b}l^+\nu_l l^-\bar{\nu}_l$ in the lab frame for a centre-of-mass energy of 500 GeV with (a) unpolarised incoming beams, (b) negatively polarised electrons and positively polarised positrons and (c) positively polarised electrons and negatively polarised positrons.

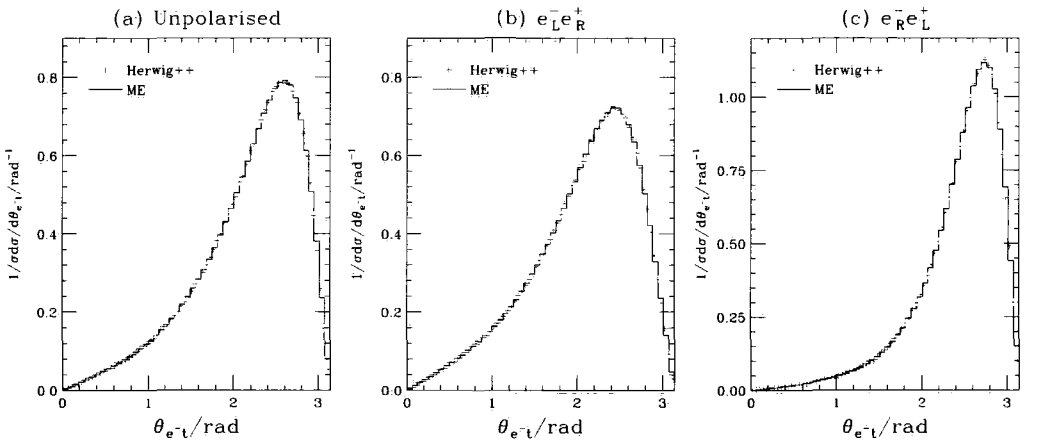

Figure 2.3: Angle between the lepton and the top quark in $e^+e^- \to t\bar{t} \to b\bar{b}l^+\nu_l l^-\bar{\nu}_l$ in the lab frame for a centre-of-mass energy of 500 GeV with (a) unpolarised incoming beams, (b) negatively polarised electrons and positively polarised positrons and (c) positively polarised electrons and negatively polarised positrons.

the results for the angle between the final-state lepton/anti-lepton pair showing the correct implementation of the decay matrix that encodes the information about the $\bar{t}$ decay. Again there is good agreement between our numerical results and the full matrix element calculation giving us confidence in the validity of the spin correlation algorithm.

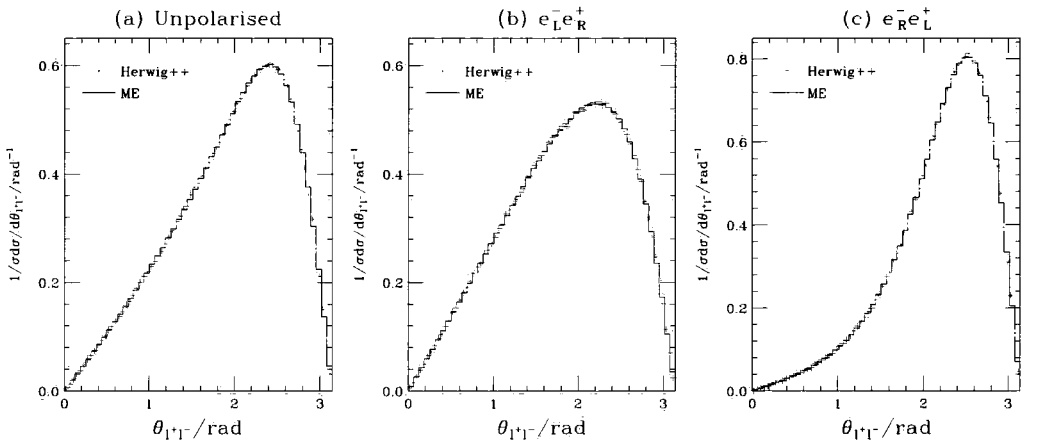

Figure 2.4: Angle between the outgoing lepton and anti-lepton in $e^+e^- \to t\bar{t} \to b\bar{b}l^+\nu_l l^-\bar{\nu}_l$ in the lab frame for a centre-of-mass energy of 500 GeV with (a) unpolarised incoming beams, (b) negatively polarised electrons and positively polarised positrons and (c) positively polarised electrons and negatively polarised positrons.

The above procedure is ideally suited for implementation in an event generator, as demonstrated, where one would like additional processes to occur between the hard production and decay such as showering of a coloured particle. Throughout this thesis, spin correlations will play a vital role when discussing the new physics scenarios discussed in Chapter 1, therefore the algorithm presented here will be used extensively.

2.3 Summary

In this chapter we have introduced the basic ideas of Monte Carlo techniques as a method of numerically evaluating complex integrals. We have shown that by treating the integral as an average over a set of selected points, a solution is obtained with a well defined error. This technique was carried into the particle physics domain by the concept of an event generator, which uses the Monte Carlo method to produce events that are distributed as they would be in an experiment. The main

steps of the event simulation were briefly described with the hard scattering and decay phases discussed in more detail, including an algorithm for preserving spin correlations throughout the simulation, as they are most relevant to this thesis.

The next chapter introduces a general framework, which has been implemented in the Herwig++ event generator [28], for the simulation of physics beyond the Standard Model.

Chapter 3

Simulations of New Physics

'The most exciting phrase to hear in science, the one that heralds new discoveries, is not 'Eureka!' (I found it!) but 'That's funny ...'.'

— Isaac Asimov

The LHC, currently being built at CERN, will usher in a new era for high-energy physics. It will become possible, for the first time, to probe physics at the TeV scale and attempt to address some of the problems with the Standard Model that were discussed in Chapter 1. As we do not know what type of new physics the LHC will uncover, it is important to be able to explore a wide variety of models and analyse their signals within a realistic setting. This, essentially, means implementing the required model in a Monte Carlo event generator.

In the past each model was hard coded in to a generator, making the addition of new models a time consuming process. Here we present a method, which we have implemented in Herwig++ [28], aimed at minimising this effort. Our approach requires two basic ingredients to be specified with each model, namely:

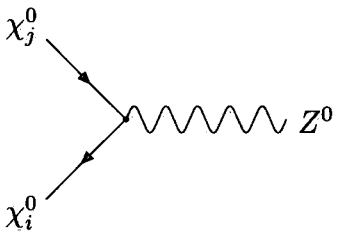

$$i\frac{g}{2\cos\theta_W}\gamma^\mu\left[O'^L_{ij}(1-\gamma_5)+O'^R_{ij}(1+\gamma_5)\right]$$

Figure 3.1: Feynman rule for the $\chi_i^0\chi_j^0Z^0$ vertex where $O'^{L,R}_{ij}$ are defined in the text.

- the Feynman rules which specify the interactions among the new particle spectrum;
- a mass spectrum for the new particles.

The calculations, such as matrix element evaluation, are performed based upon the spin structure of a process rather than hard-coding specific processes.

3.1 Feynman Rules

For a given combination of spins interacting at a vertex, if we assume the perturbative form of the interaction, there is a specific Lorentz structure and a limit on the number of possible couplings for any given interaction. In our approach, each Feynman rule is factorised into a part depending on the Lorentz structure of the interaction and a part governing the exact form for a specific interaction. For example, consider the $\chi_i^0\chi_j^0Z^0$ vertex in the MSSM as shown in Fig. 3.1. A more general rule for any fermion-anti-fermion interacting with a vector boson is given by:

$$ic\gamma^\mu\left[a^LP_L+a^RP_R\right], \tag{3.1}$$

where c is the overall normalisation, $P_{L,R}$ are the left- and right-handed helicity projection operators and $a^{L,R}$ are the left and right couplings respectively. To specify the exact vertex for the interaction in Fig. 3.1 simply requires setting $c = g/\cos\theta_W$, $a^L = O'^L_{ij}$ and $a^R = O'^R_{ij}$ where $O'^L_{ij} = -\frac{1}{2}N_{i3}N^*_{j3} + \frac{1}{2}N_{i4}N^*_{j4}$ and $O'^R_{ij} = O'^{L\,*}_{ij}$.

To use the vertex we need to be able to either evaluate it as a complex number or calculate an off-shell wave function that can be used as input to another calculation. The ability to calculate not just the vertex as a complex number but off-shell components as well, underlies the HELAS [52] method for matrix element calculations. As an example, consider the three-body decay of the top quark as discussed in Chapter 2. The HELAS approach factorises the problem into two parts. First, for each helicity combination of the top and bottom quarks, a vector wave function ϵ_ν for an off-shell W^+ with momentum $q = p_t - p_b$ is calculated,

$$\epsilon_\nu = \bar{u}(p_b)\gamma^\mu \left(-\frac{ig_W}{\sqrt{2}}V_{tb}\right) P_L u(p_t) \frac{i(g_{\mu\nu} - \frac{q_\mu q_\nu}{m_W^2})}{q^2 - m_W^2 + im_W\Gamma}. \tag{3.2}$$

This is used as an input, along with the spinors for the light fermions, at the second vertex to calculate the final matrix element for that helicity combination,

$$\mathcal{M}_{t\to b\bar{f}'f} = \bar{u}(p_f)\gamma^\nu \left(-\frac{ig_W}{\sqrt{2}}V_{tb}\right) P_L v(p_{\bar{f}'})\epsilon_\nu. \tag{3.3}$$

To obtain the spin-summed matrix element the procedure is repeated for all possible helicities of the external particles.

In our approach, the HELAS calculations are performed in terms of the Lorentz structure of each perturbative vertex so that they can be reused with each specific interaction of that vertex type. In addition, the HELAS formalism has a number of advantages:

- the basis states for the particles are provided, which can be stored and passed between production and decay to ensure the spin correlations are consistently implemented using the algorithm described in the previous chapter;
- we can use the spinors and polarisation vectors calculated when the particle is produced to calculate their decays in a different frame, after an appropriate Lorentz transformation, so that each step of the calculation can be done in the most relevant frame;
- more complicated matrix elements can be evaluated from the basic building blocks rather than calculated from scratch;
- the inclusion of particles other than scalars, spin-$\frac{1}{2}$ fermions and massless spin-1 bosons is relatively simple.

Appendix B describes our conventions for the wave functions and vertices used in the HELAS method.

3.2 Hard Processes

The previous chapter discussed generating the outgoing momenta for the initial hard scattering in a general purpose event generator. The cross-section integral in Eqn. (2.8) depends on the matrix element of the process being generated and is evaluated for each phase-space point chosen by the Monte Carlo procedure. The general method of choosing these points does not depend on the process being generated, so the matrix element evaluation is separated from the generation of the phase space. In our approach, we limit the production mechanisms to $2 \to 2$ scatterings and as such the only piece of information that will change with each BSM process is the computation of the matrix element.

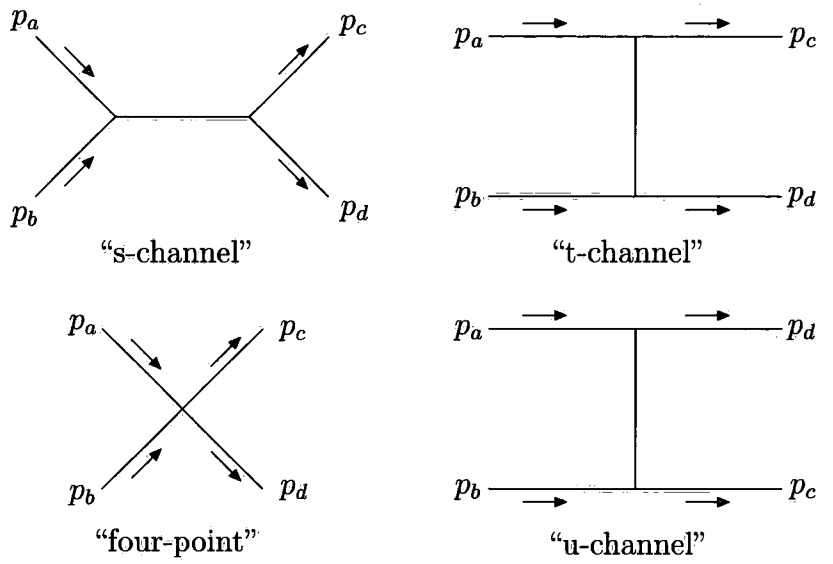

Figure 3.2: Tree-level topologies for a $2 \rightarrow 2$ process. The arrows denote the flow of momenta.

Using the factorised approach described above, the matrix element for a given process can be written down based upon its external spin structure rather than for an exact process. In Fig. 3.2 the possible topologies for a $2 \rightarrow 2$ process at tree level are shown, along with the labels that we will use to refer to a specific diagram type. To compute the matrix element squared for a given process, the tree-level diagrams are calculated and split into so-called *colour flows*. An individual colour flow is identified as a specific combination of colour matrices multiplying an amplitude and a single diagram can contribute to more than one colour flow. For example, consider the process $gg \rightarrow \tilde{g}\tilde{g}$ shown in Fig. 3.3. If the amplitude for the ith diagram, stripped of its colour information, is denoted by $\mathcal{M}_i$ the full amplitude for the 3 diagrams is given by,

$$g_1 = if^{aci}if^{bid}\mathcal{M}_1, \tag{3.4a}$$

$$g_2 = if^{adi}if^{bic}\mathcal{M}_2, \tag{3.4b}$$

$$g_3 = -if^{aib}if^{icd}\mathcal{M}_3, \tag{3.4c}$$

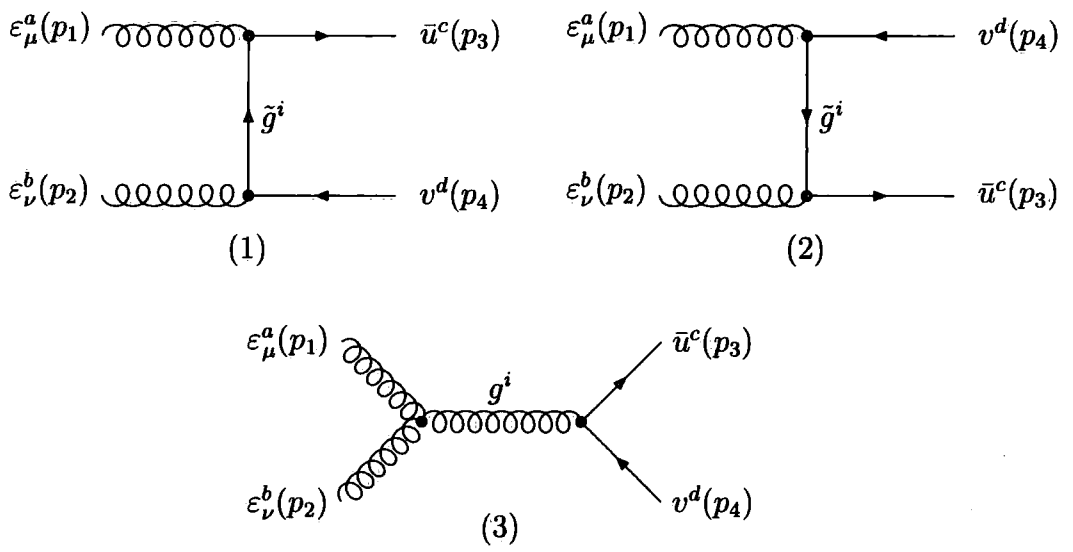

Figure 3.3: Diagrams contributing to the process $gg \to \tilde{g}\tilde{g}$ where lowered Greek letters denote space-time indices and raised Roman letters denote colour indices in the adjoint representation. u, v are the spinors for the gluinos and $\varepsilon_{\mu,\nu}$ are the polarisation vectors of the gluons. The momenta (p_1, p_2) are incoming and (p_3, p_4) are outgoing.

where g_i denotes the full amplitude and f^{abc} denotes the anti-symmetric structure constants of $SU(3)$.

The combination of structure constants in Eqn. (3.4c) can be rewritten using the Jacobi identity to give

$$g_3 = \left(f^{aci}f^{bid} - f^{bci}f^{aid}\right)\mathcal{M}_3, \tag{3.5}$$

where it is apparent that the colour structure of the s-channel gluon exchange diagram is simply a combination of the other two colour structures. The full colour amplitude can therefore be written as

$$\mathcal{M}_T = -\left[c_1(\mathcal{M}_1 - \mathcal{M}_3) + c_2(\mathcal{M}_2 + \mathcal{M}_3)\right], \tag{3.6}$$

where c_i denotes the combination of structure constants from above and the combination of diagram amplitudes are the colour flows, *i.e.* $\mathcal{M}_1 - \mathcal{M}_3$, denoted by f_i[1].

To square the amplitude given in Eqn. (3.6) requires both squaring the colour flows $\mathcal{M}_1 - \mathcal{M}_3$ and $\mathcal{M}_2 + \mathcal{M}_3$ and squaring the colour structures $c_{1,2}$. Given that we are performing the amplitude evaluation using a numerical approach, squaring these is a trivial task. However, to square the colour structures we need to perform colour sums on each combination of structure constants. Taking the above example, the two colour structures are given by $c_1 = if^{aci}if^{bid}$ and $c_2 = if^{adi}if^{bic}$, so that, in theory, there are four colour sums to perform, but in practice since $|c_1|^2 = |c_2|^2$ and $c_1c_2^* = c_2c_1^*$ there are in fact only two. Using the identity

$$f^{abc} = it^a_{bc}, \tag{3.7}$$

we can rewrite the colour structures in terms of the colour matrices of $SU(3)$ such that

$$|c_1|^2 = t^b_{di'}t^a_{i'c}t^a_{ci}t^b_{id}. \tag{3.8}$$

Using the identity $\sum_A t^A_{ab}t^A_{bc} = C_F\delta_{ac}$ gives

$$|c_1|^2 = |c_2|^2 = N_C C_F^2 = \frac{16}{3}, \tag{3.9}$$

where for $SU(3)$ $N_C = 3$ and $C_F = 4/3$. A similar calculation involving the identity $t^at^bt^a = (C_F - \frac{C_A}{2})t^b$ gives $c_1c_2^* = c_2c_1^* = -2/3$. It is noteworthy that the ratio $|c_1|^2/c_1c_2^* \propto (N_C^2 - 1)$, the number of gluons, so that the interference term is suppressed by a factor of $(N_C^2 - 1)$. While there are algorithms available to perform such colour algebra [53], given the limited set of colour structures we are

[1]Note that the overall minus sign in Eqn. (3.6) can be dropped since it simply corresponds to a phase that will not contribute to the final answer.

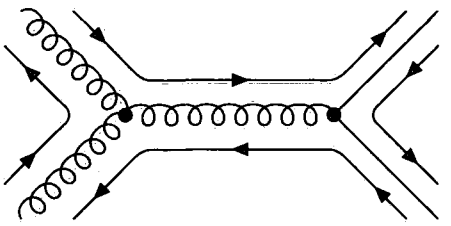

Figure 3.4: A possible colour topology, in the large N_C limit, for the s-channel gluon exchange diagram contributing to the process $gg \to \tilde{g}\tilde{g}$. The three remaining possibilities are found by reversing the arrows appropriately.

dealing with, we choose to calculate those required by hand and store the answers for later use.

The full matrix element squared for a general process $ab \to cd$, summed over final-state spins and colours and averaged over initial-state spins and colours, is given by

$$\overline{\sum}|\mathcal{M}|^2 = Z\frac{1}{S_a}\frac{1}{S_b}\frac{1}{C_a}\frac{1}{C_b}\sum_{\lambda} C_{ij} f_i^{\lambda} f_j^{*\lambda} \tag{3.10}$$

where C_{ij} is a matrix containing the squared colour factors $c_i c_j^*$, f_i^{λ} denotes the ith colour flow for the set of helicities λ, Z is an identical particle symmetry factor, $S_{a,b}$ is the number of polarisation states for each incoming particle and $C_{a,b}$ is the number of colour states for each incoming particle.

In addition to calculating the matrix element for a given scattering process, we must also construct the colour topology that is associated with it so that the parton shower and hadronization stages can proceed correctly. This is achieved by choosing a colour flow probabilistically, based upon its contribution to the total matrix element for the given process. Depending on the colours of the internal and external states involved, there may be more than one possible colour structure for each diagram. For the example in Fig. 3.3 each diagram has 4 possible colour topologies, one of which is shown in Fig. 3.4 for the s-channel exchange, since

Process Type		
$\Psi\ \Psi'$	$\rightarrow$	$\Psi''\ \Psi'''$
$\Psi\ \Psi'$	$\rightarrow$	$\phi\ \phi'$
$\Psi\ \Psi'$	$\rightarrow$	$V\ V'$
$\Psi\ V$	$\rightarrow$	$\Psi\ \phi$
$V\ V'$	$\rightarrow$	$\phi\ \phi'$
$V\ V'$	$\rightarrow$	$\Psi\ \Psi'$
$\Psi\ V$	$\rightarrow$	$V'\ \Psi'$
$V\ V'$	$\rightarrow$	$V''\ V'''$

Table 3.1: Spin structures for $2 \rightarrow 2$ scattering processes where ϕ is a scalar field, Ψ is a fermion field and V is a vector field.

both the gluon and gluino carry a colour and an anti-colour line in the large N_C limit. If a diagram such as this is chosen, one of the possible topologies is selected at random. While this does rely upon using the large N_C limit, given the colour structures that we are dealing with, it is a good approximation.

As discussed above, our approach is based on the external spin structure of a $2 \rightarrow 2$ scattering process so that the above procedure is only implemented for each possible type of spin structure, a list of which is shown in Table 3.1. Coupled with the Feynman rules for a given model, the so-called matrix elements listed produce numerical answers for the spin-summed matrix element squared. In each case all possible s-, t- and u-channel diagrams involving scalar, fermion, vector and tensor exchange are included together with all possible four-point vertices so that the cross section for a selected process can be estimated. To ensure that the method described above is correct, each matrix element was written and compared to an analytical expression in the MSSM [30, 54] and the MUED model [55], once the Feynman rules for each of these models were included.

As an example, the production cross sections for a range of processes in the MSSM at SPS point 1a and the MUED model with the mass spectrum shown in

Particle	Mass (GeV)	Particle	Mass (GeV)
g_1	626.32	$W_1^{\pm}$	535.49
$t_1'^{\circ}$	600.43	H_1^0	517.65
$b_1^{\bullet}$	588.28	$\tau_1^{\bullet}$	514.79
$c_1^{\bullet}$	588.27	$\mu_1^{\bullet}$	514.78
$s_1^{\bullet}$	588.27	$e_1^{\bullet}$	514.78
$d_1^{\bullet}$	588.27	$\nu_{\tau 1}^{\bullet}$	514.78
$u_1^{\bullet}$	588.27	$\nu_{\mu 1}^{\bullet}$	514.78
c_1°	576.32	$\nu_{e 1}^{\bullet}$	514.78
u_1°	576.31	A_1^0	512.88
b_1°	574.91	$H_1^{\pm}$	511.08
s_1°	574.90	τ_1°	504.25
d_1°	574.90	μ_1°	504.25
$t_1'^{\bullet}$	574.20	e_1°	504.25
Z_1^0	535.81	γ_1	500.98

Table 3.2: The mass spectrum for the MUED model, calculated using Herwig++ with the information given in Appendix A, where $R^{-1} = 500\,\text{GeV}$, $\Lambda R = 20$, $\bar{m}_H = 0$ and $m_{h^0} = 115\,\text{GeV}$.

Table 3.2, are given in Table 3.3. Given that the mass spectra are not the same in each of the models, a fair comparison based upon the helicity structure of the underlying model cannot be drawn. However, it is instructive to note that a typical MUED mass spectrum does give production cross sections that are significantly higher than those in the MSSM.

3.2.1 Majorana Particles

Supersymmetry introduces Majorana fermions[2], namely the gauginos, into the new particle landscape. This complicates matrix element calculations as some interactions violate fermion number conservation. For example, consider the production

[2]A fermion field that is its own conjugate

(a)

Process	Cross Section (pb)
$ug \to \tilde{g}\tilde{u}_R$	5.04
$ug \to \tilde{g}\tilde{u}_L$	4.84
$gg \to \tilde{g}\tilde{g}$	3.93
$dg \to \tilde{g}\tilde{d}_R$	2.18
$dg \to \tilde{g}\tilde{d}_L$	1.97
$ud \to \tilde{u}_R\tilde{d}_R$	0.64
$ud \to \tilde{u}_L\tilde{d}_L$	0.57
$uu \to \tilde{u}_L\tilde{u}_R$	0.50
$uu \to \tilde{u}_R\tilde{u}_R$	0.44
$uu \to \tilde{u}_L\tilde{u}_L$	0.41
$ud \to \tilde{u}_L\tilde{d}_R$	0.26
$ud \to \tilde{u}_R\tilde{d}_L$	0.25
$u\bar{u} \to \tilde{u}_R\tilde{u}_L^*$	0.18
$u\bar{u} \to \tilde{u}_R\tilde{u}_R^*$	0.11
$gg \to \tilde{u}_R\tilde{u}_R^*$	0.16
$gg \to \tilde{u}_L\tilde{u}_L^*$	0.14
$u\bar{u} \to \tilde{u}_L\tilde{u}_L^*$	0.10

(b)

Process	Cross Section (pb)
$ug \to g_1 u_1^\circ$	26.14
$ug \to g_1 u_1^\bullet$	25.35
$gg \to g_1 g_1$	23.58
$dg \to g_1 d_1^\circ$	10.70
$dg \to g_1 d_1^\bullet$	10.21
$ud \to u_1^\circ d_1^\circ$	3.46
$ud \to u_1^\bullet d_1^\bullet$	3.29
$uu \to u_1^\bullet u_1^\circ$	5.05
$uu \to u_1^\circ u_1^\circ$	2.82
$uu \to u_1^\bullet u_1^\bullet$	2.76
$ud \to u_1^\bullet d_1^\circ$	2.54
$ud \to u_1^\circ d_1^\bullet$	2.51
$u\bar{u} \to u_1^\circ \bar{u}_1^\bullet$	0.83
$u\bar{u} \to u_1^\circ \bar{u}_1^\circ$	1.00
$gg \to u_1^\circ \bar{u}_1^\circ$	0.53
$gg \to u_1^\bullet \bar{u}_1^\bullet$	0.46
$u\bar{u} \to u_1^\bullet \bar{u}_1^\bullet$	0.96

Table 3.3: Partonic cross sections, produced using Herwig++ after 1×10^6 events, for a range of strong interaction processes at the LHC in (a) the MSSM at SPS point 1a and (b) the MUED model with $R^{-1} = 500\,\text{GeV}$ and $\Lambda R = 20$. The processes are ordered in decreasing magnitude of the MSSM cross section.

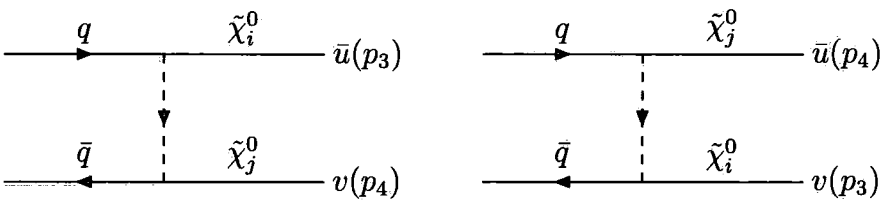

Figure 3.5: Neutralino pair production via t- and u-channel diagrams. The spinors associated the neutralinos are denoted as $u(p)$ and $v(p)$, where the momentum p is outgoing. There is also an additional s-channel diagram involving the exchange of a Z^0 boson but this is not relevant to the discussion here.

of a pair of neutralinos in the MSSM, as shown in Fig. 3.5. The spinor assignments for each of the neutralinos follow from rules introduced by Denner *et al.* in

Refs. [56, 57]. The u-channel diagram arises because the neutralinos do not carry a fermion flow arrow, so the outgoing particles can be exchanged. When calculating the matrix element for this type of process, the spinors for the t-channel diagram are calculated first, followed by the two extra spinors for the exchange diagram, where care must be taken to associate the two extra spinors with the correct momentum and helicity.

3.2.2 Resonant Processes

Often we are interested in the study of s-channel resonances which decay to Standard Model particles rather than the production of a new particle in a $2 \to 2$ scattering process. We therefore include a mechanism to study this type of process. We will take as an example here the virtual exchange of a graviton, the lowest lying state of a Kaluza-Klein tower. The graviton is predicted by various models with extra dimensions where gravity is allowed to propagate in the bulk, an example process is shown in Fig. 3.6. Here, the same procedure as above is used to compute the matrix elements but now there is less work since there is only a single s-channel diagram and hence a single colour flow.

In Randall-Sundrum type models, narrow graviton resonances at the TeV scale are predicted that can be detectable by the LHC [58] through various hard subprocesses. An implementation of the simplest RS model is included in Herwig++ and we have picked three processes involving graviton exchange, $gg \to G \to e^+e^-$, $u\bar{u} \to G \to e^+e^-$ and $u\bar{u} \to G \to \gamma\gamma$, to demonstrate the properties of processes involving a spin-2 particle. The plots of the angular distribution of the outgoing fermion/boson with respect to the beam axis in the centre-of-mass frame are shown in Fig. 3.7 and were produced with our general matrix elements.

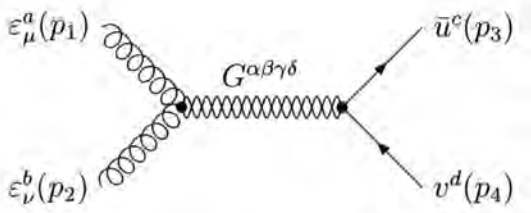

Figure 3.6: Resonant graviton exchange from gluon fusion to produce two fermions.

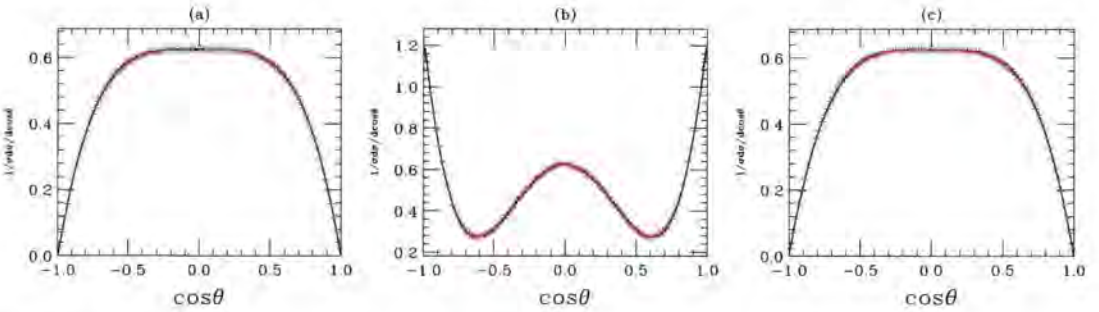

Figure 3.7: Angular distributions for fermion and boson production through a resonant graviton. The graviton has a mass of 1 TeV. The black line denotes the analytical result and the red crosses show the simulation data for (a) $gg \to G \to e^+e^-$ (b) $u\bar{u} \to G \to e^+e^-$ and (c) $u\bar{u} \to G \to \gamma\gamma$.

These distributions show the characteristic behaviour of an exchanged spin-2 particle. The angular dependence of an exchanged spin-1 boson on the other hand is notably different and therefore this kind of distribution is extremely useful in identifying the two cases and eliminating possible background spin-1 exchange when searching for this new mode in future experiments [59]. Discovery of the kind of behaviour shown in Fig. 3.7 would certainly be a very strong indication of the existence of some type of extra dimensional model.

3.3 Perturbative Decays

A new particle spectrum will introduce a rich structure of possible decay modes, the exact form of which will depend on the model parameters. In a SUSY model,

since the phenomenology has been much more widely studied, there are spectrum generators [60–63] which give the mass spectrum and mixing matrices for a given set of input parameters. All of this information is transmitted between these programs in a standard format called the SUSY Les Houches Accord [64, 65]. In addition to calculating the mass spectrum, some programs will also generate a decay table with corresponding widths and branching ratios.

If, on the other hand, a non-SUSY model is being studied, the mass spectrum and decay information must be determined by another means. Our approach takes this into account by including a mechanism to automatically determine the possible two- and three-body decay modes once the new mass spectrum for a non-supersymmetric type model has been calculated[3]. For a further discussion of the details concerning the three-body decay modes, see Section 4.5. To determine the branching ratios we calculate the partial width for each decay mode of a given particle and the branching fraction of a specific mode i is given by

$$\mathrm{BR}_i = \frac{\Gamma_i}{\sum_{j=1}^{N} \Gamma_j}, \tag{3.11}$$

where Γ_i is the partial width of decay mode i and the sum in the denominator extends over the N possible decays of the particle. A sample of the decay modes generated by Herwig++ for the MSSM and the MUED model is shown, along with their corresponding partial widths, in Table 3.4[4].

For a two-body decay, the matrix element only depends on the mass-squared values of each particle so the phase-space factor can be integrated separately and

[3]This mechanism can also be used with a SUSY model if the spectrum generator does not provide a decay table.

[4]An example of a complete decay table generated by Herwig++, for both the MSSM and MUED model, is given in Appendix B.4.

(a)

Decay Mode	Γ_i (GeV)
$\tilde{d}_L \to \tilde{\chi}_1^+, d$	3.31
$\tilde{d}_R \to \tilde{\chi}_1^0, d$	0.29
$\tilde{e}_L \to \tilde{\chi}_1^0, e$	0.12
$\tilde{e}_R \to \tilde{\chi}_1^0, e$	0.21
$\tilde{\chi}_2^0 \to \tilde{\tau}_1^\pm, \tau^\mp$	0.01
$\tilde{\chi}_2^+ \to \tilde{\tau}_1^+, \nu_\tau$	2.02
$\tilde{g} \to \tilde{b}_1, \bar{b}$	0.56

(b)

Decay Mode	Γ_i (GeV)
$d_1^\bullet \to W_1^-, u$	0.11
$d_1^\circ \to \gamma_1, d$	0.02
$e_1^\bullet \to \gamma_1, e$	1.94×10^{-3}
$e_1^\circ \to \gamma_1, e$	3.22×10^{-4}
$Z_1^0 \to \nu_{\tau 1}^\bullet, \nu_\tau$	7.24×10^{-3}
$W_1^+ \to e_1^{\bullet +}, \nu_e$	0.01
$g_1 \to d_1^\circ, \bar{d}$	0.11

Table 3.4: A sample of decay modes for (a) the MSSM at SPS point 1a and (b) the MUED model with the mass spectrum shown in Table 3.2 where the mode with the highest partial width is shown.

the partial width is given by

$$\Gamma(a \to bc) = \frac{p_{cm}}{8\pi m_a^2} \overline{\sum} |\mathcal{M}|^2, \tag{3.12}$$

where $\overline{\sum}|\mathcal{M}|^2$ is the matrix element squared summed over final-state colours and spins and averaged over initial-state colours and spins, $m_{a,b,c}$ are the masses of the initial and two final-state particles respectively and p_{cm} is the centre-of-mass momentum

$$p_{cm} = \frac{1}{2m_a} \left[\left(m_a^2 - (m_b + m_c)^2\right) \left(m_a^2 - (m_b - m_c)^2\right) \right]^{1/2}. \tag{3.13}$$

Therefore, in a two-body decay with given kinematics, the matrix element squared is the only quantity which will change depending on the specific decay. As a result, when calculating the partial width for a particular two-body decay mode, we use a hard-coded formula that is based on the Lorentz structure of the decay rather than using the HELAS approach. The spin structures for the general two-body decays are shown in Table 3.5 and the corresponding analytical expressions are given in Appendix B.3. While, in principle, these expressions could also be used

Two-Body	
$\phi \to \Psi\ \Psi'$	$V \to \Psi\ \Psi'$
$\phi \to V\ V'$	$V \to \phi\ \phi'$
$\phi \to \phi'\ \phi''$	$V \to V'\ V''$
$\phi \to \phi\ V$	$T \to \phi\ \phi'$
$\Psi \to \Psi'\ \phi$	$T \to \Psi\ \Psi'$
$\Psi \to \Psi'\ V$	$T \to V\ V'$

Table 3.5: Spin structures for general two-body decays where ϕ is a scalar, Ψ is a fermion, V is a vector boson and T is a tensor field.

to generate the momenta when a two-body decay is simulated in an event, in practice we want to include spin correlations so we must use the HELAS approach during event generation.

The partial width for a three-body decay is given by [66]

$$\Gamma(a \to b,c,d) = \frac{1}{(2\pi)^3}\frac{1}{32m_a^3}\int_{(m_b+m_c)^2}^{(m_a-m_d)^2} \mathrm{d}m_{bc}^2 \int_{(m_{cd}^2)_{\min}}^{(m_{cd}^2)_{\max}} \mathrm{d}m_{cd}^2 \overline{\sum}|\mathcal{M}|^2, \qquad (3.14)$$

where $\overline{\sum}|\mathcal{M}|^2$ is the matrix element squared summed over final-state colours and spins and averaged over initial-state colours and spins and

$$(m_{cd}^2)_{\max} = (E_c^* + E_d^*)^2 - \left(\sqrt{E_d^{*2} - m_d^2} - \sqrt{E_d^{*2} - m_d^2}\right)^2, \qquad (3.15a)$$

$$(m_{cd}^2)_{\min} = (E_c^* + E_d^*)^2 - \left(\sqrt{E_c^{*2} - m_c^2} + \sqrt{E_d^{*2} - m_d^2}\right)^2, \qquad (3.15b)$$

with $E_c^* = (m_{ab}^2 - m_b^2 + m_c^2)/2m_{bc}$ and $E_d^* = (m_a^2 - m_{bc}^2 - m_d^2)/2m_{bc}$. In general, the phase-space integration can no longer be performed analytically since the matrix element is a complicated function of the invariant mass combinations m_{bc} and m_{cd}, therefore it must be performed numerically. Given the low number of dimensions of the phase-space integral in Eqn. (3.14), they are performed using standard techniques rather than by the Monte Carlo method.

Three-Body
$\phi \rightarrow \phi\ \Psi\ \Psi'$
$\phi \rightarrow \Psi\ \Psi'\ V$
$\Psi \rightarrow \Psi'\ \Psi''\ \Psi'''$
$\Psi \rightarrow \Psi'\ V\ V'$
$V \rightarrow \Psi\ \Psi'\ V$

Table 3.6: Spin structures relevent to this work for general three-body decays where ϕ is a scalar, Ψ is a fermion and V is a vector boson.

In a general three-body decay there will be multiple diagrams that contribute to the full matrix element and as a result the calculation will follow similar lines to a $2 \rightarrow 2$ scattering process. For a particular decay, the diagrams are evaluated, using the HELAS method, for a given set of helicities and added to an appropriate colour flow. The full matrix element is given by summing over all possible helicities of the external particles and including relevant polarisation, colour and symmetry factors. Again the work is done at the level of the spin structures of a decay and those included in our work are appropriate to the helicity structures of the models discussed here and are shown in Table 3.6.

3.4 Results

3.4.1 Squark Decay

The spin correlation algorithm discussed in Chapter 2 was shown to work in the case of $t\bar{t}$ production and decay. One of the simplest cases to consider for a SUSY model is the different decay modes of a left-handed squark. Considering the decay of the squark via the two modes (a) $\tilde{u}_L \rightarrow \tilde{\chi}_2^0 q \rightarrow \tilde{l}_R^- l^+ u$ and (b) $\tilde{u}_L \rightarrow \tilde{\chi}_2^0 q \rightarrow \tilde{l}_R^+ l^- u$ and plotting the mass distribution of the produced quark and (anti-)lepton allows

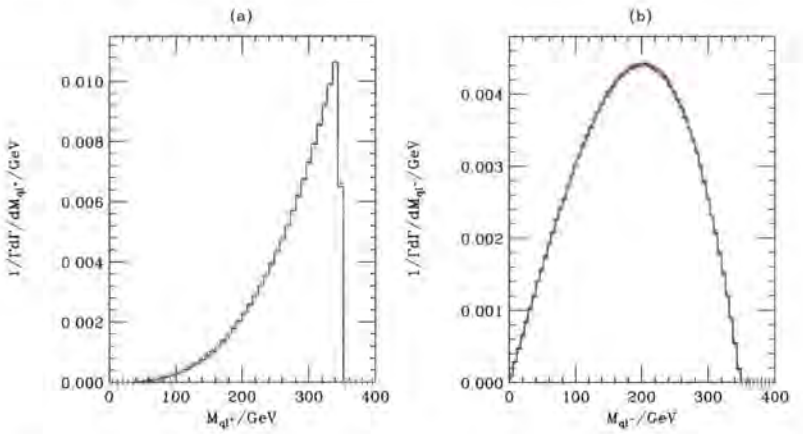

Figure 3.8: The invariant mass distribution of (a) the anti-lepton-quark and (b) the lepton-quark produced in $\tilde{u}_L \to \tilde{\chi}_2^0 u \to e^{\pm}\tilde{e}_R^{\mp} u$. The black line denotes the results from HERWIG and the red crosses denote the results from Herwig++.

the effect of spin correlations to be demonstrated.

The plots in Fig. 3.8 were produced at Snowmass point 5 [67] where $\tan\beta = 5$, $\text{sign}(\mu) > 0$, $m_0 = 150\,\text{GeV}$, $m_2 = 300\,\text{GeV}$ and $A_0 = -1000\,\text{GeV}$. This parameter set, along with SOFTSUSY 2.0.8 [61], gives $m_{\tilde{u}_L} = 672.82\,\text{GeV}$, $m_{\tilde{\chi}_2^0} = 231.29\,\text{GeV}$ and $m_{\tilde{l}_R} = 192.87\,\text{GeV}$.

There is a stark difference in the quark-lepton mass distribution for the two decay modes considered above, which is due to the helicities of the external particles. At the mass scale of the squark the quark can be considered massless and left-handed, the anti-lepton will also be left-handed and the lepton will be right-handed. When back-to-back the lepton-quark system will have net spin-1 and as such can not be produced in a scalar decay while the anti-lepton-quark system will have spin-0 and is able to proceed.

The end-point in both of the distributions is due to a kinematic cut-off where the invariant mass of the quark-lepton pair is at its maximum. The value of this end-point can be calculated by considering the mass-squared when the pair is

back-to-back. The value is given in [68] as

$$(m)^2_{\text{max}} = \frac{\left(m^2_{\tilde{u}_l} - m^2_{\tilde{\chi}^0_2}\right)\left(m^2_{\tilde{\chi}^0_2} - m^2_{\tilde{e}_R}\right)}{m^2_{\tilde{\chi}^0_2}}. \tag{3.16}$$

Using the values for the sparticle masses above one finds a value for the end-point of 348.72 GeV which is consistent with the plots in Fig. 3.8.

3.4.2 Gaugino Production

As discussed previously, supersymmetry introduces Majorana fermions and it is necessary to ensure that their spin correlations are implemented correctly in our new framework. We consider three production processes and the angular distributions of the leptons produced in the subsequent decays. The SUSY spectrum for each was again generated using SOFTSUSY and the masses for the points used in each process are given in the relevant section.

$e^+e^- \rightarrow \tilde{\chi}^0_2\tilde{\chi}^0_1$

Here we consider the production of the lightest and next-to-lightest neutralinos with the decay of the $\tilde{\chi}^0_2$ proceeding through (i) $\tilde{\chi}^0_2 \rightarrow \tilde{l}^{\pm}_R l^- \rightarrow l^+l^-\tilde{\chi}^0_1$ and (ii) $\tilde{\chi}^0_2 \rightarrow Z^0\tilde{\chi}^0_1 \rightarrow l^-l^+\tilde{\chi}^0_1$ at SPS point 1b. The relevant sparticle masses are $m_{\tilde{\chi}^0_2} = 306.55\,\text{GeV}$, $m_{\tilde{\chi}^0_1} = 161.78\,\text{GeV}$, $m_{\tilde{l}_R} = 253.82\,\text{GeV}$. Fig. 3.9 shows how the polarisation of the beam affects the angular distribution of the lepton produced in the $\tilde{\chi}^0_2$ decay.

The lepton shows a correlation with the beam polarisation because the neutralino is a fermion and spin information is preserved when it decays. Figures 3.10 and 3.11 show the angular dependence of the final-state lepton for the case of

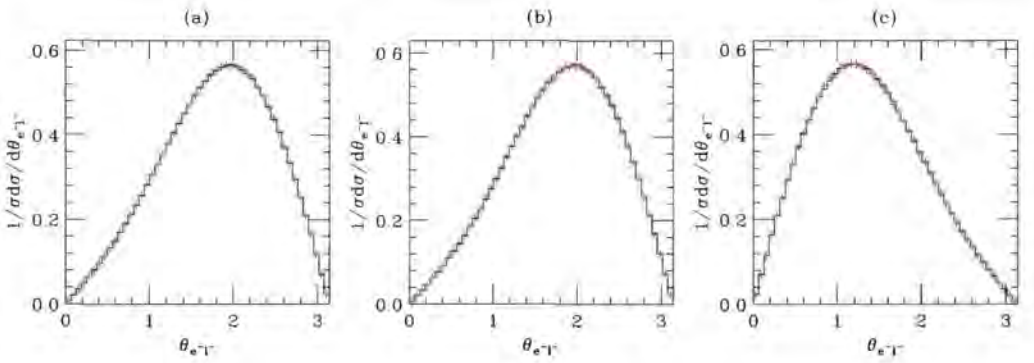

Figure 3.9: The angular correlation between the lepton produced in $e^+e^- \to \tilde{\chi}_2^0\tilde{\chi}_1^0 \to \tilde{l}_R^+ l^- \tilde{\chi}_1^0$ and the beam in the lab frame for a centre-of-mass energy of 500 GeV and (a) unpolarised incoming beams, (b) negatively polarised electrons and positively polarised positrons and (c) positively polarised electrons and negatively polarised positrons. The black histogram is from HERWIG and the red crosses from Herwig++.

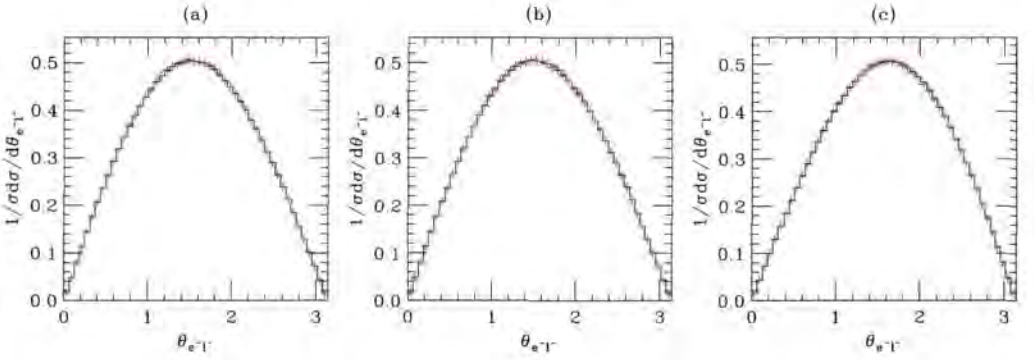

Figure 3.10: The angular correlation between the lepton produced in $e^+e^- \to \tilde{\chi}_2^0\tilde{\chi}_1^0 \to Z^0\tilde{\chi}_1^0 \to l^-l^+\tilde{\chi}_1^0$ and the beam in the lab frame for a centre-of-mass energy of 500 GeV and (a) unpolarised incoming beams, (b) negatively polarised electrons and positively polarised positrons and (c) positively polarised electrons and negatively polarised positrons. The black histogram is from HERWIG and the red crosses from Herwig++.

an intermediate Z^0 boson and $\tilde{l}_R$ respectively. As is to be expected for an intermediate slepton, the incoming beam polarisation has little effect on the angular distribution of the final-state lepton due to its scalar nature[5]. The plots are in good agreement with the HERWIG results.

[5]There is some residual effect due to the correlation of the $\tilde{l}_R$ direction with the beam in the $\tilde{\chi}_2^0$ decay.

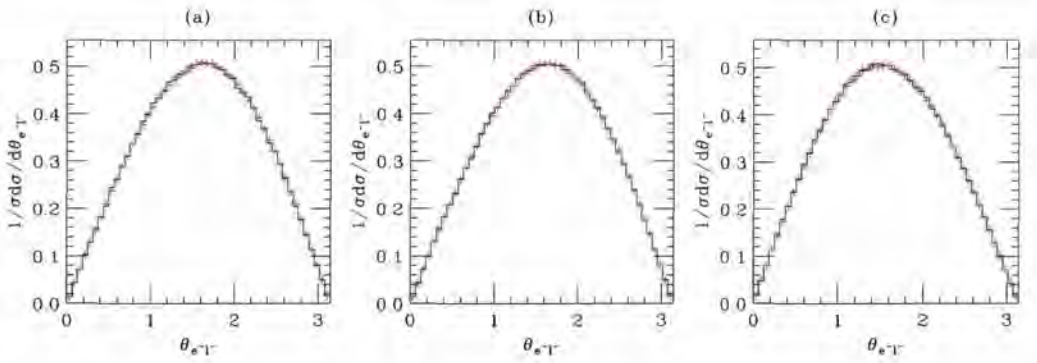

Figure 3.11: The angular correlation between the lepton produced in $e^+e^- \to \tilde{\chi}_2^0\tilde{\chi}_1^0 \to \tilde{l}_R^- l^+ \to l^- l^+ \tilde{\chi}_1^0\tilde{\chi}_1^0$ and the beam in the lab frame for a centre-of-mass energy of 500 GeV and (a) unpolarised incoming beams, (b) negatively polarised electrons and positively polarised positrons and (c) positively polarised electrons and negatively polarised positrons. The black histogram is from HERWIG and the red crosses from Herwig++.

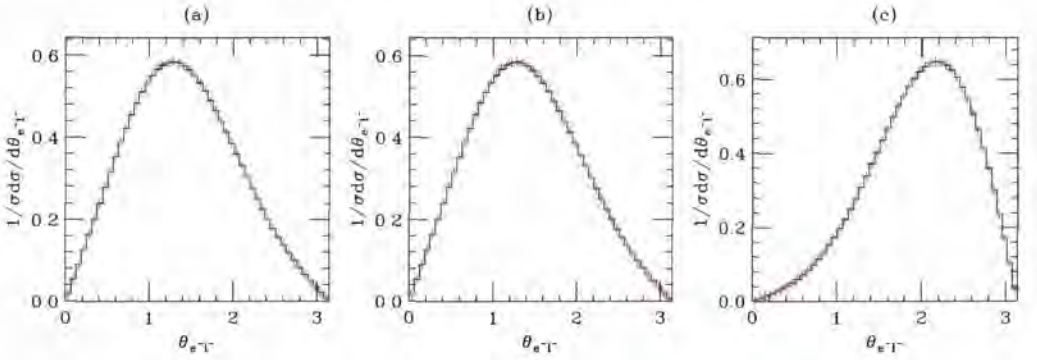

Figure 3.12: The angle between the lepton produced in $e^+e^- \to \tilde{\chi}_1^+\tilde{\chi}_1^- \to W^+W^-\tilde{\chi}_1^0\tilde{\chi}_1^0 \to l^- l^+ \nu_l \bar{\nu}_l \tilde{\chi}_1^0\tilde{\chi}_1^0$ and the beam in the lab frame for a centre-of-mass energy of 500 GeV and (a) unpolarised incoming beams, (b) negatively polarised electrons and positively polarised positrons and (c) positively polarised electrons and negatively polarised positrons. The black histogram is from HERWIG and the red crosses from Herwig++.

$e^+e^- \to \tilde{\chi}_i^+\tilde{\chi}_i^-$

We now consider the production of chargino pairs and their associated decays. Two possible decay modes of the $\tilde{\chi}_i^\pm$ are (a) $\tilde{\chi}_i^\pm \to W^\pm\tilde{\chi}_1^0$ and (b) $\tilde{\chi}_i^\pm \to \tilde{\nu}_\alpha l^\pm$. Here we use the W decay mode for the lightest chargino and the sneutrino decay mode for the heaviest chargino in order to consider final-states with differing spins.

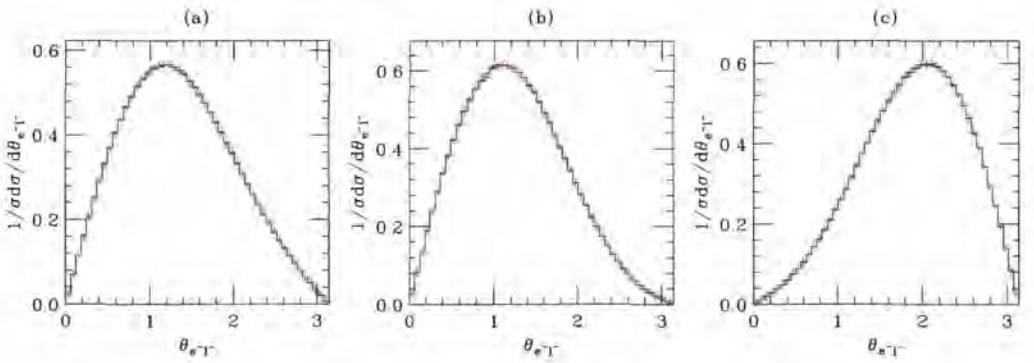

Figure 3.13: The angle between the lepton produced in $e^+e^- \to \tilde{\chi}_2^+\tilde{\chi}_2^- \to \tilde{\nu}_L l^+ \tilde{\nu}_L l^-$ and the beam in the lab frame for a centre-of-mass energy of 1 TeV and (a) unpolarised incoming beams, (b) negatively polarised electrons and positively polarised positrons and (c) positively polarised electrons and negatively polarised positrons. The black histogram is from HERWIG and the red crosses from Herwig++.

The mass spectrum was generated for SPS point 1a where $m_{\tilde{\chi}_2^+} = 377.39\,\text{GeV}$, $m_{\tilde{\chi}_1^+} = 181.53\,\text{GeV}$, $m_{\tilde{\nu}_L} = 185.42\,\text{GeV}$ and $m_{\tilde{\chi}_1^0} = 97.00\,\text{GeV}$.

Figure 3.12 shows the angle of the produced electron for the production of the lightest chargino. As expected, the beam polarisation affects the lepton distribution because of the intermediate W boson carrying the spin correlations through to the final state. The effects are similar for the sneutrino decay of the heaviest chargino shown in Fig. 3.13. The lepton accompanying the $\tilde{\nu}_L$ still shows correlation with the beam on account of the chargino being a fermion. If the lepton had come from the decay of a scalar, there would have been no such correlation.

3.4.3 Tau Decays

One Prong Decays

The tau has a number of leptonic and hadronic decay modes. A more detailed analysis of these decays shows interesting features in the distribution of energy to the decay products. A typical tau decay involving several mesons has the form

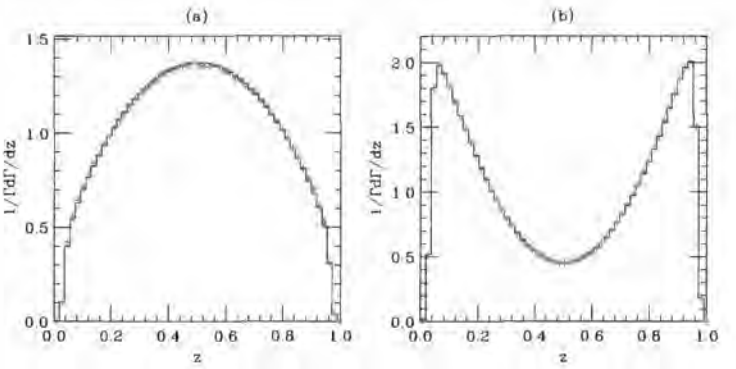

Figure 3.14: Energy fraction, z, carried away by the charged meson in the one prong τ decay $\rho^{\pm} \to \pi^{\pm}\pi^0$ for (a) left-handed $\tilde{\tau}_1$ and (b) right-handed $\tilde{\tau}_1$. The black histogram shows the results from HERWIG with the TAUOLA [70] decay package and the red crosses indicate the Herwig++ results.

$\tau^{\pm} \to (nm^{\pm})(qm^0)\nu_\tau$ where $nm^{\pm}$ denotes $n \geq 1$ charged mesons, *i.e.* the number of prongs, while qm^0 denotes $q \geq 0$ neutral mesons. Here we will consider the one prong decay $\tau^{\pm} \to \rho^{\pm}\nu_\tau \to \pi^{\pm}\pi^0\nu_\tau$ where the τ is produced from the decay of a $\tilde{\tau}_1$. Fig. 3.14 shows our results for the fraction of visible energy carried away by the charged meson in the two cases where the $\tilde{\tau}_1$ is (a) 100% left-handed and (b) 100% right-handed.

There is a stark difference in the energy distribution for two possible mixings of the $\tilde{\tau}_1$ in Fig. 3.14 due to the resulting helicity of the decaying ρ. For the case where the $\tilde{\tau}_1$ is entirely $\tilde{\tau}_L$ the ρ has a higher probability of being transversely polarised, from the results of [69], which favours the equal splitting of energy between the two pions as confirmed by the first plot. A $\tilde{\tau}_1$ that is entirely $\tilde{\tau}_R$ however, will give rise to mostly longitudinally polarised ρ mesons that prefer to distribute their energy unequally and favour a distribution where one meson receives most of the visible energy from the τ decay. This is again confirmed in our second plot. The Herwig++ results are plotted together with those from HERWIG with the TAUOLA decay package [70] that is designed specifically for the decay of polarised τ leptons.

Squark Decay

The use of the effects described above in the study of SUSY models has long been recognised. In Ref. [71] a mechanism for the determining the spin properties of particles involved in SUSY cascade decays using τ polarisation was suggested. The method involves analysing invariant mass distributions of different particle pairs along the decay chain $\tilde{q}_\alpha \to q\tilde{\chi}_2^0 \to q\tau_n^\pm\tilde{\tau}_1^\mp \to q\tau_f^\mp\tilde{\chi}_1^0$ with the τ decay restricted to $\tau^\pm \to \pi^\pm\nu_\tau$. The various normalised invariant mass distributions are shown in Fig. 3.15 for $\tilde{q}_\alpha = \tilde{q}_L$ at SPS point 1a where $m_{\tilde{q}_L} = 558.40\,\text{GeV}$, $m_{\tilde{\chi}_2^0} = 180.96\,\text{GeV}$, $m_{\tilde{\tau}_1} = 134.56\,\text{GeV}$ and $m_{\tilde{\chi}_1^0} = 97.00\,\text{GeV}$. Since an experiment would be unable to distinguish a near or far τ/π their distributions are combined. The plots are normalised to the appropriate maximum invariant mass where

$$\left(m^2_{\tau\tau}\right)_{\max} = \left(m^2_{\pi\pi}\right)_{\max} = \left(m^2_{\tilde{\chi}_2^0} - m^2_{\tilde{\tau}_1}\right)\left(1 - m^2_{\tilde{\chi}_1^0}/m^2_{\tilde{\tau}_1}\right), \tag{3.17a}$$

$$\left(m^2_{q\tau}\right)_{\max} = \left(m^2_{q\pi}\right)_{\max} = \max\left\{\left(m^2_{\tilde{q}_L} - m^2_{\tilde{\chi}_2^0}\right)\left(1 - m^2_{\tilde{\tau}_1}/m^2_{\tilde{\chi}_2^0}\right), \left(m^2_{\tilde{q}_L} - m^2_{\tilde{\chi}_2^0}\right)\left(1 - m^2_{\tilde{\chi}_2^0}/m^2_{\tilde{\tau}_1}\right)\right\}. \tag{3.17b}$$

The differences in shape of the charge conjugate plots in Fig. 3.15 for the τ and π are due to the different helicities of the τ and π as explained in Section 3.4.1. The kinks in these distributions show the change from near to far leptons or pions making up the main components of the event. Again our results are plotted along with those from HERWIG with the TAUOLA package and there is excellent agreement between the two sets of results and the distributions follow those of Fig. 3 in Ref. [71].

For comparison, the results from the analogous cascade in the MUED model are also included in Fig. 3.15. These show a stark difference to the MSSM results, with the exception of the $\tau\tau$ distribution, due to the different helicity structure of

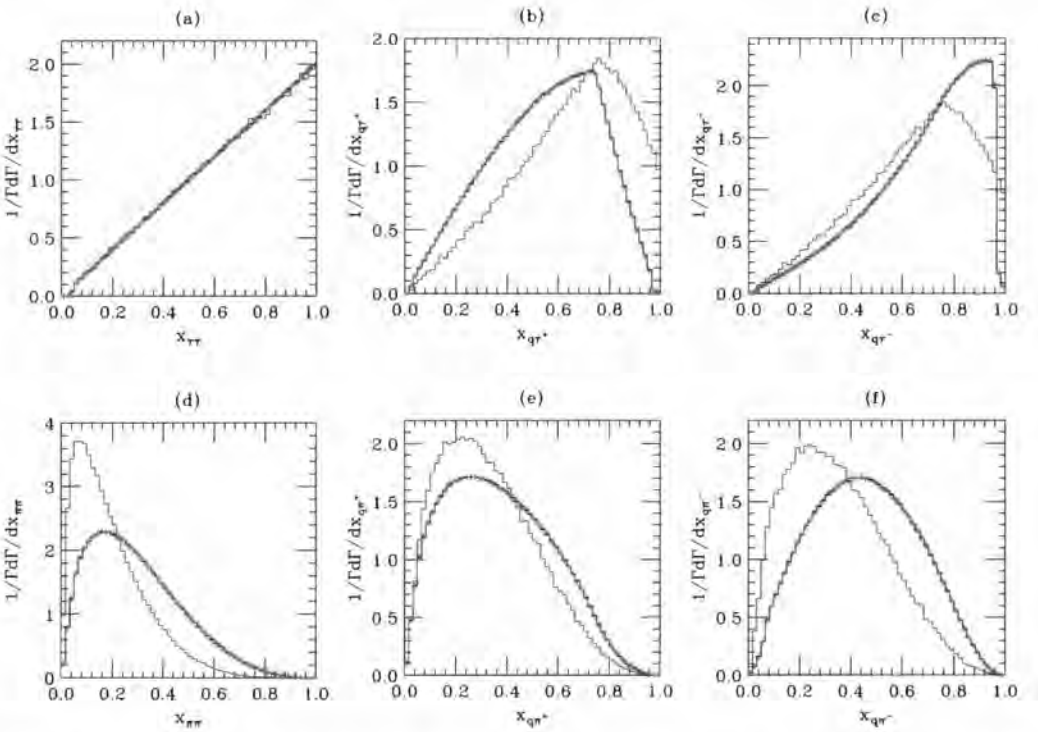

Figure 3.15: Normalised invariant mass distributions $x_{ij} = m_{ij}/(m_{ij})_{max}$ for various pairs of decay products along the chain $\tilde{q}_\alpha \to q\tilde{\chi}_2^0 \to q\tau_n^\pm \tilde{\tau}_1^\mp \to q\tau_f^\mp \tilde{\chi}_1^0$ where the τ decays via $\tau \to \pi\nu_\tau$ only. The black histogram denotes the results from HERWIG with the TAUOLA package and the red crosses are the results from Herwig++ for (a) $\tau\tau$, (b) $q\tau^+$, (c) $q\tau^-$, (d) $\pi\pi$, (e) $q\pi^+$ and (f) $q\pi^-$. The blue histogram shows the results from Herwig++ for the counterpart cascade in the MUED model with a matched mass spectrum.

the underlying cascade. The $\tau\tau$ result should also deviate from the phase-space distribution, however from the discussion in Ref. [55], the deviation is sensitive to the mass spectrum and at SPS 1a the spectrum is such that the spin correlations all but vanish.

These kind of invariant mass distributions serve as a good indication of the spin properties of the particles involved in cascade decays. This information is important when trying to confirm an exact model of new physics since it is possible for two different BSM models to imitate each other in certain decays, as shown, even though the new particles introduced into each model have different

spin assignments [55]. This behaviour will be studied in more detail in Chapter 5.

3.5 Summary

This chapter has described a general approach to the simulation of new physics scenarios, with the aim of reducing the amount of work required to incorporate further models into the Herwig++ event generator. The HELAS method of calculating amplitudes was introduced so that the information necessary for the spin correlation algorithm, described in the previous chapter, could be calculated. After implementing the Feynman rules for the MSSM, various distributions showing the propagation of spin correlation information throughout production and decay were shown and compared to the HERWIG program. All were in excellent agreement, demonstrating that this approach is viable for simulating models of new physics.

Throughout this chapter we have assumed that all particle states are produced on mass shell. Given that we do not have a measured spectrum this approximation may not be valid if some decays occur close to threshold. In the next chapter we will describe a general procedure for extending the simulation to include the effects of finite particle widths.

Chapter 4

Finite Width Effects

'In physics, you don't have to go around making trouble for yourself - nature does it for you.'

— Frank Wilczek

When introducing the concept of a Monte Carlo event generator in Chapter 2, we described how a width in a scattering process originates from corrections to the propagator of an unstable particle. In the subsequent work we ignored the effects of these widths entirely and worked soley within the narrow width approximation. However, given our lack of knowledge of a specific mass spectrum, we cannot be certain that the assumptions used in the narrow width approximation are strictly satisfied. While there have been studies recently of the validity of narrow width limit for some SUSY scenarios [72–74], nothing has been studied in relation to other popular new physics models. In this chapter we describe a systematic method for including off-shell effects in a Monte Carlo event generator with our main focus on BSM studies.

As discussed in Chapter 2, the narrow width approximation allows the propa-

gator connecting production and decay of successive decays to be integrated out. This essentially means that part of the phase-space integral is approximated to a constant when the correct assumptions are satisfied. Therefore, to improve the accuracy of our simulation we wish to move away from the on-shell approximation and include the effects from integrating over the connecting propagator. In the past this has been accomplished in a variety of ways. For example, the FORTRAN HERWIG [29] program included:

1. the full three-body matrix element, with an off-shell $W^{\pm}$ boson, for top decay;
2. smearing of fundamental particle masses using a Breit-Wigner distribution;
3. a more sophisticated Higgs boson lineshape [75].

To improve our simulation of BSM physics, we include the weight factor

$$\frac{1}{\pi}\int_{m^2_{\text{min}}}^{m^2_{\text{max}}} \mathrm{d}m^2 \frac{m\Gamma(m)}{(m^2-M^2)^2+m^2\Gamma^2(m)}, \tag{4.1}$$

throughout the production and decay stages, where $\Gamma(m)$ is the running width of the particle, M is the pole mass and $m_{min,max}$ are defined such that the maximum deviation from the pole mass is a constant times the on-shell width. The factor can be derived by considering a three-body decay that consists entirely of scalar particles[1]. Using the notation in Fig. 4.1, the decay rate is given by

$$\Gamma(a \to b,d,e) = \frac{(2\pi)^4}{2m_a}\int \mathrm{d}\phi_3\left(p_a;p_b,p_d,p_e\right)\sum_{i=1}^{n}\overline{|\mathcal{M}_{3_i}|}^2 \tag{4.2}$$

where $\mathrm{d}\phi_3$ is the three-body phase-space and $\overline{|\mathcal{M}|}^2 = \overline{\sum}|\mathcal{M}|^2$, the spin-averaged

[1]We in fact apply the same weight factor regardless of the spin of the particles involved. Therefore in the derivation, although it is a slight abuse of terminology, we refer to the matrix element squared as being summed over final-state spins and averaged over initial-state spins.

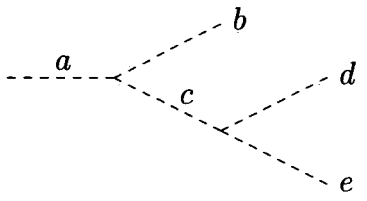

Figure 4.1: A three-body decay consisting entirely of scalar particles where the external particles a, b, d and e are all on-shell.

matrix element. The phase space can be written recursively as [66, 76]

$$\mathrm{d}\phi_3\left(p_a; p_b, p_d, p_e\right) = \mathrm{d}\phi_2\left(p_a; p_b, q\right)\mathrm{d}\phi_2\left(q; p_d, p_e\right)\left(2\pi\right)^3 \mathrm{d}q^2, \tag{4.3}$$

where $\mathrm{d}\phi_2$ is a two-body phase-space factor and q is the momentum of the intermediate.

For the matrix element we assume that the intermediate particle of mass M has n two-body decay modes so that

$$\sum_{i=1}^{n} \overline{|\mathcal{M}_{3_i}|}^2 = \frac{\overline{|\mathcal{M}_a|}^2}{\left(q^2 - M^2\right)^2 + q^2\Gamma^2(q)} \sum_{i=1}^{n} \overline{|\mathcal{M}_{c_i}|}^2, \tag{4.4}$$

where $\overline{|\mathcal{M}_a|}^2$ and $\overline{|\mathcal{M}_{c_i}|}^2$ are the two-body spin-averaged matrix elements and $\Gamma(q)$ is the width of the intermediate particle at scale q. Substituting Eqns. (4.3, 4.4) into Eqn. (4.2) gives

$$\begin{aligned}\Gamma(a \to b, d, e) \;=\; & \frac{(2\pi)^3}{m_a} \int_{m_{\min}^2}^{m_{\max}^2} \mathrm{d}q^2 \frac{q}{\left(q^2 - M^2\right)^2 + q^2\Gamma^2(q)} \\ & \times \int \mathrm{d}\phi_2 \overline{|\mathcal{M}_a|}^2 \int \mathrm{d}\phi_2 \frac{(2\pi)^4}{2q} \sum_{i=1}^{n} \overline{|\mathcal{M}_{c_i}|}^2,\end{aligned} \tag{4.5}$$

where we have limited the integral over q to the region defined by the width cut described above. The third integral in Eqn. (4.5) can be recognised as $\Gamma(c \to d, e)$ using

$$\Gamma(a \to b, c) = \frac{(2\pi)^4}{2m_a} \int \overline{|\mathcal{M}_a|}^2 \mathrm{d}\phi_2 \tag{4.6}$$

and the second as $\Gamma(a \to b, c)$, with the intermediate particle at scale q, giving

$$\Gamma(a \to b, d, e) = \frac{1}{\pi} \int_{m_{\min}^2}^{m_{\max}^2} \mathrm{d}q^2 \, \Gamma_a \frac{q\Gamma_c(q)}{\left(q^2 - M^2\right)^2 + q^2\Gamma_c^2(q)}. \tag{4.7}$$

The weight factor is then identified as

$$w = \frac{1}{\pi} \int_{m_{\min}^2}^{m_{\max}^2} \mathrm{d}q^2 \frac{q\Gamma(q)}{\left(q^2 - M^2\right)^2 + q^2\Gamma^2(q)}. \tag{4.8}$$

The case for either production followed by decay or high multiplicity decays follows similar arguments and the same factor is found.

It should be noted from the discussion in Ref. [75] that use of the running width in the propagator of Eqn. (4.5) is only valid if $\Gamma(q) \sim q$ for large q. If $\Gamma(q)$ were to grow faster than this then the width terms are dominant and the propagator becomes of $\mathrm{O}(1/\alpha)$, since $\Gamma \sim \sqrt{\alpha}$, the coupling of the $c \to d, e$ decay. If $\Gamma(q)$ grows linearly with q the extra terms do not become dominant and are simply unenhanced higher order corrections.

The weight includes a momentum dependence into the calculation of cross sections and decay widths thereby improving the approximation to the full matrix element. The approximation is not without its problems as there can be issues with gauge cancellations, which will be commented on in more detail and other problems such as unitarity violations. Despite these issues, it is still a better treatment than having all particles on mass shell.

While for the latter case convoluting the weight with the partial width calculation for a particular decay mode is relatively simple, this is not the case for the production stage, so we will consider them separately.

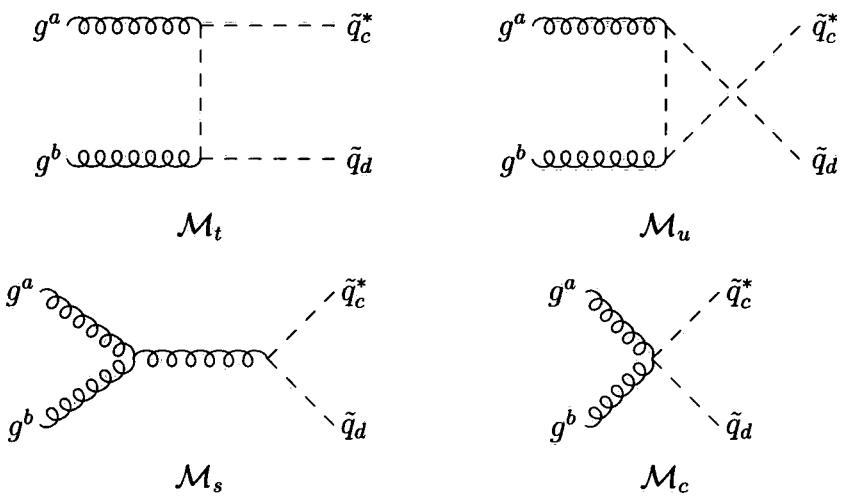

Figure 4.2: Feynman diagrams for the process $gg \to \tilde{q}^*\tilde{q}$ where the Roman indices give the colour representation.

4.1 Off-Shell Masses in Particle Production

For production we need to convolute the weight factor described above with the cross-section integral. We achieve this by distributing the masses of the outgoing particles according to Eqn. (4.1). This in itself is a simple task but what we will show here, with an example from supersymmetry, is that gauge invariance can be violated if these masses are used naïvely when calculating the matrix elements.

Consider the process $gg \to \tilde{q}^*\tilde{q}$, for which the diagrams are shown in Fig. 4.2, where we wish the outgoing squarks to have masses m_3 and m_4 respectively. Due to the presence of external gluons, the Ward identity

$$p_{1\mu}p_{2\nu}\mathcal{M}^{\mu\nu}(p_1, p_2) = 0, \tag{4.9}$$

where p_i are the momenta of the gluons and $\mathcal{M}$ is the total amplitude, must be satisfied.

The amplitudes $\mathcal{M}_i$, after replacing the external polarisation vectors with their

momenta, are given by

$$\mathcal{M}_t = -g_s^2 \frac{(t-m_3^2)}{(t-m_{t-diag}^2)} \left(m_4^2 - t\right) t_{di}^b t_{ic}^a, \tag{4.10a}$$

$$\mathcal{M}_u = -g_s^2 \frac{(u-m_4^2)}{(u-m_{u-diag}^2)} \left(m_3^2 - u\right) t_{di}^a t_{ic}^b, \tag{4.10b}$$

$$\mathcal{M}_s = -\frac{g_s^2}{2} (t-u) \left(t_{di}^b t_{ic}^a - t_{di}^a t_{ic}^b\right), \tag{4.10c}$$

$$\mathcal{M}_c = \frac{g_s^2}{2} s \left(t_{di}^a t_{ic}^b + t_{di}^b t_{ic}^a\right), \tag{4.10d}$$

where s, t and u are the Mandelstam variables, $m_{t-,u-diag}$ are the t- and u-channel masses and t_{ij}^a are the SU(3) colour matrices. Equations (4.10a, 4.10b) show that for any hope of achieving the correct cancellation we must set $m_t = m_3$ and $m_u = m_4$. This also shows why, even in the on-shell case, one must take care when using widths in scattering diagram calculations as these alone can give rise to violations of gauge invariance. The total amplitude saturated with the gluon momenta for the $g\,g \to \tilde{q}^*\tilde{q}$ process is then

$$\frac{g_s^2}{2} \left(m_3^2 - m_4^2\right) \left[t^b, t^a\right], \tag{4.11}$$

so that Eqn. (4.9) is only satisfied if $m_3 = m_4$.

This requirement means that, in general, we cannot use off-shell masses when calculating matrix elements since if we generate a process such as that shown, we would violate gauge invariance. In our procedure the off-shell masses are used when calculating the momenta of the outgoing particles involved in the hard interaction but are rescaled, such that $m_3 = m_4$, for the matrix element calculations. To demonstrate the validity of this procedure we compare the line shape of the top quark from Herwig++ and Madgraph for the production of a top quark at the ILC, the Tevatron and the LHC. In Herwig++ the top quark width is computed

using the full three-body matrix element whereas in the Madgraph case just the two-body decay of the top quark is used, due to rapid growth in the number of diagrams that are required. In all cases Herwig++ generates the $2 \to 2$ production process for the $t\bar{t}$ pair followed by the three-body decay of the top quark using the treatment of off-shell effects described in the text. Madgraph was used to calculate the $2 \to 4$ matrix element for the production of $b\bar{b}W^-W^+$ including the non-resonant diagrams.

To ensure that the amplitudes generated by Madgraph [34] were gauge invariant, the "fudge-factor" scheme [77–79] was used. This involves calculating the full amplitude without the inclusion of the width for any off-shell propagators and multiplying the full amplitude, including non-resonant contributions, by

$$\frac{p^2 - M^2}{p^2 - M^2 + iM\Gamma} \tag{4.12}$$

for any propagator that can be on-shell, *i.e.* for which it is possible for $p^2 = M^2$ within the physically allowed phase space. This is the simplest approach that ensures the amplitude is gauge invariant [77], although it has the drawback that the non-resonant diagrams are affected. A more detailed discussion of the issue of gauge-invariance when including non-resonant diagrams can be found in [79].

For the ILC case, Fig. 4.3, the Madgraph result is shown for both the process including only the diagrams with a top quark line and also the process including all electroweak diagrams, resonant and non-resonant, excluding the Higgs. There is excellent agreement between our results and those performed with the full matrix element giving us confidence in our procedure.

For hadron colliders we must consider the rescaling since there will be many processes, not just those initiated by a vector boson, that will violate gauge invari-

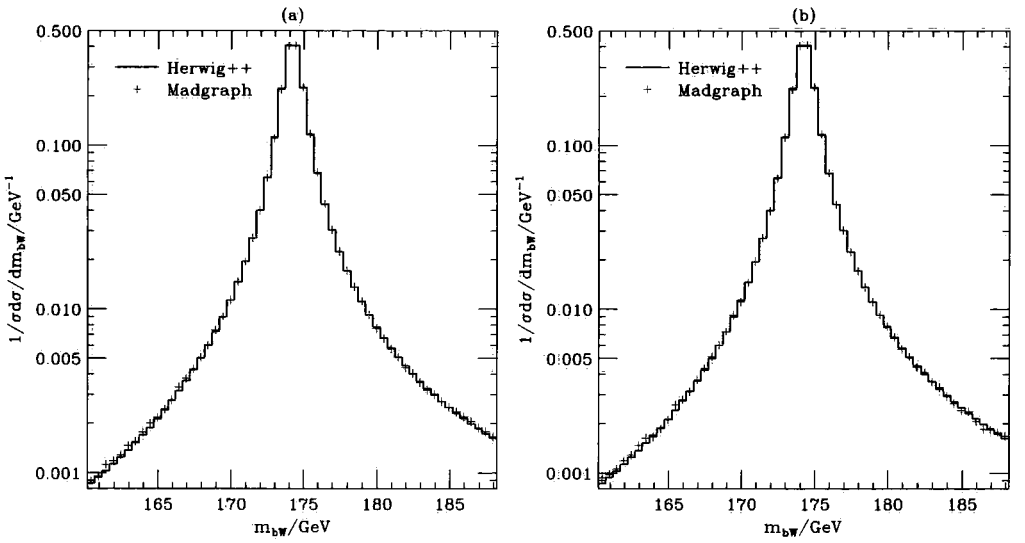

Figure 4.3: The line shape of the top quark for $m_t^{\text{pole}} = 174.20\,\text{GeV}$ and $\Gamma_t(m_t^{\text{pole}}) = 1.40\,\text{GeV}$ at the ILC with the results of **Herwig++** for $e^+e^- \to t\bar{t} \to b\bar{b}W^+W^-$ compared to the Madgraph calculation of $e^+e^- \to b\bar{b}W^+W^-$ with the Madgraph result including (a) all diagrams containing a top quark line and (b) all diagrams excluding those containing a Higgs boson. In both cases the **Herwig++** result uses our off-shell treatment while the Madgraph result includes all diagrams for the $2 \to 4$ scattering process, including the non-resonant contributions.

ance when we take the top quark off-shell. Here we will compare two choices for the momenta rescaling, first rescaling such that the masses have their on-shell value and second rescaling to the average value of the outgoing masses $(m_3 + m_4)/2$, where the momenta are rescaled so as to conserve $\hat{s}$ and θ in the centre-of-mass frame. The results for the Tevatron and LHC are shown in Fig. 4.4. The Tevatron results are in excellent agreement with the matrix element for both choices of rescaling and the LHC is in good agreement except for the tail where there is a small deviation. It is clear that either choice for the value of the rescaled mass gives good agreement with the matrix element but in the LHC case choosing to rescale to the average value of the outgoing masses gives slightly better agreement with the full calculation.

Figure 4.5 shows the mass distributions for a left-handed up squark in the

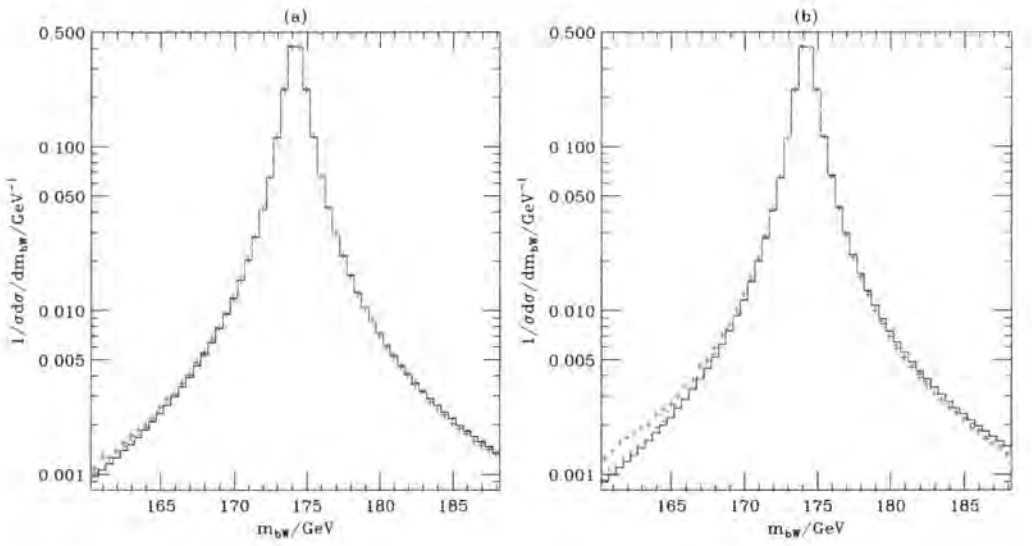

Figure 4.4: The line shape of the top quark for $m_t^{\text{pole}} = 174.20\,\text{GeV}$ and $\Gamma_t(m_t^{\text{pole}}) = 1.40\,\text{GeV}$ at (a) the Tevatron and (b) the LHC. The black line denotes the results from Herwig++ with the outgoing masses rescaled to their on-shell value, the blue dot-dash line denotes Herwig++ with the outgoing masses rescaled to their average value and the red crosses denote the Madgraph results. The Herwig++ results were generated using the $2 \to 2$ production process for $t\bar{t}$ followed by the three-body decay of the top quarks. The Madgraph results use the full matrix element for the production of $b\bar{b}W^+W^-$ to order $\alpha_S^2\alpha_W^2$, including all diagrams, both resonant and non-resonant diagrams, containing a top quark line.

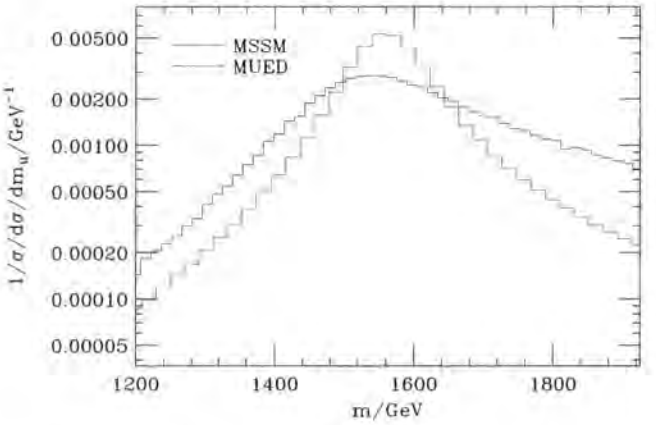

Figure 4.5: The lineshapes for the SUSY partner to the u-type doublet field and the level-1 KK partner to the u-type doublet field.

MSSM and the KK-partner of the doublet quark in the MUED model respectively. The mass spectrum for the MUED case is matched to the SUSY spec-

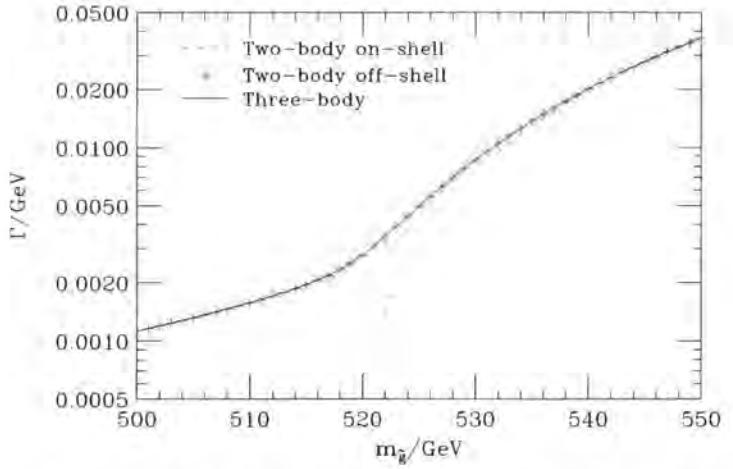

Figure 4.6: The partial width for the decay mode $\tilde{g} \to \bar{b}\tilde{b}_1 \to \tilde{\chi}_2^0 b$ in the MSSM.

trum at SPS point 2 [67] where $m_{\tilde{u}_L} = 1560.97\,\text{GeV}$, $\Gamma_{MSSM} = 70.22\,\text{GeV}$ and $\Gamma_{MUED} = 312.76\,\text{GeV}$. It should be noted that this example is at the extreme of where this method should be applied since, especially in the MUED case, the width is large and in general there could be sizeable non-resonant contributions.

4.2 Off-Shell Effects in Particle Decay

Many new physics models have spectra that result in long chains between the production of a resonance and a stable state. As mentioned previously the simplest approach in dealing with these chains is via a series of on-shell cascade decays. While this may be an appropriate approximation in some kinematic regions, in others, *i.e.* when the decaying particle is close to threshold, the effects from the off-shell propagator must be taken into account.

This can be achieved by including the weight factor from Eqn. (4.1) in the calculation of the partial width of a selected decay mode. For example, consider

the decay $\tilde{g} \to \bar{b}\tilde{b}_1 \to \tilde{\chi}_2^0 b\bar{b}$, the partial width is

$$\Gamma\left(\tilde{g} \to \tilde{\chi}_2^0 b\bar{b}\right) = \frac{1}{\pi}\int_{m_{\min}^2}^{m_{\max}^2} \mathrm{d}m^2 \frac{m\Gamma\left(\tilde{b}_1 \to \tilde{\chi}_2^0 b\right)}{\left(m^2 - M^2\right)^2 + m^2\Gamma(m)^2}\Gamma\left(\tilde{g} \to \bar{b}\tilde{b}_1\right), \qquad (4.13)$$

where the widths inside the integral are evaluated for the off-shell mass m. The limits on the integration are determined by the on-shell width and are set such that the maximum deviation from the pole mass of $\tilde{b}_1$ is 5Γ. As the intermediate particle is a scalar, the inclusion of the weight factor should give exact agreement with the full three-body calculation providing the integral is performed over the same phase space and the width is calculated in the same manner. Fig. 4.6 demonstrates this for SPS point 1a where the three-body phase-space is restricted to the same as the two-body case. The spectrum was produced using SPheno 2.2.3 [62] where $m_{\tilde{b}_1} = 515.27\,\mathrm{GeV}$, $\Gamma(m_{\tilde{b}_1}) = 3.83\,\mathrm{GeV}$ and $m_{\tilde{\chi}_2^0} = 180.58\,\mathrm{GeV}$. The mass of the b-quark is $m_b = 4.20\,\mathrm{GeV}$, which is the default value in Herwig++. The on-shell result is also included for reference and the agreement between the full matrix element calculation and our results show that the approximation is valid.

4.3 Examples

Here we present a range of processes in the MSSM and the MUED model demonstrating the consistency of the inclusion of off-shell effects in Herwig++. In the decay examples the comparison is always to the full three-body result.

4.3.1 Decay via an Off-Shell Fermion

A possible two-body decay of the $\tilde{t}_1$ squark in the MSSM is $\tilde{t}_1 \to \tilde{\chi}_1^0 t$, where if $m_{\tilde{t}_1} \approx m_{\tilde{\chi}_1^0} + m_t$ the effect of the width of the top quark must be considered.

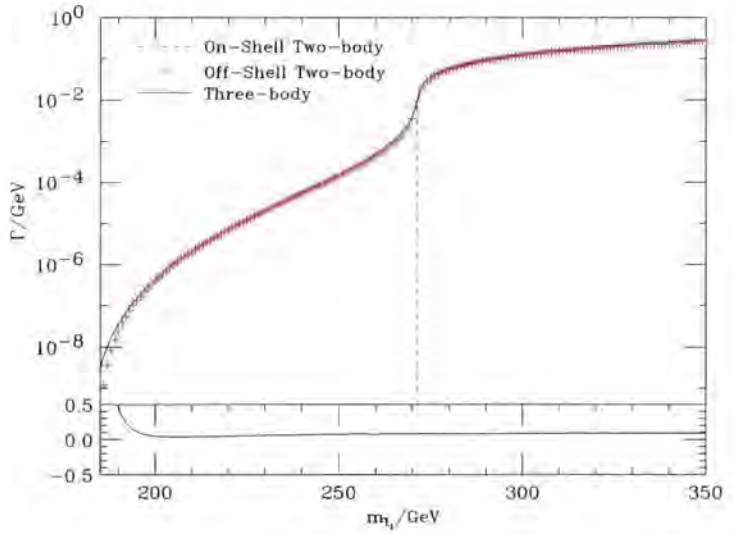

Figure 4.7: The partial width for the decay mode $\tilde{t}_1 \to \tilde{\chi}_1^0 t \to W^+ b \tilde{\chi}_1^0$. The lower panel gives the value of $(\Gamma_{\text{three}}/\Gamma_{\text{off}} - 1)$.

We choose the decay mode $\tilde{t}_1 \to \tilde{\chi}_1^0 t \to \tilde{\chi}_1^0 W^+ b$ at SPS point 1a [67] where $m_{\tilde{\chi}_1^0} = 97.04\,\text{GeV}$ with $m_t = 174.20\,\text{GeV}$, $m_W = 80.40\,\text{GeV}$ and $m_b = 4.20\,\text{GeV}$. The threshold values for the on-shell two- and three-body decays of the $\tilde{t}_1$ are 271.24 GeV and 181.64 GeV respectively. Figure 4.7 shows the partial width of the $\tilde{t}_1$ as a function of its mass for the three-body, two-body off-shell and two-body on-shell results.

Unlike the gluino decay example in Section 4.2 the $W^\pm$ boson, like the top quark, has a measured decay width and this should be treated properly. In the example shown in Fig. 4.7 the running width for the top quark is calculated from its full three-body matrix element to a b-quark and a pair of light fermions which includes the full effects of the $W^\pm$ width. The agreement between the two-body off-shell and three-body results shows that this is a valid approximation to use. Also, despite the extra factor of $(\not{p}+m)$ in the numerator of the fermion propagator, there is still good agreement between the full three-body result and the two-body result with weight factor even though the factor does not attempt to include this.

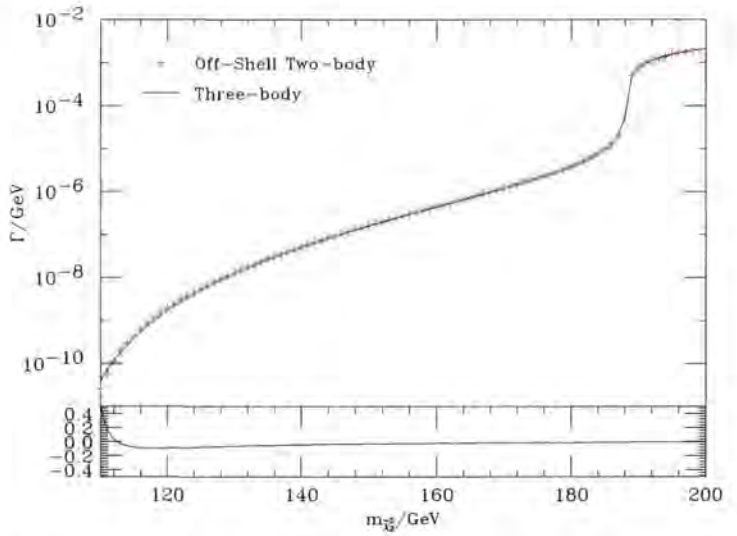

Figure 4.8: The partial width for $\tilde{\chi}_2^0 \to \tilde{\chi}_1^0 Z^0 \to b\bar{b}\tilde{\chi}_1^0$ in the MSSM. The lower panel gives the value of $(\Gamma_{\text{three}}/\Gamma_{\text{off}} - 1)$.

This is due to the numerator factor being largely responsible for propagating spin information rather than altering the kinematics.

4.3.2 Decay via an Off-Shell Gauge Boson

In the MSSM there is a coupling between the Z^0 boson and the gaugino sector allowing for a three-body decay of the second neutralino, via an intermediate Z^0 boson, to a pair of light fermions and the lightest neutralino. The presence of a spin-1 rather than a spin-0 particle alters the form of the partial width as the decay is now p-wave and not s-wave, as in Fig. 4.6. To illustrate that the weight formula works just as well in this situation we choose the decay chain $\tilde{\chi}_2^0 \to \tilde{\chi}_1^0 Z^0 \to \tilde{\chi}_1^0 b\bar{b}$ at SPS point 1a where $m_{\tilde{\chi}_1^0} = 97.04\,\text{GeV}$ with $M_{Z^0} = 91.19\,\text{GeV}$ and $m_b = 4.20\,\text{GeV}$.

Figure 4.8 shows the results for the above decay and demonstrates that there is good agreement between the full three-body result and the two-body approxi-

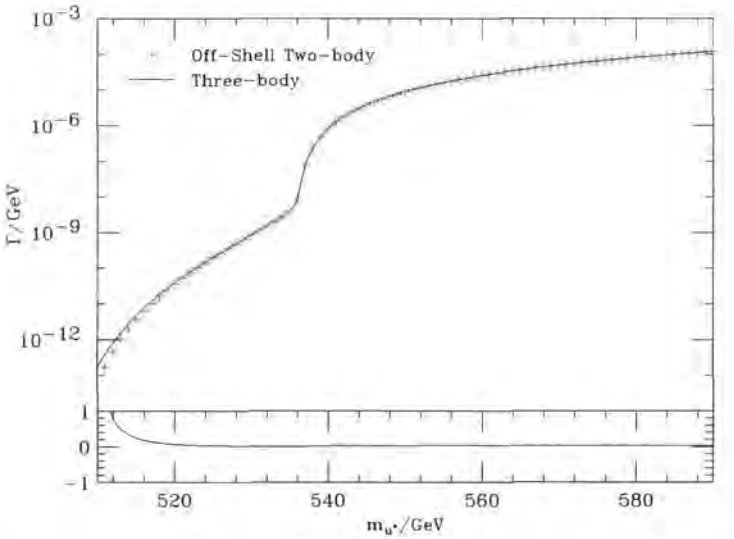

Figure 4.9: The partial width for $u^\bullet \to u\, e_1^{\circ -} e^+$ in the MUED model. The lower panel gives the value of $(\Gamma_{\text{three}}/\Gamma_{\text{off}} - 1)$.

mation for an intermediate vector particle. Another example of a possible p-wave decay is $u^\bullet \to u\, e_1^{\circ -} e^+$ in the MUED model where the intermediate particle is the level-1 KK-Z^0 boson. For parameter values $R^{-1} = 500\,\text{GeV}$ and $\Lambda R = 20$ the relevant masses are $M_{Z_1^0} = 535.81\,\text{GeV}$ and $M_{e_1^\circ} = 504.25\,\text{GeV}$. The partial width is shown in Fig. 4.9, again with both the three-body result and two-body via an off-shell Z_1^0.

4.4 Off-Shell Cross Sections

In the narrow width approximation, the cross section for a particular final state is computed by taking the on-shell production cross section to an intermediate resonance and multiplying by the branching fraction to the final state of interest. If the on-shell mass of the resonance is close the threshold for the decay into the final state, the narrow width approximation is invalid and one should calculate the full matrix element. As described and demonstrated above, we can include a

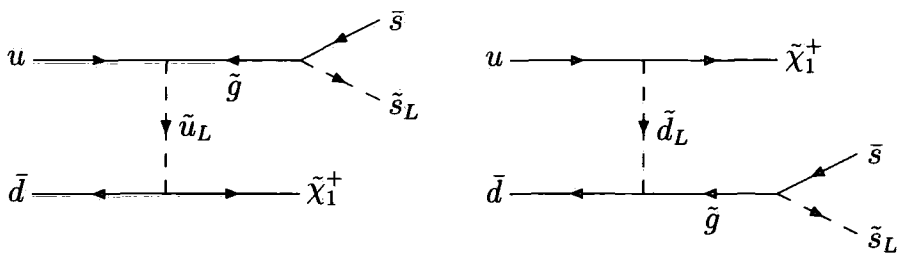

Figure 4.10: The diagrams contributing to the process $u\bar{d} \to \tilde{\chi}_1^+ \tilde{g}$ followed by the decay of the gluino to a strange quark and a left-handed strange squark.

weight factor in production and decay to simulate off-shell behaviour. In the case of calculating cross sections for specific processes, this amounts to including the effect of propagator widths in the Monte Carlo estimate of such a quantity. It is important to note, however, that a general purpose event generator, which starts from a $2 \to 2$ hard scattering and perturbatively decays the produced resonances, will, in general, not include non-resonant contributions. This is a fundamental limit of the approximations used to generate the events. Nevertheless, a good approximation can still be achieved providing one uses the simulations with care[2].

An example of a process that has no non-resonant contributions is the production of a strange squark via $u\bar{d} \to \tilde{\chi}_1^+ \tilde{g} \to \tilde{\chi}_1^+ \tilde{s}_L \bar{s}$, the diagrams for which are shown in Fig. 4.10. The results for the ratio of the off-shell to the on-shell cross section as a function of the strange squark mass are shown in Fig. 4.11 for SPS point 1a. The ratio is constant, with the off-shell result smaller due to the integration limits no longer being taken to infinity, until $m_{\tilde{s}_L} \approx 0.8 m_{\tilde{g}}$ where we are in the threshold region for the decay of the gluino. The sudden steep rise as the mass ratio approaches unity is due to the on-shell cross section going to zero at threshold.

There is a counterpart process to that in Fig. 4.10 for MUED, where the $\tilde{\chi}_1^+$ is

[2]In some specific cases non-resonant effects can be modelled by using a modified form of Eqn. (4.1), for example the Higgs lineshape [75].

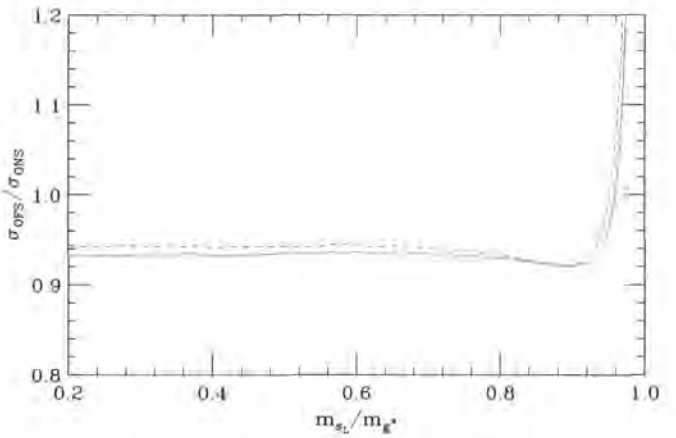

Figure 4.11: The ratio of the off-shell and on-shell cross section for the process $u\bar{d} \to \tilde{\chi}_1^+ \tilde{s}_L \bar{s}$ (red line) and its counterpart in the MUED model (blue dashes).

replaced by the W_1^+ boson, the $\tilde{g}$ by the g_1 and $\tilde{s}_L$ by the $s_1^\bullet$. The ratio of the on-shell to the off-shell cross section for this process is also shown in Fig. 4.11 where the masses for the MUED particles have been matched to the SUSY spectrum to give a fair comparison. It is apparent here that the spins of the underlying model play only a small role in determining the value of this ratio as the results are similar and while the absolute values of the cross sections may differ greatly, taking the colour octet object off-shell affects only the kinematics.

4.5 Merging Two- and Three-Body Decays

In Section 4.3 we demonstrated the accuracy of including an off-shell weight factor by comparison with the full three-body matrix element for a variety of processes. For each process considered the width was plotted over the entire kinematic range, rather than restricting to the region where the decay would be applicable, to give a full comparison. In a real simulation there is a choice over which point we should change between using a two- and three-body decay of the particle. If both decays were treated on-shell the point would simply be the threshold of the two-body

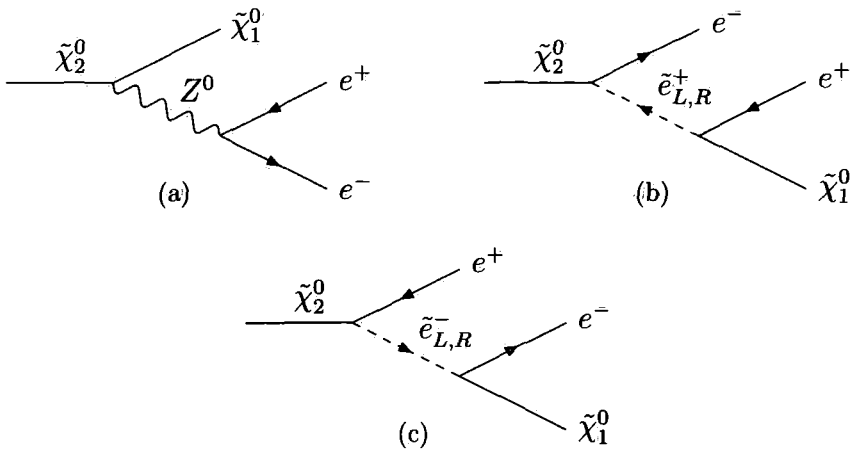

Figure 4.12: Feynman diagrams for the three-body decay $\tilde{\chi}_2^0 \to \tilde{\chi}_1^0 e^+ e^-$ with a (a) Z^0 boson intermediate, (b) left- and right-handed anti-selectron intermediate and (c) left- and right-handed selectron intermediate.

decay but when including of off-shell effects for the two-body decay, the choice is not so simple.

Here we use the three-body decay $\tilde{\chi}_2^0 \to \tilde{\chi}_1^0 e^+ e^-$ in the MSSM to study this effect. The full three-body decay is mediated by a Z^0 boson and both the left- and right-handed selectron, as shown in Fig. 4.12, giving an interference between the different channels. If the decay occurs as a series of cascades with a weight factor, these interference effects will be neglected. To judge the extent of the interference we compare the partial width for the decay via the full three-body matrix element and the three-body matrix element with the Z^0 diagram, Fig. 4.12(a), removed and performed as a cascade decay.

Figure 4.13 shows the results for a range of selectron masses, where both $\tilde{e}_L$ and $\tilde{e}_R$ are degenerate, with $M_{\tilde{\chi}_1^0} = 120.00\,\text{GeV}$ and $M_{Z^0} = 91.19\,\text{GeV}$. For a sufficiently large selectron mass there is good agreement between the two methods as there is only a small interference with the Z^0 boson diagram. However, as the mass is lowered so that the decay of the $\tilde{\chi}_2^0$ through the selectron mode becomes

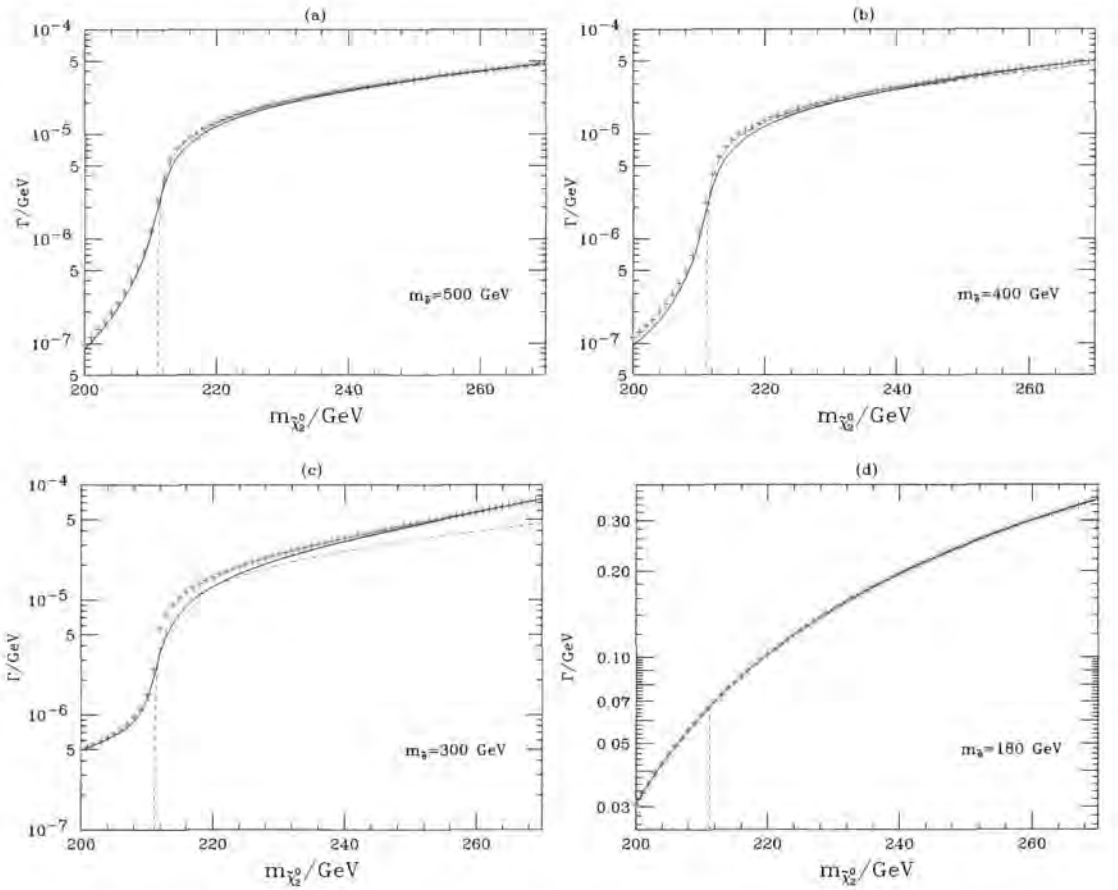

Figure 4.13: The partial width for the decay $\tilde{\chi}^0_2 \to \tilde{\chi}^0_1 e^+ e^-$ where the selectron masses are indicated on the plot. The solid line is the full three-body partial width and the red crosses are for the three-body decay with the Z^0 diagram removed plus $\Gamma(\tilde{\chi}^0_2 \to \tilde{\chi}^0_1 Z^0) \times BR(Z^0 \to e^+ e^-)$. The blue dashed line shows the two-body on-shell cascade.

closer to being on-shell, the interference effects, particularly just above the Z^0 threshold, become significant and the full three-body calculation is necessary in this region. For the final case, Fig. 4.13(d), where the selectron modes are on-shell for the whole range there is quite different behaviour. The partial width now smoothly passes over the Z^0 threshold and there is exact agreement with the full three-body result indicating that there is very little or no interference. Given these results it seems reasonable to use the threshold of the on-shell two-body decay as the point where the change from a three-body to a two-body decay with weight

factor occurs.

4.6 Summary

Incorporating the effects of finite widths into the simulation significantly improves the accuracy of the physics description, especially close to threshold. In BSM models, given our lack of knowledge of a particular mass spectrum, these effects could play an important role in many situations. For example, if a decay mode is close to threshold and also taggable at a collider, the naïve branching ratio expectation from the narrow width approximation could deviate significantly from the results with width effects included. This would cause problems when attempting to reconstruct theoretical parameters from experimental data.

Bearing this in mind we have demonstrated a model independent method for including these effects in a Monte Carlo event generator and compared our results using the Herwig++ event generator with the full three-body matrix elements for a range of processes in the MSSM and the MUED model. The importance of interference effects when considering the crossover between two- and three-body decays was also studied and it was found that the on-shell cut-off was an adequate point to switch between the two methods.

Chapter 5

Cascade Decays

'Welcome to the real world.'

— Morpheus, The Matrix

A common property of the new physics models introduced in Chapter 1 is the presence of a discrete symmetry, namely R-, KK- and T-parity. Since all of the new particles in each model are odd under the action of the relevant symmetry, they can only be pair-produced and the lightest particle in the spectrum is stable. This particle provides a natural termination point for decay chains which are initiated by the production of a particle from the new spectrum. In general these decay chains, so-called cascade decays, can be long and the spin correlation algorithm is ideally suited for studying such cascades. In this chapter we will use the method discussed in Chapter 3, along with the Feynman rules defined in Appendix D, to compare the invariant mass distributions of various combinations of particles along a decay chain with the counterpart chains in the other models. First we present the parton-level distributions for two types of decay chain, namely neutral and charged cascades. Finally, an analysis using a fast detector simulation is presented

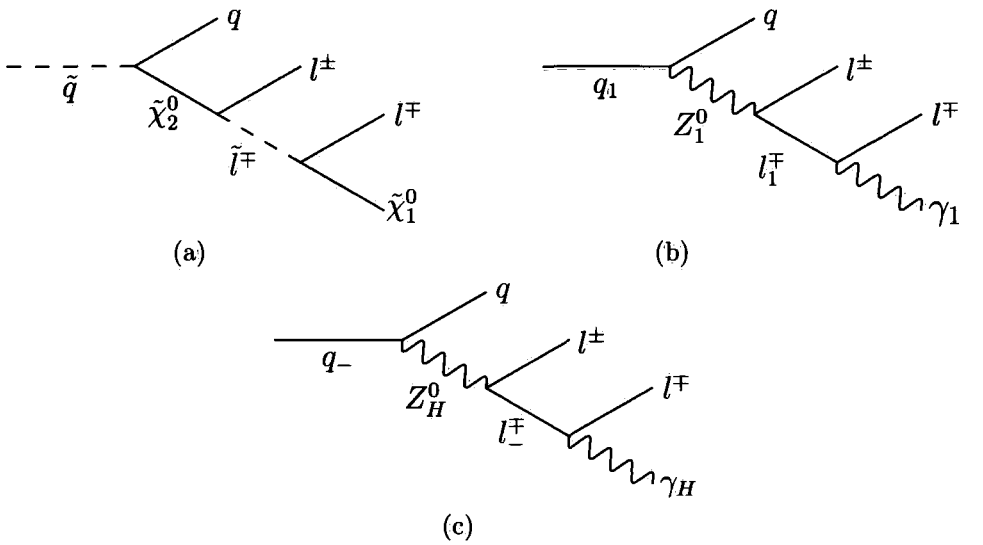

Figure 5.1: A neutral chain cascade decay in (a) the MSSM, (b) the MUED model and (c) the LHT. In the MSSM and the MUED model, these chains can also be initiated by the decay of the heavy partner of the gluon, assuming the mass spectrum will allow it.

with the aim of studying more realistic signals.

5.1 Parton Level

5.1.1 Neutral Cascades

We define a "neutral cascade" for each of the models being discussed as those shown in Fig. 5.1, where for our purposes the lepton is either an electron or a muon. At the parton level we can trace the origin of the quark and each of the leptons that emerge from the cascade and form invariant mass distributions of these particles. The distributions are highly sensitive to the helicity structure of the cascade and therefore act as a probe of the underlying physics. To illustrate the effects of the helicity structure of the cascades we match the mass spectra of the LHT and the MUED model with a parameter point, namely SPS 3, in the MSSM. The masses of the relevant particles are given in Table 5.1 and were produced using SPheno

MSSM	MUED	LHT	SPS 3
$\tilde{g}$	g_1	–	930.59
$\tilde{d}_L$	$d_1^\bullet$	d_-	863.90
$\tilde{u}_L$	$u_1^\bullet$	u_-	860.39
$\tilde{d}_R$	d_1°	–	827.70
$\tilde{u}_R$	u_1°	–	829.94
$\tilde{\chi}_2^0$	Z_1^0	Z_H^0	303.59
$\tilde{\chi}_2^\pm$	$W_1^\pm$	$W_H^\pm$	543.154
$\tilde{l}_L$	$l_1^\bullet$	l_-	288.51
$\tilde{l}_R$	l_1°	–	180.80
$\tilde{\chi}_1^0$	γ_1	γ_H	161.04

Table 5.1: The mass spectrum for the particles in the MSSM at parameter point SPS 3 with the counterpart states from the MUED model and the LHT also shown. A dash indicates that no partner of this type exists in that model. All values are in GeV.

2.2.3 [62].

The numerical distributions for the three models are compared to the analytical distributions, given in Refs. [55, 80], in Fig. 5.2. Each plot is normalised to unit area so that the distributions are only dependent on the helicity structure of the chain and not the exact couplings. Figure 5.2(a) shows the same behaviour as shown in Section 3.4.1 except that the lepton and anti-lepton curves have been interchanged. This is expected since the slepton is left-handed in Fig. 5.1(a), whereas in Section 3.4.1 we considered a right-handed slepton and therefore the opposite helicity projections are involved. Comparing Figs. 5.2(a) and 5.2(b) with Figs. 5.2(c) and 5.2(d), one can immediately see differences in the shapes of the invariant mass distributions which are a result of different underlying spin structures, *i.e.* *scalar* $\rightarrow$ *fermion* and *fermion* $\rightarrow$ *vector*. This is confirmed by considering the plots in Figs. 5.2(e) and 5.2(f) for the LHT where the spins of the particles in-

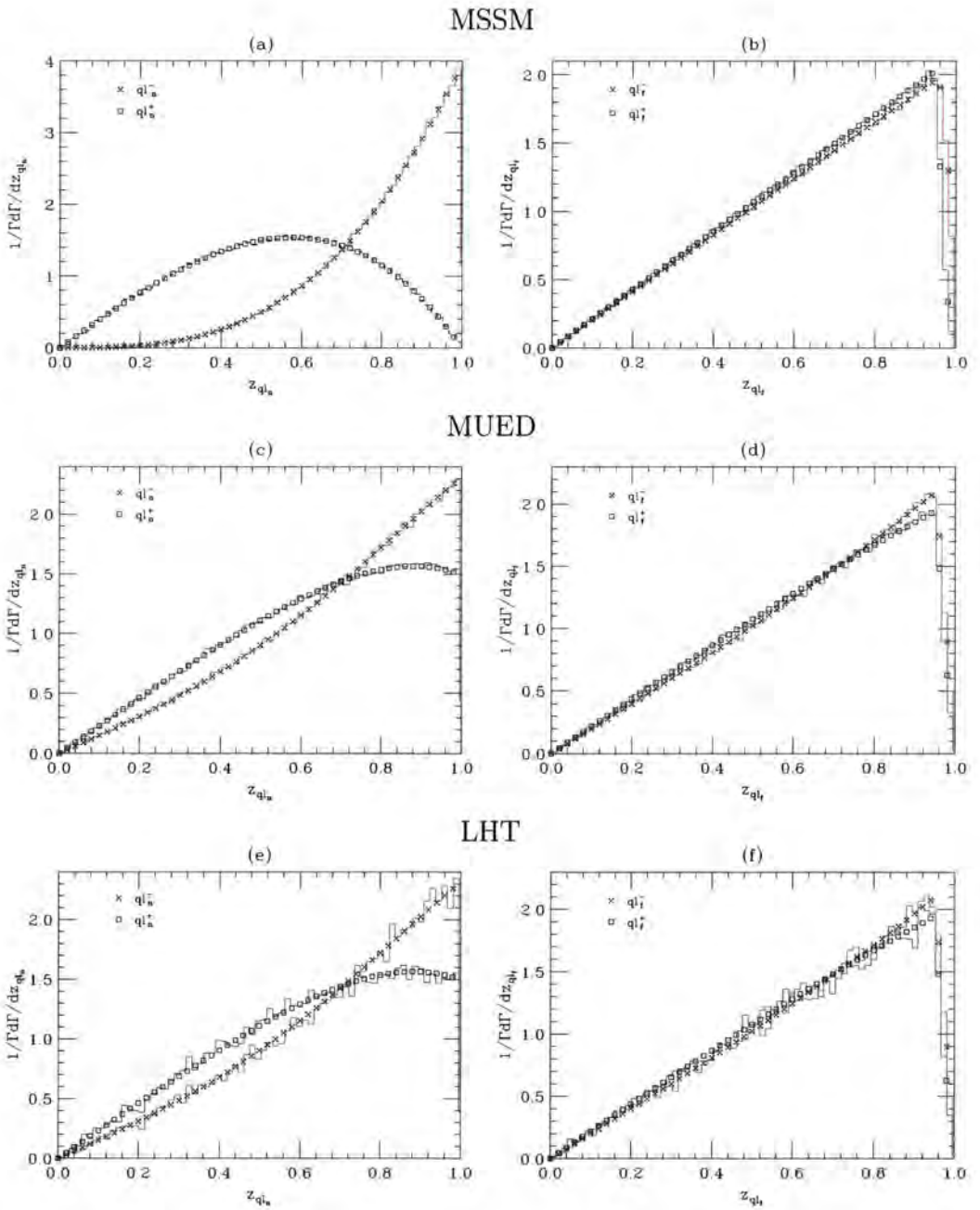

Figure 5.2: Invariant mass distributions for the near and far quark-lepton/quark-anti-lepton pairs for the cascade decays shown in Fig. 5.1, where $z = m_{ql}/(m_{ql})_{\max}$ and the name of the model is indicated above each pair of plots. The lines denote our numerical results.

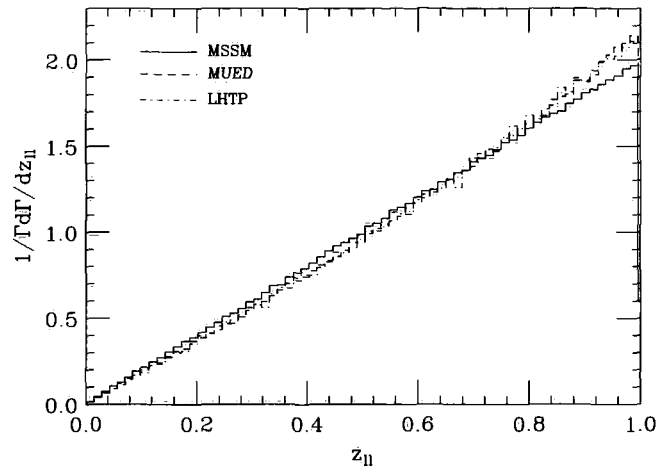

Figure 5.3: Numerical results for the lepton/anti-lepton invariant mass distributions in the three models discussed here, where $z = m_{ll}/(m_{ll})_{\max}$.

volved are the same as in the MUED model and therefore, given our normalisation, their shapes must be the same.

The effects of a non-zero spin can also be seen in the dilepton invariant mass distributions, shown in Fig. 5.3, where the MSSM distribution follows the phase-space result since the intermediate particle is a scalar. However, for the MUED model and the LHT, both distributions deviate slightly due to the intermediate particle having spin one.

5.1.2 Charged Cascades

The cascades considered in the previous section all contained the partner to the Z^0 boson for that model. If the spectrum allows it, the initial quark partner will also decay via a charged intermediary, so-called "charged cascades", as shown in Fig. 5.4. The spin correlations depend on whether the decay proceeds through a W^+ or a W^- boson [81] and the numerical distributions, again compared to the

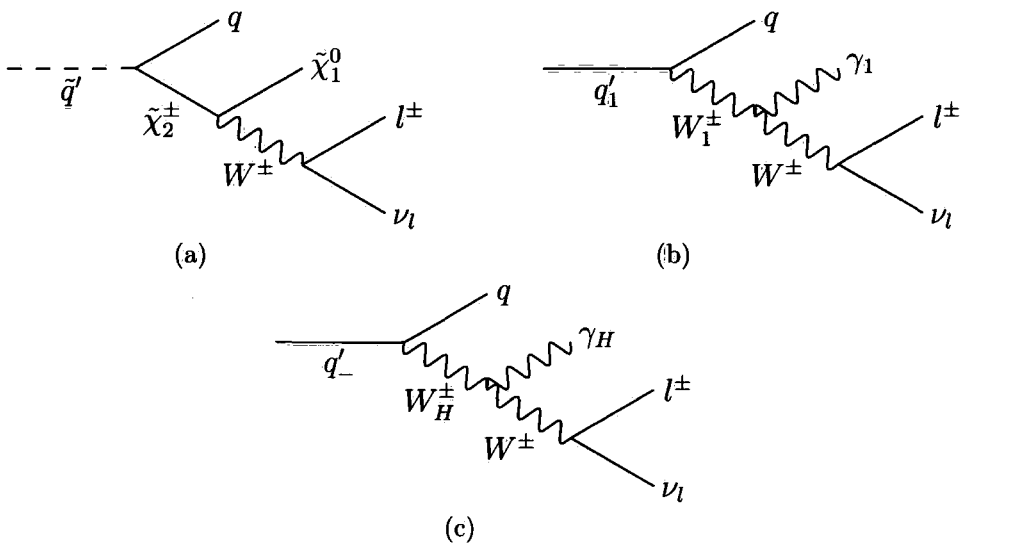

Figure 5.4: A charged chain cascade decay in (a) the MSSM, (b) the MUED model and (c) the LHT. In the MSSM and the MUED model, these chains can also be initiated by the decay of the heavy partner of the gluon if it is allowed by the mass spectrum.

analytical ones, are shown in Fig. 5.5 with

$$\hat{z}_{ql} = 2\left(m_C^2 - m_B^2\right)^{-1/2} m_{ql}, \tag{5.1}$$

where $C = \{\tilde{q}, q_1, q_-\}$ and $B = \{\tilde{\chi}_2^\pm, W_1^\pm, W_H^\pm\}$.

Comparing the results from the MSSM in Fig. 5.5(a) with those from the MUED model and the LHT in Figs. 5.5(b) and 5.5(c) shows that it is very difficult to distinguish between the two decay chains in the latter two models. This is due to the presence of a triple-vector-boson vertex in both the MUED model and the LHT, which is blind to the helicity of the decaying particle, *i.e.* it does not contain any projection operators. However, the MSSM decay still proceeds through three vertices that distinguish between left- and right-handed states, thereby giving a larger difference in the two distributions. Again, with the above normalisation, the distributions for the LHT are identical to the MUED model because the same helicity structures are involved.

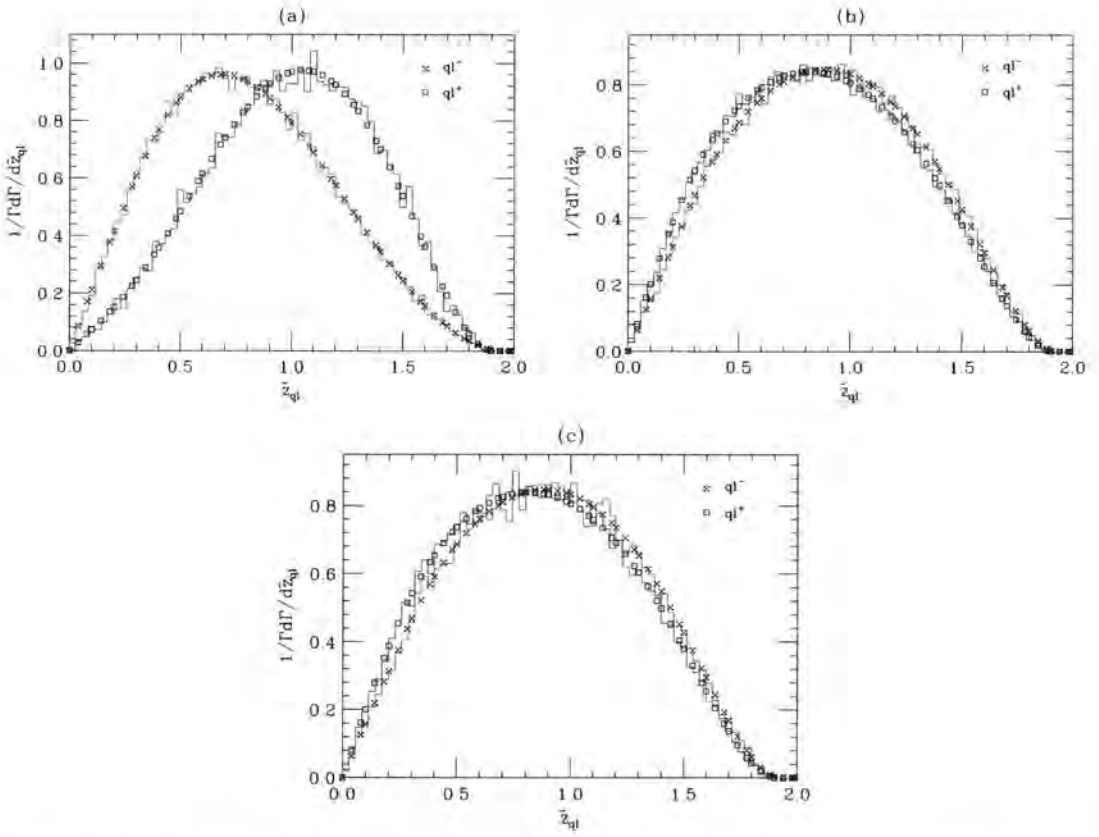

Figure 5.5: Invariant mass distributions for the quark-lepton/quark-anti-lepton pair in the decay chains shown in Fig. 5.4 for (a) the MSSM, (b) the MUED model and (c) the LHT at SPS 3. The rescaled mass $\hat{z}$ is defined in Eqn. (5.1) and the lines curves denote our numerical results.

In both of the above discussions the lepton was restricted to either an electron or a muon so that a massless approximation would suffice. However, if the lepton were a τ particle, there would be further decays to consider. Since the spin correlation algorithm can be applied to decay chains of an arbitrary length, we can now consider further distributions, similar to those presented in Section 3.4.3, with the decay products of the τ-lepton.

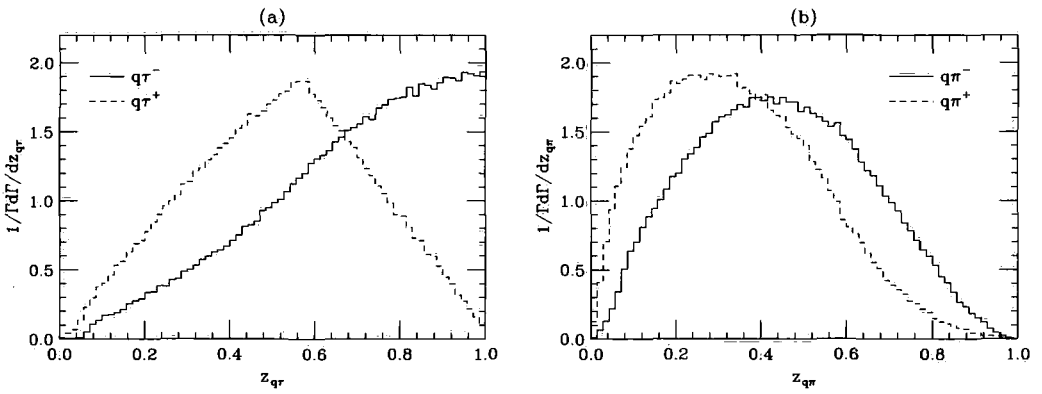

Figure 5.6: Normalised invariant mass distributions where $z = m_{ij}/(m_{ij})_{\max}$ for (a) $q\tau$ and (b) $q\pi$ pairs along the chain $\tilde{q}_L \to q\tilde{\chi}_2^0 \to q\tau_n^{\pm}\tilde{\tau}_1^{\mp} \to q\tau_f^{\pm}\tilde{\chi}_1^0$ in the MSSM with the τ decays restricted to $\tau \to \pi\nu_\tau$ only.

5.2 Tau Decays

In the above sections we considered separate distributions depending on whether the lepton was first or second in the cascade. In reality it would not be possible to determine this information, therefore the leptons would be paired with the quark and shown in the same histogram. Here we present similar distributions involving a quark and τ-lepton to those shown above but we do not attempt to locate the exact origin of each lepton. In addition, we present the distributions involving a π meson from the decay $\tau \to \pi\nu_\tau$.

The MSSM and MUED results, shown in Figs. 5.6 and 5.7, have already been discussed in Section 3.4.3 but are given here for the mass spectrum at SPS 3 for clarity. It is apparent from comparing Fig. 5.6 to Figs. 5.7 and 5.8 that the spin correlation effects are most notable in the MSSM where there is a greater difference between the distributions involving a τ^+ and a τ^-. This is due to the initial scalar particle restricting the form of the $ql_n^{\pm}$ distributions so as to conserve angular momentum and therefore cause a greater difference when the ql_n and ql_f plots are combined.

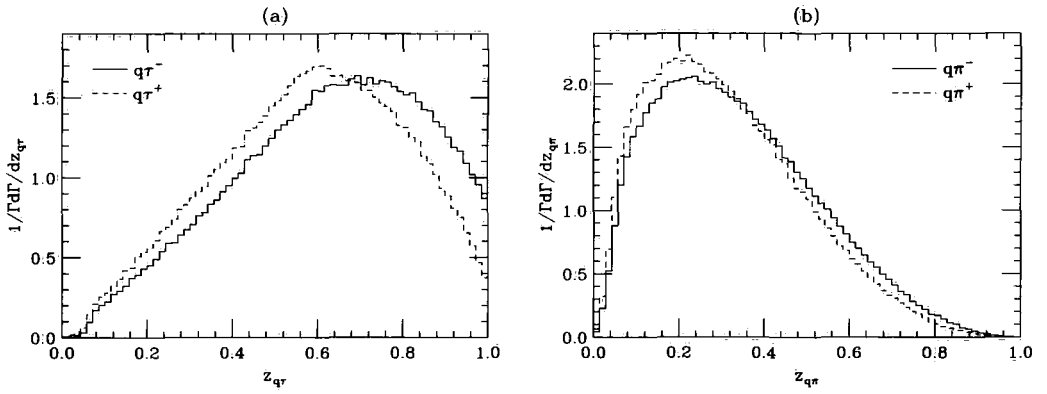

Figure 5.7: Normalised invariant mass distributions where $z = m_{ij}/(m_{ij})_{\max}$ for (a) $q\tau$ and (b) $q\pi$ pairs along the chain $q^\bullet \to qZ_1^0 \to q\tau_n^\pm \tau_1^{\bullet\mp} \to q\tau_f^\mp \gamma_1$ in the MUED model with the τ decays restricted to $\tau \to \pi\nu_\tau$ only.

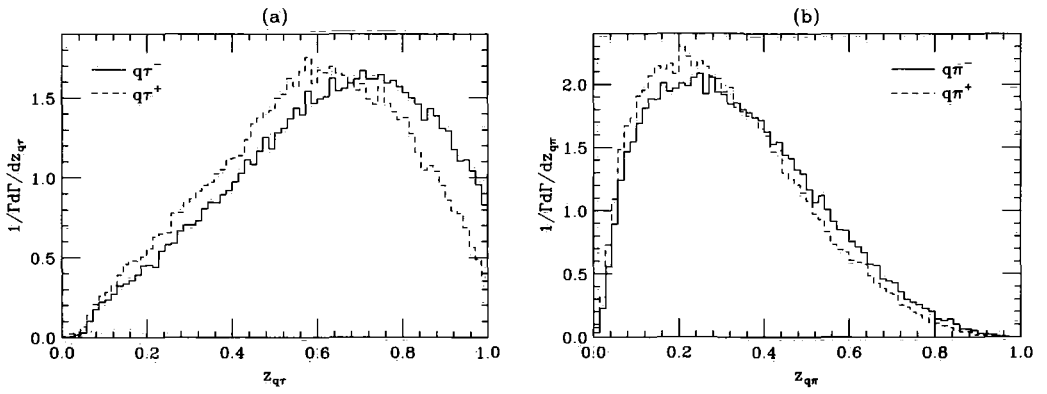

Figure 5.8: Normalised invariant mass distributions where $z = m_{ij}/(m_{ij})_{\max}$ for (a) $q\tau$ and (b) $q\pi$ pairs along the chain $q_- \to qZ_H^0 \to q\tau_n^\pm \tau_-^\mp \to q\tau_f^\mp \gamma_H$ in the LHT with the τ decays restricted to $\tau \to \pi\nu_\tau$ only.

Figure 5.9 shows the $\tau\tau$ and $\pi\pi$ mass distributions for the three models under discussion. The $\tau\tau$ plot for the MSSM has the expected phase-space form, while the MUED model and the LHT results show a similar deviation as before. However, the dilepton result for the MUED model is in contrast to that shown in Fig. 3.15, where there was no deviation from phase space, confirming that the spin correlations in the dilepton invariant mass distributions are sensitive to the mass spectrum. The distributions for the $\pi\pi$ invariant mass, Fig. 5.9(b), show significant differences depending upon whether the underlying spin structure is that of

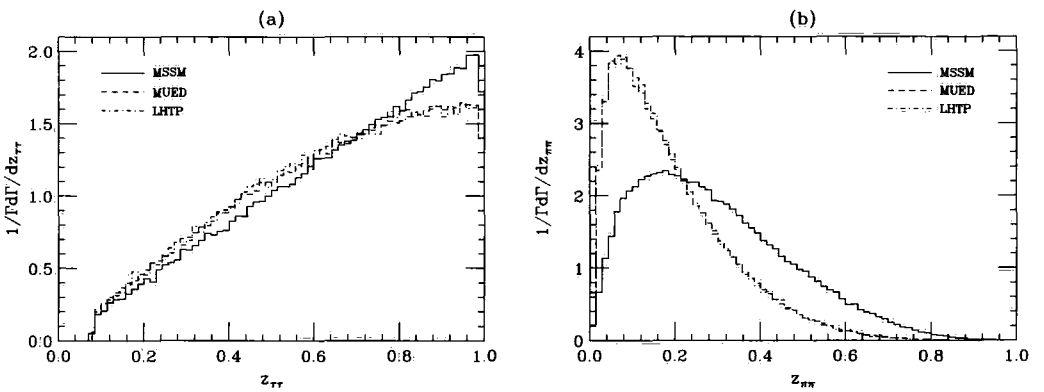

Figure 5.9: Normalised invariant mass distributions for $\tau\tau$ and $\pi\pi$ pairs in neutral cascade decays involving a τ lepton for the MSSM, the MUED model and the LHT.

the MSSM or the MUED model.

While here we have not attempted to determine the exact origin of the taus and pions in the decay chain, we have still both exactly identified the quark from the initial decay and precisely determined the momentum of each of the particles in the decay chain. In a real experiment however, this is impossible since free quarks cannot be detected and resolution effects mean that measurements of energy and momentum cannot be 100% accurate.

5.3 Fast Detector Simulation

We can approximate the effects discussed above using so-called fast detector simulation packages, which take the output of an event generator and attempt to model the interactions of the particles with a detector. We choose to use the AcerDet [41] package as this is the simplest to interface with Herwig++. After running the fast detector simulation, we are no longer able to isolate single quarks and the output gives lists of jets and leptons with their associated momenta along with data describing the missing transverse energy in the event. Both the lepton's flavour and

MSSM	MUED	LHT	SPS 9
$\tilde{g}$	g_1	–	1152.61
$\tilde{d}_L$	$d_1^\bullet$	d_-	1279.81
$\tilde{u}_L$	$u_1^\bullet$	u_-	1277.51
$\tilde{d}_R$	d_1°	–	1292.20
$\tilde{u}_R$	u_1°	–	1282.82
$\tilde{\chi}_2^0$	Z_1^0	Z_H^0	548.84
$\tilde{\chi}_2^\pm$	$W_1^\pm$	$W_H^\pm$	1020.94
$\tilde{l}_L$	$l_1^\bullet$	l_-	387.45
$\tilde{l}_R$	l_1°	–	374.95
$\tilde{\chi}_1^0$	γ_1	γ_H	197.34

Table 5.2: The mass spectrum for the particles in the MSSM at parameter point SPS 9 with the counterpart states from the MUED model and the LHT also shown. A dash indicates that no partner of this type exists in that model. All values are in GeV.

charge can be distinguished so that we are able to perform an analysis similar to those above. In addition to presenting the distributions for SPS 3, we also compare this with a different mass spectrum, SPS 9, which is shown in Table 5.2.

In order to try and observe the behaviour shown previously we must define cuts and selection criteria to discard the events that we assume do not contain a decay chain of the required type. First we will analyse the neutral cascades, shown in Fig. 5.1, with one set of cuts and then the charged chains, shown in Fig. 5.4, with a different set.

Neutral Cascades

For this analysis we require the following:

- exactly two leptons of opposite sign, either electron or muon, each with a

$p_T > 10\,\text{GeV}$;

- a total missing transverse momentum, $\not{p}_T$, greater than 100 GeV;
- a minimum of 4 jets, where the 4 highest p_T jets have a $p_T > 50\,\text{GeV}$;
- an effective mass $M_{\text{eff}} = \not{p}_T + \sum_{i=1}^{4} p_{Ti}^{\text{jet}} > 400\,\text{GeV}$;
- $m_{jl} < (m_{ql})_{\text{max}}$, where the jet used to form the invariant mass is the jet which forms $(m_{jll})_{\text{min}}$;
- $m_{ll} < (m_{ll})_{\text{max}}$;

where $(m_{ql})_{\text{max}}$ and $(m_{ll})_{\text{max}}$ are the parton-level quantities. When considering the jet-lepton invariant mass distributions, rather than show the individual lepton and anti-lepton plots it is more instructive to use a quantity called the asymmetry, defined as

$$A^{\pm} = \frac{dP/dm_{jl^+} - dP/dm_{jl^-}}{dP/dm_{jl^+} + dP/dm_{jl^-}}, \tag{5.2}$$

where $dP/dm_{jl^{\pm}}$ denotes the invariant mass distribution with respect to either an anti-lepton or a lepton. Our results for the asymmetry at both mass points are shown in Fig. 5.10, where in both the MSSM and MUED model, the production of the heavy colour octet state and both left- and right-handed quark partners was included. These plots demonstrate the dependence of this quantity on the mass spectrum since for SPS 9, Fig. 5.10(b), there is a much greater asymmetry in both the MSSM and MUED model.

The cuts defined above do not require the two leptons in the final state to be of the same flavour, only of the opposite charge. This was deliberate so that the events containing two different flavour leptons could be used to model background events where the leptons are uncorrelated. By subtracting the distribution containing only opposite flavour leptons from that containing all dilepton pairs we can achieve

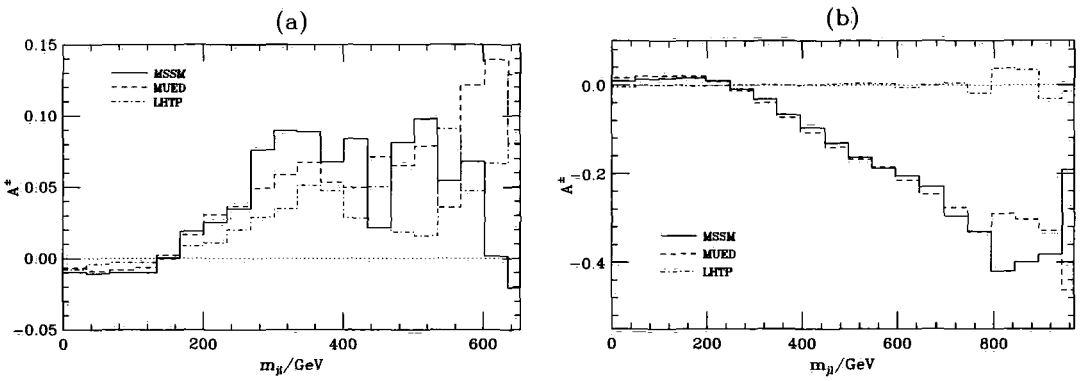

Figure 5.10: The jet-lepton asymmetry obtained using the first set of cuts defined in the text for the mass spectrum at (a) SPS 3 and (b) SPS 9.

a better approximation of the required distribution. The main background events will come from other processes in each of the three models, as Standard Model background should be minimised with the above set of cuts. For example, in SUSY there will be decays to other types of neutralino with different masses that will skew the distributions.

The results, after the application of this subtraction procedure, are shown in Fig. 5.11 for the three models considered here. For SPS 3, Fig. 5.11(a), all three models approximate to the phase-space result whereas there is slight deviation from this form at SPS 9, Fig. 5.11(b). Given this fact and the small amount of asymmetry seen in the jet-lepton distributions shown in Fig. 5.10(a), it is logical to conclude that for the mass spectrum at SPS 3 the relative numbers of different production mechanisms and decays has the net effect of cancel the spin correlations and very little difference between each model can be seen. The mass spectrum at SPS 9 would seem to give more hope of discriminating between the models but even here the differences are still quite small[1].

[1]The peak in Fig. 5.11(b) for the LHT is at the lightest CP-even Higgs boson mass $\approx$ 116 GeV. It appears here because there is a coupling between the heavy Z^0 boson and the h^0 which gives a large enough rate to be detectable. It does not, however, affect the conclusions drawn here.

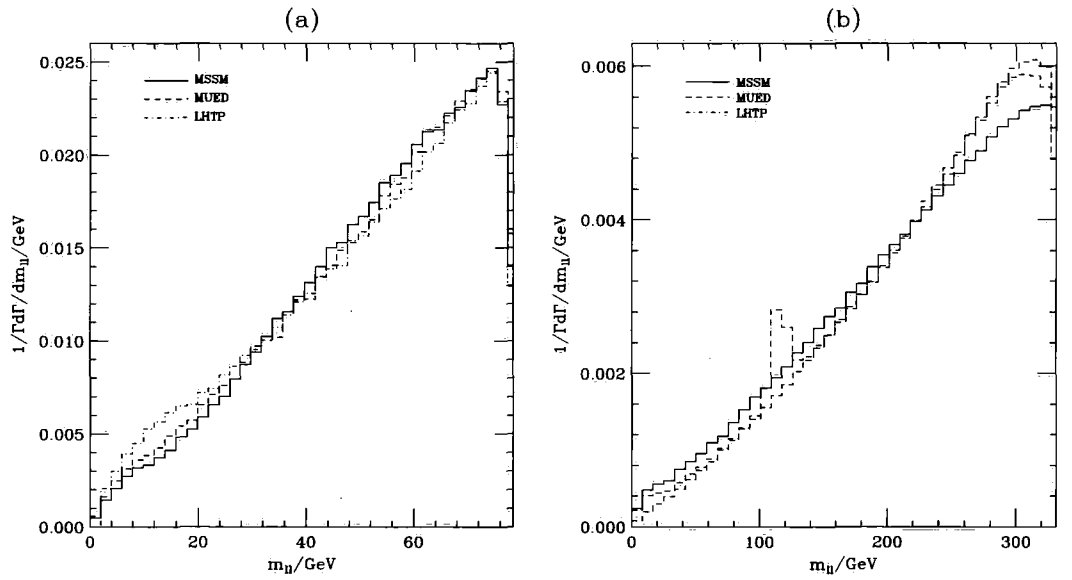

Figure 5.11: The dilepton invariant mass distributions obtained using the first set of cuts defined in the text for the mass spectrum at (a) SPS 3 and (b) SPS 9.

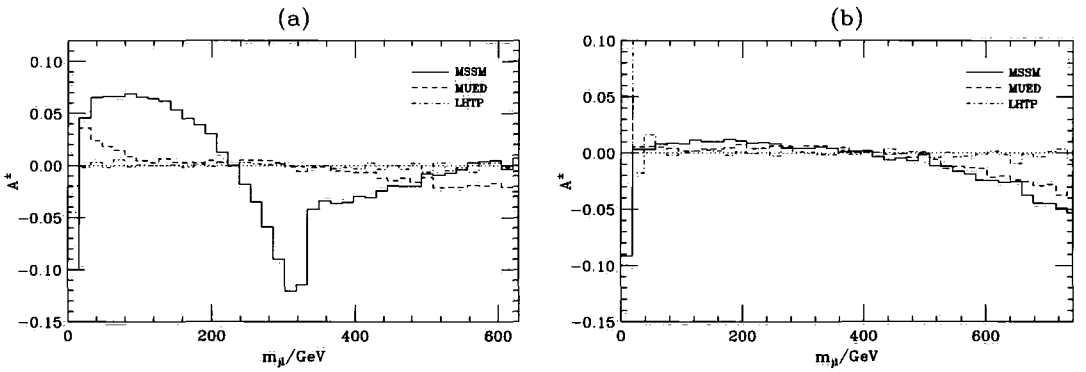

Figure 5.12: The jet-lepton asymmetry obtained using the second set of cuts defined in the text for the mass spectrum at (a) SPS 3 and (b) SPS 9.

Charged Cascades

For this analysis we require the following:

- a single lepton with a $p_T > 10$ GeV;
- a total missing transverse momentum, $\not{p}_T$, greater than 200 GeV;
- a minimum of four jets, where the four highest p_T jets have a $p_T > 50$ GeV;

Model	Parameter Point	Cross Section (pb)
MSSM	SPS 3	2.39
	SPS 9	0.32
MUED	SPS 3	17.24
	SPS 9	2.76
LHT	SPS 3	0.17
	SPS 9	0.012

Table 5.3: Production cross sections for the MSSM, the MUED model and the LHT for both of the mass spectra considered here.

- an effective mass $M_{\text{eff}} = \not{p}_T + \sum_{i=1}^{4} p_{Ti}^{\text{jet}} > 500\,\text{GeV}$;
- $m_{jl} < \max(m_{ql})$, where the j is the highest-p_T jet.

As there is only a single lepton in the final state, the only quantity that can be analysed is the jet-lepton invariant mass, where again we use the asymmetry defined in Eqn. (5.2) to show the difference in the lepton and anti-lepton distributions. In contrast to the neutral cascade, the plots for SPS 3 in Fig. 5.12(a) show a bigger discrepancy between the MSSM, the MUED model and the LHT. However, upon moving to SPS 9, shown in Fig. 5.12(b), the differences are again negligible and it is difficult to distinguish between the three models. In particular, the LHT gives virtually zero asymmetry in this and the neutral cascade cuts. The main reason is due to the lack of a heavy partner for the gluon. In the MSSM and MUED model, subprocesses such as $ug \to \tilde{g}\tilde{q}$ and $ug \to g_1 q_1$ tend to dominate the production cross section due to the relative abundance of u-quarks in the proton [80]. This gives rise to slightly higher numbers of chains initiated by the partner of a quark rather an anti-quark, leading to an asymmetry. However, in the LHT each production mechanism gives a $f_- \bar{f}_-$ final state which go on to decay with opposite correlations, thereby destroying any asymmetry.

Model	Parameter Point	Set 1	Set 2	$N^1_{100\,\text{fb}^{-1}}$	$N^2_{100\,\text{fb}^{-1}}$
MSSM	SPS 3	0.08	0.38	18777	91451
	SPS 9	0.35	0.43	11050	13595
MUED	SPS 3	0.09	0.31	150715	527969
	SPS 9	0.42	0.35	116385	97451
LHT	SPS 3	0.12	0.52	1983	8252
	SPS 9	0.47	0.32	554	382

Table 5.4: Fraction of events passing the two sets of cuts defined in the text, along with the number of events after 100 fb^{-1} for set of cuts 1 and 2. The total number of events generated was 1×10^7.

Table 5.3 gives the cross sections generated by Herwig++ after running both of the above detector simulations. The values are consistently lower in all three models for the second mass spectrum at SPS point 9, which is to be expected as there is less phase space available due to the larger rest mass of each particle in the spectrum, see Table 5.2. The differences in the values of the cross sections for each model are due to both the helicity structures involved in each subprocess and also the type of subprocess that can be generated. As discussed above, processes such as $ug \to \tilde{g}\tilde{q}$ and $ug \to g_1 q_1$ will enhance the cross section in the MSSM and the MUED model whereas this type of process is absent in the LHT, thereby giving it a lower overall cross section in each case. We can see from Table 5.4 that a much smaller fraction of events survive the first set of cuts for the first mass spectrum in each model, which is most likely due to the lower masses producing jets that are too soft to satisfy the cut requirements. The second set of cuts does provide a larger event sample but as we have already discussed, the resulting asymmetry is still small due to abundance of cascades with both sets of correlations.

5.4 Summary

It is crucial that in future experiments at the LHC and any other collider, we are able to distinguish between different possible types of new physics. This will enable us to state with some confidence that the underlying physics in nature is due to a particular model. Here we have shown some of possibilities that can arise for the MSSM, the MUED model and the LHT, which all relate to the use of cascade decays in order to determine spin information. It is quite clear that to pin down a certain model we will need more information than the types of distribution presented here since there is very little discrimination between the three models that we have investigated.

The results presented in this chapter have shown that the method described in Chapter 3 is ideally suited to this kind of work since it allows the production of a wide variety of processes with a minimal amount of work when implementing a new model.

Chapter 6

Conclusions

'Life is infinitely stranger than anything which the mind of man could invent.'

— Sherlock Holmes, 'A Case of Identity'

Throughout this thesis we have argued that the simulation of new physics scenarios should be as all encompassing as possible, given the lack of data concerning physics at the TeV scale. The advent of the LHC will give us access to this scale for the first time and it is important that we are able to study a wide variety of models of new physics so that we can attempt to establish the true underlying physics. In this thesis we have motivated three minimal models of new physics that each attempt to address the problems with the Standard Model in different ways, namely the Minimal Supersymmetric Standard Model, Minimal Universal Extra Dimensions model and the Littlest Higgs model with T-parity.

A common feature of most BSM scenarios, including those discussed here, is the addition of a new particle spectrum that is expected to be produced at a collider with sufficient energy. To study the signals from the new particle spectrum most effectively requires implementing each model in a Monte Carlo event generator.

However, given the potentially large number of production and decay processes that can occur, hard-coding each new model becomes a time consuming process. To alleviate these issues, we have designed a new framework that requires only a minimal amount of work to include a model of new physics in to an event generator, namely Herwig++. Our new approach does not compromise on the simulation of the underlying physics as we include a state-of-the-art simulation of spin correlation and off-shell effects, so that effective comparisons between different models can be made. While implementing our method to incorporate off-shell effects in to the simulation we studied the effects of particle widths on various production and decay processes in the MSSM and the MUED model. It was found that they can play a significant role in the calculation of partial widths and cross sections when these processes occur close to threshold. Given that we do not have a measured mass spectrum, it is vital that these effects are included in studies since if a real mass spectrum possessed a high degree of degeneracy, many processes would be close to threshold and a naïve study may misinterpret data.

Our final study used the general method already described to compare and contrast the invariant mass distributions of cascade decays in the three different models discussed. It was found that the Littlest Higgs model with T-parity and the Minimal Universal Extra Dimensions model are very similar due to the presence of the same helicity structures in the decay chains. A simulation incorporating a minimal set of effects from a detector was also performed and it was found that, mostly due to the presence of cascades with opposite correlations, it would be difficult to distinguish the different behaviour predicted by each model under real world conditions.

We have produced the state-of-the-art event generator for the simulation of BSM physics including, for the first time, a generic framework for the treatment of

off-shell effects. In addition, the Minimal Universal Extra Dimensions model and Littlest Higgs model with T-parity have been simulated with full spin correlations throughout production and decay. For the future we anticipate this approach will be used to implement other models of new physics, for example the Next-to-Minimal Supersymmetric Standard Model and the general Little Higgs model and hope that more extensive studies in comparing different models can be performed.

In conclusion, our framework combines the state-of-the art physics simulation of BSM physics in an event generator with the ability to easily add new models and will allow easy comparison of the predictions of many models with data at the LHC.

Appendix A

Kaluza-Klein Masses

As discussed in Section 1.2.2, the masses of the KK excitations are approximately degenerate at each level if loop effects are ignored. Here we present the corrections to each of the propagators from the bulk and boundary terms.

The bulk corrections are well-behaved and depend simply on the compactification scale R such that [82]

$$\delta_1(m_{B_j}^2) = -\frac{39}{2}\frac{e^2\zeta(3)}{16\pi^4\cos^2\theta_W}\frac{1}{R^2}, \tag{A.1a}$$

$$\delta_1(m_{W_j}^2) = -\frac{5}{2}\frac{e^2\zeta(3)}{16\pi^4\sin^2\theta_W}\frac{1}{R^2}, \tag{A.1b}$$

$$\delta_1(m_{g_j}^2) = -\frac{3}{2}\frac{g_s^2\zeta(3)}{16\pi^4}\frac{1}{R^2}, \tag{A.1c}$$

$$\delta_1(m_{f_j}) = \delta(m_{H_j}^2) = 0, \tag{A.1d}$$

where $\zeta(3) \approx 1.2020\ldots$ and the couplings e and g_s are evaluated at the compactification scale.

The boundary terms are more complex as they are divergent and require renormalization where the assumption is that the boundary kinetic terms vanish at a

cut-off scale Λ, which becomes another parameter in the theory. This can be thought of as parameter that conceals our naïvety about the UV behaviour of the theory in the same way that the soft supersymmetric breaking terms hide our ignorance of a supersymmetry breaking mechanism. The boundary bosonic corrections are given by [82]

$$\delta_2(m^2_{B_j}) = -\frac{1}{3}\left(\frac{j}{R}\right)^2 \frac{e^2}{16\pi^2\cos^2\theta_W}\ln\left(\frac{\Lambda R}{j}\right), \tag{A.2a}$$

$$\delta_2(m^2_{W_j}) = \frac{15}{2}\left(\frac{j}{R}\right)^2 \frac{e^2}{16\pi^2\sin^2\theta_W}\ln\left(\frac{\Lambda R}{j}\right), \tag{A.2b}$$

$$\delta_2(m^2_{g_j}) = \frac{23}{2}\left(\frac{j}{R}\right)^2 \frac{g_s^2}{16\pi^2}\ln\left(\frac{\Lambda R}{j}\right), \tag{A.2c}$$

$$\delta_2(m^2_{H_j}) = \left(\frac{j}{R}\right)^2 \left(\frac{3e^2}{2}\left(\frac{1}{\sin^2\theta_W} + \frac{1}{2\cos^2\theta_W} - \lambda_H\right)\right)\frac{1}{16\pi^2}\ln\left(\frac{\Lambda R}{j}\right) + \bar{m}^2_H, \tag{A.2d}$$

where λ_H is the quartic coupling of the Higgs field, $\bar{m}^2_H$ is the mass of the Higgs at the boundary and is usual taken to be zero. The mass eigenstates for the level-1 electroweak gauge bosons γ_1 and Z_1 arise from diagonalising their mass matrix, which in the B_1, W_1^3 basis is given by [22]

$$\begin{pmatrix} R^{-2} + \delta_{B_1} + \frac{1}{4}g'^2v^2 & \frac{1}{4}g'gv^2 \\ \frac{1}{4}g'gv^2 & R^{-2} + \delta_{W_1} + \frac{1}{4}g^2v^2 \end{pmatrix}, \tag{A.3}$$

where g' and g are the $U(1)$ and $SU(2)$ couplings respectively, v is the vacuum expectation value of the Standard Model Higgs field and $\delta_{B_1}, \delta_{W_1}$ are the sum of the two corrections factors given above. The masses are then

$$m^2_{Z_1,\gamma_1} = \frac{1}{2}\left[(2R^{-2} + m_Z^2 + \delta_{B_1} + \delta_{W_1}) \pm \sqrt{(\delta_{B_1} - \delta_{W_1} - 2m_W^2 + m_Z^2)^2 + 4m_W^2(m_Z^2 - m_W^2)}\right], \tag{A.4}$$

where $m_{W,Z}$ are the masses of the Standard Model $W^{\pm}$ and Z^0 bosons respectively.

The corrections to the fermion modes have a similar form and are given by [82]

$$\delta_2 m_{Q_j} = \frac{j}{8\pi^2 R}\left(3g_s^2 + \frac{27e^2}{16\sin^2\theta_W} + \frac{e^2}{16\cos^2\theta_W}\right)\ln\left(\frac{\Lambda R}{j}\right), \quad \text{(A.5a)}$$

$$\delta_2 m_{u_j} = \frac{j}{8\pi^2 R}\left(3g_s^2 + \frac{e^2}{\cos^2\theta_W}\right)\ln\left(\frac{\Lambda R}{j}\right), \quad \text{(A.5b)}$$

$$\delta_2 m_{d_j} = \frac{j}{8\pi^2 R}\left(3g_s^2 + \frac{e^2}{4\cos^2\theta_W}\right)\ln\left(\frac{\Lambda R}{j}\right), \quad \text{(A.5c)}$$

$$\delta_2 m_{L_j} = \frac{j}{8\pi^2 R}\left(\frac{27e^2}{16\sin^2\theta_W} + \frac{9e^2}{16\cos^2\theta_W}\right)\ln\left(\frac{\Lambda R}{j}\right), \quad \text{(A.5d)}$$

$$\delta_2 m_{e_j} = \frac{j}{8\pi^2 R}\frac{9e^2}{4\cos^2\theta_W}\ln\left(\frac{\Lambda R}{j}\right), \quad \text{(A.5e)}$$

with the third generation doublet and singlet quarks receiving addition contributions due to their large Yukawa coupling g_t,

$$\delta_2 m_{Q_{3j}} = -\frac{3j}{32\pi^2 R}g_t^2\ln\left(\frac{\Lambda R}{j}\right), \quad \text{(A.6a)}$$

$$\delta_2 m_{t_j} = -\frac{3j}{16\pi^2 R}g_t^2\ln\left(\frac{\Lambda R}{j}\right). \quad \text{(A.6b)}$$

Using these corrections, the masses of the jth level KK-mode are given by [82]

$$m_j^2 = \begin{cases} m_0^2 + \left(\frac{j}{R}\right)^2 + \delta_1(m^2) + \delta_2(m^2), \\ m_0^2 + \left(\frac{j}{R} + \delta_1(m) + \delta_2(m)\right)^2, \end{cases} \quad \text{(A.7)}$$

for the spin-1 bosons and spin-1/2 fermions respectively, while the KK-Higgs masses are given by

$$m_{H_j^0}^2 = m_{h^0}^2 + (j/R)^2 + \delta_1(m_{H_j}^2) + \delta_2(m_{H_j}^2), \quad \text{(A.8a)}$$

$$m_{A_j^0}^2 = m_Z^2 + (j/R)^2 + \delta_1(m_{H_j}^2) + \delta_2(m_{H_j}^2), \quad \text{(A.8b)}$$

$$m_{H_j^{\pm}}^2 = m_W^2 + (j/R)^2 + \delta_1(m_{H_j}^2) + \delta_2(m_{H_j}^2). \quad \text{(A.8c)}$$

Appendix B

Helicity Calculations

B.1 Conventions

To numerically evaluate the matrix elements using the HELAS formalism we need a specific representation for the Dirac matrices. Two options are available in Herwig++, the conventional low-energy choice used in, for example [83],

$$\gamma_i^{\text{HABER}} = \begin{pmatrix} 0 & \sigma_i \\ -\sigma_i & 0 \end{pmatrix}, \quad \gamma_0^{\text{HABER}} = \begin{pmatrix} 1 & 0 \\ 0 & -1 \end{pmatrix}, \quad \gamma_5^{\text{HABER}} = \begin{pmatrix} 0 & 1 \\ 1 & 0 \end{pmatrix}, \tag{B.1}$$

and the original choice of HELAS which is more appropriate at high energies

$$\gamma_i^{\text{HELAS}} = \begin{pmatrix} 0 & \sigma_i \\ -\sigma_i & 0 \end{pmatrix}, \quad \gamma_0^{\text{HELAS}} = \begin{pmatrix} 0 & 1 \\ 1 & 0 \end{pmatrix}, \quad \gamma_5^{\text{HELAS}} = \begin{pmatrix} -1 & 0 \\ 0 & 1 \end{pmatrix}. \tag{B.2}$$

The two representations are related by the transformation

$$\psi_{\text{HELAS}} = S\psi_{\text{HABER}} \quad \text{where} \quad S = \frac{1}{\sqrt{2}} \begin{pmatrix} 1 & -1 \\ 1 & 1 \end{pmatrix}. \tag{B.3}$$

B.1.1 Wave Functions

For the spin correlation algorithm we need to store the basis states of the particles involved in an interaction. Here we give the form of the basis states for spin-0, -$\frac{1}{2}$, -$\frac{3}{2}$ and -2 fields.

Spin-0

The basis state is a complex number. For external particles it has the value 1, however it can assume different values if it is calculated from an internal line.

Spin-$\frac{1}{2}$

The basis state for a spin-$\frac{1}{2}$ fermion is either a spinor or a barred-spinor. The four-component spinors u and v[1] are calculated in terms of two-component spinors, as in [52]

$$\chi_+(p) = \frac{1}{\sqrt{2|\mathbf{p}|\,(|\mathbf{p}| + p_z)}} \begin{pmatrix} |\mathbf{p}| + p_z \\ p_x + ip_y \end{pmatrix}, \tag{B.4a}$$

$$\chi_-(p) = \frac{1}{\sqrt{2|\mathbf{p}|\,(|\mathbf{p}| + p_z)}} \begin{pmatrix} -p_x + ip_y \\ |\mathbf{p}| + p_z \end{pmatrix}, \tag{B.4b}$$

[1]The barred-spinors are related to the spinors in the usual way, *i.e.* $\bar{u} = u^\dagger \gamma_0$.

where $p_{x,y,z}$ are the x, y and z components of the momentum respectively, E is the energy of the particle and $|\mathbf{p}|$ is the magnitude of the three momentum.

For the HELAS choice of gamma matrix representation the spinors are given by

$$u(p) = \begin{pmatrix} \omega_{-\lambda}(p)\chi_{\lambda}(p) \\ \omega_{\lambda}(p)\chi_{\lambda}(p) \end{pmatrix}, \tag{B.5a}$$

$$v(p) = \begin{pmatrix} -\lambda\omega_{\lambda}(p)\chi_{-\lambda}(p) \\ \lambda\omega_{-\lambda}(p)\chi_{-\lambda}(p) \end{pmatrix}, \tag{B.5b}$$

where $\omega_{\pm}(p) = \sqrt{E \pm |\mathbf{p}|}$ and the helicity $\lambda = \pm 1$. Similarly for the low energy definition

$$u(p) = \begin{pmatrix} \omega_{+}(p)\chi_{\lambda}(p) \\ \lambda\omega_{-}(p)\chi_{\lambda}(p) \end{pmatrix}, \tag{B.6a}$$

$$v(p) = \begin{pmatrix} \omega_{-}(p)\chi_{-\lambda}(p) \\ -\lambda\omega_{+}(p)\chi_{-\lambda}(p) \end{pmatrix}. \tag{B.6b}$$

Spin-1

The basis state for a vector boson is a polarisation vector ε^{μ}, which is calculated using, as in [52],

$$\varepsilon_1^{\mu}(p) = \frac{1}{|\mathbf{p}|p_T}\left(0, p_x p_z, p_y p_z, -p_T^2\right), \tag{B.7a}$$

$$\varepsilon_2^{\mu}(p) = \frac{1}{p_T}(0, -p_y, p_x, 0), \tag{B.7b}$$

$$\varepsilon_3^{\mu}(p) = \frac{E}{m|\mathbf{p}|}\left(\frac{|\mathbf{p}|^2}{E}, p_x, p_y, p_z\right), \tag{B.7c}$$

where m is the mass, $p_T = \sqrt{p_x^2 + p_y^2}$ and ε_3^μ only exists if $m > 0$. The HELAS choice for the polarisation vectors is

$$\varepsilon^\mu(p, \lambda = \pm 1) = \frac{1}{\sqrt{2}}\left(\mp\varepsilon_1^\mu(p) - i\varepsilon_2^\mu(p)\right), \tag{B.8a}$$

$$\varepsilon^\mu(p, \lambda = 0) = \varepsilon_3^\mu(p), \tag{B.8b}$$

which is available in Herwig++. However, by default an additional phase factor $\exp(i\lambda\phi)$, as in [83], is included in order to make the inclusion of spin correlations in the parton shower easier.

Spin-$\frac{3}{2}$

Although there are no fundamental spin-$\frac{3}{2}$ particles applicable to this thesis, we include the Rarita-Schwinger spinors both to allow the simulation of spin-$\frac{3}{2}$ hadronic resonances and the future inclusion of the gravitino. The spinors ψ^μ are calculated using the Clebsch-Gordon decomposition. For massive particles the spinors are calculated in the rest frame and then boosted to the required frame, while for massless particles the spinors are calculated in the same frame as the momentum. The decomposition is as follows:

$$\psi^\mu(p, \lambda = -2) = \varepsilon^\mu(p, -1)\psi(p, -1); \tag{B.9a}$$

$$\psi^\mu(p, \lambda = -1) = \sqrt{\frac{1}{3}}\varepsilon^\mu(p, -1)\psi(p, 1) + \sqrt{\frac{2}{3}}\varepsilon^\mu(p, 0)\psi(p, -1); \tag{B.9b}$$

$$\psi^\mu(p, \lambda = 1) = \sqrt{\frac{1}{3}}\varepsilon^\mu(p, 1)\psi(p, -1) + \sqrt{\frac{2}{3}}\varepsilon^\mu(p, 0); \tag{B.9c}$$

$$\psi^\mu(p, \lambda = 2) = \varepsilon^\mu(p, 1)\psi(p, 1). \tag{B.9d}$$

Spin-2

The basis state for a spin-2 particle is a polarisation tensor $\varepsilon^{\mu\nu}$, which is calculated using the Clebsch-Gordon decomposition:

$$\varepsilon^{\mu\nu}(p,\lambda=-2) = \varepsilon^{\mu}(p,-1)\varepsilon^{\nu}(p,-1); \tag{B.10a}$$

$$\varepsilon^{\mu\nu}(p,\lambda=-1) = \sqrt{\frac{1}{2}}\left[\varepsilon^{\mu}(p,-1)\varepsilon^{\nu}(p,0)+\varepsilon^{\mu}(p,0)\varepsilon^{\nu}(p,-1)\right]; \tag{B.10b}$$

$$\varepsilon^{\mu\nu}(p,\lambda=0) = \sqrt{\frac{1}{2}}[\varepsilon^{\mu}(p,1)\varepsilon^{\nu}(p,-1)+\varepsilon^{\mu}(p,-1)\varepsilon^{\nu}(p,1) +2\varepsilon^{\mu}(p,0)\varepsilon^{\nu}(p,0)]; \tag{B.10c}$$

$$\varepsilon^{\mu\nu}(p,\lambda=1) = \sqrt{\frac{1}{2}}\left[\varepsilon^{\mu}(p,1)\varepsilon^{\nu}(p,0)+\varepsilon^{\mu}(p,0)\varepsilon^{\nu}(p,1)\right]; \tag{B.10d}$$

$$\varepsilon^{\mu\nu}(p,\lambda=2) = \varepsilon^{\mu}(p,1)\varepsilon^{\nu}(p,1). \tag{B.10e}$$

Here this is applied in the frame in which the momentum is specified.

B.1.2 Lorentz Transformations

In addition to calculating the basis state for a given field, we need to be able to transform it between different Lorentz frames.

The Lorentz transformation for a spinor is given by

$$\psi'(x') = \psi'(ax) = S(a)\psi(x), \tag{B.11}$$

where $a^{\nu}_{\mu} = \frac{\partial x'^{\nu}}{\partial x^{\mu}}$. For a Lorentz boost along the direction specified by the unit vector $\hat{\mathbf{n}}$ with a magnitude β the transformation is given by

$$S_{\text{boost}} = \cosh\left(\frac{\chi}{2}\right) + \sinh\left(\frac{\chi}{2}\right)\hat{n}_i\gamma^0\gamma^i, \tag{B.12}$$

where $\tanh\chi = \beta$. For a rotation by an angle ϕ about the unit vector $\hat{\mathbf{n}}$ the Lorentz transformation is given by

$$S_{\text{rotation}} = \cos\left(\frac{\phi}{2}\right) + \sin\left(\frac{\phi}{2}\right)\varepsilon^{ijk}\hat{n}_k\gamma^i\gamma^j. \tag{B.13}$$

The Lorentz transformation for a four vector is given by

$$\varepsilon^{\mu}(x') = L(a)^{\mu}_{\nu}\varepsilon^{\nu}(x). \tag{B.14}$$

If we wish to boost by a factor β along a unit vector $\hat{\mathbf{n}}$ the transformation is

$$L^{\mu}_{\nu} = \begin{pmatrix} \gamma & -\gamma\beta\hat{n}_1 & -\gamma\beta\hat{n}_2 & -\gamma\beta\hat{n}_3 \\ -\gamma\beta\hat{n}_1 & 1-\hat{n}_1\hat{n}_1\omega & -\hat{n}_1\hat{n}_2\omega & -\hat{n}_1\hat{n}_3\omega \\ -\gamma\beta\hat{n}_2 & -\hat{n}_2\hat{n}_1\omega & 1-\hat{n}_2\hat{n}_2\omega & -\hat{n}_2\hat{n}_3\omega \\ -\gamma\beta\hat{n}_3 & -\hat{n}_3\hat{n}_1\omega & -\hat{n}_3\hat{n}_2\omega & 1-\hat{n}_3\hat{n}_3\omega \end{pmatrix}, \tag{B.15}$$

where $\omega = 1-\gamma$ and $\gamma = \frac{1}{\sqrt{1-\beta^2}}$. The Lorentz transformation for a rotation by an angle δ about a unit vector $\hat{\mathbf{n}}$ is

$$L^{\mu}_{\nu} = \begin{pmatrix} 1 & 0 & 0 & 0 \\ 0 & \lambda\hat{n}_1\hat{n}_1 + c_\delta & \lambda\hat{n}_1\hat{n}_2 - s_\delta\hat{n}_3 & \lambda\hat{n}_1\hat{n}_3 + s_\delta\hat{n}_2 \\ 0 & \lambda\hat{n}_2\hat{n}_1 + s_\delta\hat{n}_3 & \lambda\hat{n}_2\hat{n}_2 + c_\delta & \lambda\hat{n}_2\hat{n}_3 - s_\delta\hat{n}_1 \\ 0 & \lambda\hat{n}_3\hat{n}_1 - s_\delta\hat{n}_2 & \lambda\hat{n}_3\hat{n}_2 + s_\delta\hat{n}_1 & \lambda\hat{n}_3\hat{n}_3 + c_\delta \end{pmatrix}, \tag{B.16}$$

where $c_\delta = \cos\delta$, $s_\delta = \sin\delta$ and $\lambda = 1-\cos\delta$. The transformations for the higher-spin particles can then be constructed as products of the spin-$\frac{1}{2}$ and spin-1

transformations, *i.e.*

$$\psi^{\mu}(x') = L(a)^{\mu}_{\nu} S(a) \psi^{\nu}(x), \tag{B.17a}$$

$$\varepsilon^{\mu\nu}(x') = L(a)^{\mu}_{\alpha} L(a)^{\nu}_{\beta} \varepsilon^{\alpha\beta}. \tag{B.17b}$$

B.2 Vertices

The vertex structures given below are the perturbative forms applicable to this work. In general all of the momenta are defined as incoming.

B.2.1 Scalar Vertices

FFSVertex The vertex for the coupling of a fermion and anti-fermion to a scalar boson is defined to have the perturbative form

$$ic\bar{f}_2 a^{\lambda} P_{\lambda} f_1 \phi_3, \tag{B.18}$$

where c is the overall normalisation, a^{λ} are the left/right couplings, P_{λ} are the helicity projection operators, f_1 is the wave function for the fermion, $\bar{f}_2$ is the wave function for the anti-fermion and ϕ_3 is the wave function for the scalar boson.

GeneralSVVVertex In addition to the perturbative form for the vertex coupling a scalar and two vector bosons described below, there is a general form for this interaction so that effective vertices, for example $h^0 \to gg$, can be

implemented. The form of the vertex is

$$ic\left[a_{00}g^{\mu\nu} + a_{22}p_2^\mu p_2^\nu + a_{23}p_2^\mu p_3^\nu + a_{32}p_3^\mu p_2^\nu + a_{33}p_3^\mu p_3^\nu \right. \\ \left. + a_\epsilon \epsilon^{\mu\nu\alpha\beta} p_{2\alpha} p_{3\beta}\right] \epsilon_{2\mu}\epsilon_{3\nu}\phi_1, \tag{B.19}$$

where $p_{2,3}$ are the momenta of the vector bosons, $\epsilon_{2,3}$ are the wave functions of the vector bosons, ϕ_1 is the wave function of the scalar boson, c is the overall coupling and a_{ij} are the couplings of the different terms.

SSSVertex The vertex for the coupling of three scalar bosons is defined to have the perturbative form

$$ic\phi_1\phi_2\phi_3, \tag{B.20}$$

where $\phi_{1,2,3}$ are the wave functions for the scalar bosons and c is the coupling.

SSSSVertex The vertex for the coupling of four scalar bosons is defined to have the perturbative form

$$ic\phi_1\phi_2\phi_3\phi_4, \tag{B.21}$$

where $\phi_{1,2,3,4}$ are the wave functions for the scalar bosons and c is the coupling.

VSSVertex The vertex for the coupling of a vector boson and two scalar bosons is defined to have the perturbative form

$$-ic\left(p_2 - p_3\right) \cdot \epsilon_1 \phi_2 \phi_3, \tag{B.22}$$

where ϵ_1 is the wave function of the vector boson, $\phi_{2,3}$ are the wave functions for the scalar bosons and $p_{2,3}$ are the momenta of the scalar bosons and c is the coupling.

VVSSVertex The vertex for the interaction of two vector and two scalar bosons is defined to have the perturbative form

$$icg^{\mu\nu}\epsilon_{1\mu}\epsilon_{2\nu}\phi_3\phi_4, \tag{B.23}$$

where $\epsilon_{1,2}$ are the wave functions of the vector bosons and $\phi_{3,4}$ are the wave functions for the scalar bosons and c is the coupling.

VVSVertex The vertex for the interaction of two vector bosons and a scalar boson is defined to have the perturbative form

$$icg^{\mu\nu}\epsilon_{1\mu}\epsilon_{2\nu}\phi_3, \tag{B.24}$$

where $\epsilon_{1,2}$ are the wave functions of the vector bosons and ϕ_3 is the wave function for the scalar boson and c is the coupling.

B.2.2 Vector Vertices

There are a number of vertices involving vector bosons.

FFVVertex The interaction of a fermion, anti-fermion and a vector boson is taken to have the perturbative form

$$ic\bar{f}_2\gamma^\mu a^\lambda P_\lambda f_1\epsilon_{3\mu}, \tag{B.25}$$

where c is the overall normalisation, a^λ are the left/right couplings, f_1 is the wave function for the fermion, $\bar{f}_2$ is the wave function for the anti-fermion and ϵ_3 is the wave function for the vector boson.

VVVVertex The interaction of three vector bosons is taken to have the pertur-

bative form

$$ig\left[(p_1-p_2)^\gamma g^{\alpha\beta}+(p_2-p_3)^\alpha g^{\beta\gamma}+(p_3-p_1)^\beta g^{\alpha\gamma}\right]\epsilon_{1\alpha}\epsilon_{2\beta}\epsilon_{3\gamma}, \quad \text{(B.26)}$$

where $\epsilon_{1,2,3}$ are the wave functions of the vector bosons and $p_{1,2,3}$ are the momenta of the vector bosons.

VVVVVertex The interaction of four vector bosons is taken to have the form

$$ic^2\left[2\epsilon_1\cdot\epsilon_2\epsilon_3\cdot\epsilon_4-\epsilon_1\cdot\epsilon_3\epsilon_2\cdot\epsilon_4-\epsilon_1\cdot\epsilon_4\epsilon_2\cdot\epsilon_3\right], \quad \text{(B.27)}$$

where $\epsilon_{1,2,3,4}$ are the wave functions of the vector bosons. For the quartic gluon vertex this is the contribution of one colour structure. The others can be obtained by an appropriate reordering of the input wave functions.

B.2.3 Tensor Vertices

There are a number of vertices involving spin-2 particles. The form of the Feynman rules follows that of [84].

FFTVertex The interaction of a pair of fermions with a tensor is taken to have the perturbative form

$$-\frac{i\kappa}{8}\bar{f}_2\left[\gamma_\mu(p_1-p_2)_\nu+\gamma_\nu(p_1-p_2)_\mu-2g_{\mu\nu}(\not{p}_1-\not{p}_2)+4g_{\mu\nu}m_f\right]f_1\epsilon_3^{\mu\nu}, \quad \text{(B.28)}$$

where κ is the defined as $2/\Lambda_{\text{cut-off}}$, $p_{1,2}$ are the momenta of the fermions, f_1 is the fermion wave function, $\bar{f}_2$ is the anti-fermion wave function and $\epsilon_3^{\mu\nu}$ is the polarisation tensor for the spin-2 particle.

VVVTVertex The interaction of three vector bosons with a tensor is taken to

have the perturbative form

$$\frac{g\kappa}{2}\left[C_{\mu\nu,\rho\sigma}(p_1-p_2)_\lambda + C_{\mu\nu,\rho\lambda}(p_3-p_1)_\sigma + C_{\mu\nu,\sigma\lambda}(p_2-p_3)_\rho + \bar{F}_{\mu\nu,\rho\sigma\lambda}\right]\epsilon_1^\rho\epsilon_2^\sigma\epsilon_3^\lambda\epsilon_4^{\mu\nu}, \tag{B.29}$$

where κ is $2/\Lambda_{\text{cut-off}}$, $p_{1,2,3}$ are the momenta of the vector bosons, $\epsilon^\mu_{1,2,3}$ are the polarisation vectors and $\epsilon_4^{\mu\nu}$ is the polarisation tensor. The C and F symbols are defined as

$$C_{\mu\nu,\rho\sigma} = g_{\mu\rho}g_{\nu\sigma} + g_{\mu\sigma}g_{\nu\rho} - g_{\mu\nu}g_{\rho\sigma}, \tag{B.30a}$$

$$F_{\mu\nu,\rho\sigma\lambda} = g_{\mu\rho}g_{\sigma\lambda}(p_2-p_3)_\nu + g_{\mu\sigma}g_{\rho\lambda}(p_3-p_1)_\nu + g_{\mu\lambda}g_{\rho\sigma}(p_1-p_2)_\nu + (\mu\leftrightarrow\nu). \tag{B.30b}$$

VVTVertex The interaction of two vector bosons with a tensor is taken to have the perturbative form

$$-\frac{i\kappa}{2}\left[(m_v^2 + p_1\cdot p_2)C_{\mu\nu,\rho\sigma} + D_{\mu\nu,\rho\sigma}\right]\epsilon_1^\rho\epsilon_2^\sigma\epsilon_3^{\mu\nu}, \tag{B.31}$$

where κ is the defined as $2/\Lambda_{\text{cut-off}}$, m_v is the mass of the gauge boson, $p_{1,2}$ are the momenta of the vector bosons, $\epsilon^\mu_{1,2,3}$ are the polarisation vectors and $\epsilon_3^{\mu\nu}$ is the polarisation tensor. The C symbol is defined as above and D is defined as

$$D_{\mu\nu,\rho\sigma} = g_{\mu\nu}k_{1\sigma}k_{2\rho} - \left[g_{\mu\sigma}k_{1\nu}k_{2\rho} + g_{\mu\rho}k_{1\sigma}k_{2\nu} - g_{\rho\sigma}k_{1\mu}k_{2\nu} + (\mu\leftrightarrow\nu)\right]. \tag{B.32}$$

FFVTVertex The interaction of a pair of fermions with a vector boson and a

tensor is taken to have the perturbative form

$$\frac{ig\kappa}{4}\bar{f}_2(C_{\mu\nu,\rho\sigma} - g_{\mu\nu}g_{\rho\sigma})\gamma^\sigma f_1 \epsilon_3^\rho \epsilon_4^{\mu\nu}, \tag{B.33}$$

where κ is the defined as $2/\Lambda_{\text{cut-off}}$, ϵ_3^ρ is the polarisation vector for the boson, f_1 is the fermion wave function, $\bar{f}_2$ is the anti-fermion wave function and $\epsilon_4^{\mu\nu}$ the polarisation tensor for the spin-2 particle. The C symbol is defined above.

SSTVertex The interaction of a pair of scalars with a tensor is taken to have the perturbative form

$$-\frac{i\kappa}{2}\left[m_S^2 g_{\mu\nu} - p_{1\mu}p_{2\nu} - p_{1\nu}p_{2\mu} + g_{\mu\nu}p_1 \cdot p_2\right]\epsilon_3^{\mu\nu}\phi_1\phi_2, \tag{B.34}$$

where κ is the defined as $2/\Lambda_{\text{cut-off}}$, $\Lambda_{\text{cut-off}}$ is the ultraviolet cutoff scale, m_S is the mass of the scalar, $p_{1,2}$ are the momenta of the scalars, $\epsilon_3^{\mu\nu}$ the polarisation tensor for the spin-2 particle and $\phi_{1,2}$ are the scalar wave functions.

B.3 Two-body Decay Formulae

Here we give the matrix elements for the two-body decays using the perturbative vertex structures defined above where $m_{a,b,c}$ are the masses of the decaying particle and two final-state particles respectively and $\mu_{b,c} = m_{b,c}/m_a$. The coupling constants c and $a^{L,R}$ are defined with the relevant vertex and the formulae are summed over final-state spins and averaged over initial-state spins but no summation or averaging over colour states has been performed. Table B.1 gives the colour factors that should be included for the possible colour combinations.

a	bc	Colour factor
1	$1\,1$	1
	$3\,\bar{3}$	3
	$8\,8$	8
3	$3\,1$	1
	$3\,8$	4/3
8	$8\,1$	1
	$3\,\bar{3}$	1/2

Table B.1: The multiplicative colour factors for a two-body decay $a \to bc$ as a result of summing over final-state colours and averaging over initial-state colours with $N_C = 3$. For an anti-colour-triplet initial state, the factors are identical to those given for the colour-triplet initial state.

Scalar Decays

A scalar particle can decay into two scalars, two fermions, a scalar and a vector boson or two vector bosons. The matrix elements for the decay into a pair of scalars or fermions are

$$\overline{\sum}|\mathcal{M}(S_a \to S_b\, S_c)|^2 = c^2, \tag{B.35a}$$

$$\overline{\sum}|\mathcal{M}(S_a \to F_b F_c)|^2 = c^2 m_a^2 \left[(|a^L|^2 + |a^R|^2)(1 - \mu_b^2 - \mu_c^2) - 2\mu_b\,\mu_c(a^{l*}a^R + a^{r*}a^L)\right], \tag{B.35b}$$

while the decay where a vector boson appears in the final state is more complicated. For a single spin-1 particle in the final state the matrix element is given by

$$\overline{\sum}|\mathcal{M}(S_a \to S_b\, V_c)|^2 = \begin{cases} -2c^2 m_a^2\,(1+\mu_b^2)\,, & m_c = 0, \\ \dfrac{c^2 m_a^2}{\mu_c^2}\left[(\mu_c^2 - \mu_b^2)^2 - 2(\mu_b^2 + \mu_c^2) + 1\right], & m_c > 0. \end{cases} \tag{B.36}$$

When there are two vector bosons in the final state, the decay can proceed via the tree-level or the loop mediated vertex. In the tree-level case the matrix element is

$$\overline{\sum}|\mathcal{M}(S_a \overset{\text{tree}}{\to} V_b V_c)|^2 = \begin{cases} 4, & m_b = m_c = 0, \\ 3, & m_b = 0 \text{ or } m_c = 0, \\ \dfrac{c^2}{4\mu_b^2\mu_c^2}\left[(\mu_b^2+\mu_c^2)^2 - 2(\mu_b^2+\mu_c^2)\right. & \\ \qquad \left. + 8\mu_b^2\mu_c^2 + 1\right], & m_b > 0 \text{ and } m_c > 0. \end{cases} \tag{B.37}$$

For the loop-mediated case we only give the result for massless vector particles in the final state

$$\overline{\sum}|\mathcal{M}(S_a \overset{\text{loop}}{\to} V_b V_c)|^2 = \frac{c^2}{2}\left[\left(a_\epsilon^2 + a_{23}a_{32} + a_{22}a_{33}\right) m_a^4 + a_{00}(a_{23}+a_{32})m_a^2 + 4a_{00}^2\right]. \tag{B.38}$$

Fermion Decays

The possible two-body decay matrix elements for a fermion are

$$\overline{\sum}|\mathcal{M}(F_a \to F_b S_c)|^2 = \frac{c^2}{2}\left[(|a^L|^2+|a^R|^2)(1+\mu_b^2-\mu_c^2) + 2\mu_b(a^{*L}a^R + a^{*R}a^L)\right], \tag{B.39a}$$

$$\overline{\sum}|\mathcal{M}(F_a \to F_b V_c)|^2 = \begin{cases} c^2\left[(|a^L|^2+|a^R|^2)(1+\mu_b^2)\right. & \\ \qquad \left. - 4\mu_b(a^{*L}a^R + a^{*R}a^L)\right], & m_c = 0, \\ \dfrac{c^2}{2\mu_c^2}\left[(|a^L|^2+|a^R|^2)\right. & \\ \qquad \times(1+\mu_b^2\mu_c^2+\mu_c^2-2\mu_b^2+\mu_b^4-2\mu_c^4) & \\ \qquad \left. - 6\mu_b\mu_c^2(a^{*L}a^R + a^{*R}a^L)\right], & m_c > 0. \end{cases} \tag{B.39b}$$

Vector boson decays

The possible two-body decay matrix elements for a vector boson are

$$\overline{\sum}|\mathcal{M}(V_a \to S_b\, S_c)|^2 = \frac{c^2 m_a^2}{3}\left[2(\mu_b^2+\mu_c^2) - (\mu_b^2-\mu_c^2)^2\right], \tag{B.40a}$$

$$\overline{\sum}|\mathcal{M}(V_a \to F_b\, F_c)|^2 = -\frac{c^2 m_a^2}{3}\left[(|a^L|^2+|a^R|^2)(\mu_b^2+\mu_c^2+(\mu_b^2-\mu_c^2)^2-2) - 6(a^{*L}a^R + a^{*R}a^L)\mu_b\mu_c\right], \tag{B.40b}$$

$$\overline{\sum}|\mathcal{M}(V_a \to V_b\, S_c)|^2 = \begin{cases} c^2 & m_b = 0, \\ \dfrac{c^2}{3\mu_b^2}\left[2\mu_b^2 + (1+\mu_b^2-\mu_c^2)\right] & m_b > 0. \end{cases} \tag{B.40c}$$

$$\overline{\sum}|\mathcal{M}(V_a \to V_b\, V_c)|^2 = \begin{cases} \dfrac{c^2 m_a^2}{6\mu_c^2}\left[(\mu_c^2+1)(5\mu_c^4-22\mu_c^2+5)\right] & m_b = 0, \\ \dfrac{c^2 m_a^2}{6\mu_b^2}\left[(\mu_b^2+1)(5\mu_b^4-22\mu_b^2+5)\right] & m_c = 0, \\ \dfrac{c^2 m_a^2}{12\mu_b^2\mu_c^2} \times \left[(\mu_b^4+\mu_c^4-2(\mu_b^2\mu_c^2-\mu_b^2-\mu_c^2)+1)\times (\mu_b^4+\mu_c^4+10(\mu_b^2+\mu_c^2+\mu_b^2\mu_c^2)+1)\right] & m_{b,c} > 0. \end{cases} \tag{B.40d}$$

Tensor Decays

The possible two-body decay matrix elements for a tensor particle are given by

$$\overline{\sum}|\mathcal{M}(T_a \to S\, S)|^2 = \frac{c^2 m_a^2}{120}\left(1-4\mu_s^2\right)^2, \tag{B.41a}$$

$$\overline{\sum}|\mathcal{M}(T_a \to F\, F)|^2 = \frac{c^2 m_a^2}{120}\left[3-4\mu_F^2-32\mu_F^4\right], \tag{B.41b}$$

$$\overline{\sum}|\mathcal{M}(T_a \to V\, V)|^2 = \frac{c^2 m_a^2}{120}\left[13+56\mu_V^2+48\mu_V^2\right], \tag{B.41c}$$

where the final-state particles each have the same mass due the structure of each vertex, as in Eqns. (B.28,B.31, B.34).

B.4 Sample Decay Tables

Below we give a sample decay table for the MSSM at SPS point 1a and the MUED model with $R^{-1} = 500$ GeV and $\Lambda R = 20$, the mass spectrum shown in Table 3.2.

B.4.1 Minimal Supersymmetric Standard Model

The output shown below is result of running Herwig++ for the MSSM with the mass spectrum at parameter point SPS 1a, produced by SPheno 2.2.3 [62]. Any decay modes with a branching fraction lower than 1×10^{-4}, a parameter that is controllable, are not included.

```
# Parent: ~d_L  Mass (GeV): 570.67  Total Width (GeV): 5.51428
#                                      Partial Width/GeV   BR
~d_L->~chi_10,d;                       0.128924            0.02338
~d_L->~chi_20,d;                       1.68235             0.305089
~d_L->~chi_30,d;                       0.00884194          0.00160346
~d_L->~chi_40,d;                       0.0856625           0.0155347
~d_L->~chi_1-,u;                       3.30826             0.599944
~d_L->~chi_2-,u;                       0.240787            0.043666
~d_L->~chi_1-,Z0,u;                    0.0125989           0.00228478
~d_L->~chi_20,W-,u;                    0.00966365          0.00175248
~d_L->~chi_1+,W-,d;                    0.0197032           0.00357313
~d_L->~chi_1-,W+,d;                    0.00672106          0.00121885
~d_L->~nu_eLbar,e-,u;                  0.00174899          0.000317174
~d_L->~e_L-,nu_ebar,u;                 0.0021417           0.000388391
~d_L->~nu_muLbar,mu-,u;                0.00174936          0.000317241
~d_L->~mu_L-,nu_mubar,u;               0.00214082          0.000388233
~d_L->~nu_tauLbar,tau-,u;              0.00186514          0.000338239
~d_L->~tau_2-,nu_taubar,u;             0.00112602          0.0002042
#
# Parent: ~u_L  Mass (GeV): 565.263  Total Width (GeV): 5.76653
#                                      Partial Width/GeV   BR
```

```
~u_L->~chi_10,u;                          0.0351368          0.00609322
~u_L->~chi_20,u;                          1.79926            0.312017
~u_L->~chi_30,u;                          0.00520609         0.000902812
~u_L->~chi_40,u;                          0.0626142          0.0108582
~u_L->~chi_1+,d;                          3.68437            0.638924
~u_L->~chi_2+,d;                          0.0772829          0.013402
~u_L->~chi_10,W+,d;                       0.000608353        0.000105497
~u_L->~chi_20,W+,d;                       0.0524849          0.00910165
~u_L->~chi_1-,W+,u;                       0.00135626         0.000235196
~u_L->~chi_1+,Z0,d;                       0.0269893          0.00468034
~u_L->~chi_1+,W-,u;                       0.00652142         0.00113091
~u_L->~nu_eL,e+,d;                        0.00427371         0.000741123
~u_L->~nu_muL,mu+,d;                      0.00427423         0.000741213
~u_L->~nu_tauL,tau+,d;                    0.0044388          0.000769752
~u_L->~e_L+,nu_e,d;                       0.000856598        0.000148547
~u_L->~mu_L+,nu_mu,d;                     0.000856106        0.000148461
#
# Parent: ~s_L  Mass (GeV): 570.67  Total Width (GeV): 5.51435
#                                         Partial Width/GeV  BR
~s_L->~chi_10,s;                          0.128931           0.023381
~s_L->~chi_20,s;                          1.68237            0.305088
~s_L->~chi_30,s;                          0.00889967         0.00161391
~s_L->~chi_40,s;                          0.085708           0.0155427
~s_L->~chi_1-,c;                          3.30822            0.599928
~s_L->~chi_2-,c;                          0.241018           0.0437074
~s_L->~chi_1-,Z0,c;                       0.0123559          0.00224068
~s_L->~chi_20,W-,c;                       0.00966353         0.00175243
~s_L->~chi_1+,W-,s;                       0.0197023          0.0035729
~s_L->~chi_1-,W+,s;                       0.00672113         0.00121884
~s_L->~nu_eLbar,e-,c;                     0.00174894         0.000317161
~s_L->~e_L-,nu_ebar,c;                    0.00214161         0.00038837
~s_L->~nu_muLbar,mu-,c;                   0.00174931         0.000317229
~s_L->~mu_L-,nu_mubar,c;                  0.00214074         0.000388212
~s_L->~nu_tauLbar,tau-,c;                 0.0018651          0.000338226
~s_L->~tau_2-,nu_taubar,c;                0.00112597         0.000204189
#
# Parent: ~c_L  Mass (GeV): 565.271  Total Width (GeV): 5.76698
#                                         Partial Width/GeV  BR
~c_L->~chi_10,c;                          0.035139           0.00609314
~c_L->~chi_20,c;                          1.79927            0.311995
~c_L->~chi_30,c;                          0.00531543         0.000921701
~c_L->~chi_40,c;                          0.0627224          0.0108761
~c_L->~chi_1+,s;                          3.68449            0.638895
~c_L->~chi_2+,s;                          0.0773735          0.0134166
~c_L->~chi_10,W+,s;                       0.000608482        0.000105511
~c_L->~chi_20,W+,s;                       0.0524912          0.00910204
~c_L->~chi_1-,W+,c;                       0.00135634         0.000235191
```

```
~c_L->~chi_1+,Z0,s;                          0.0269887          0.00467987
~c_L->~chi_1+,W-,c;                          0.00652143         0.00113082
~c_L->~nu_eL,e+,s;                           0.0042739          0.000741099
~c_L->~nu_muL,mu+,s;                         0.00427443         0.00074119
~c_L->~nu_tauL,tau+,s;                       0.004439           0.000769728
~c_L->~e_L+,nu_e,s;                          0.000856658        0.000148545
~c_L->~mu_L+,nu_mu,s;                        0.000856166        0.00014846
#
# Parent: ~b_1  Mass (GeV): 515.268  Total Width (GeV): 4.21614
#                                            Partial Width/GeV  BR
~b_1->~t_1,W-;                               0.550572           0.130587
~b_1->~chi_10,b;                             0.199242           0.0472569
~b_1->~chi_20,b;                             1.46034            0.34637
~b_1->~chi_30,b;                             0.0637949          0.0151311
~b_1->~chi_40,b;                             0.0650385          0.0154261
~b_1->~chi_1-,t;                             1.85381            0.439694
~b_1->~chi_1-,Z0,t;                          0.000816592        0.000193682
~b_1->~chi_10,W-,t;                          0.000427699        0.000101443
~b_1->~chi_20,W-,t;                          0.000724339        0.000171801
~b_1->~chi_1+,W-,b;                          0.00457917         0.00108611
~b_1->~chi_1-,W+,b;                          0.00373815         0.000886628
~b_1->~nu_eLbar,e-,t;                        0.000617642        0.000146494
~b_1->~e_L-,nu_ebar,t;                       0.000422605        0.000100235
~b_1->~nu_muLbar,mu-,t;                      0.000618048        0.000146591
~b_1->~mu_L-,nu_mubar,t;                     0.00042232         0.000100167
~b_1->~nu_tauLbar,tau-,t;                    0.000739157        0.000175316
~b_1->~tau_2-,nu_taubar,t;                   0.00099249         0.000235402
~b_1->~tau_1-,nu_taubar,t;                   0.00923994         0.00219156
#
# Parent: ~t_1  Mass (GeV): 400.717  Total Width (GeV): 2.24131
#                                            Partial Width/GeV  BR
~t_1->~chi_10,t;                             0.402674           0.179661
~t_1->~chi_20,t;                             0.266753           0.119017
~t_1->~chi_1+,b;                             1.53441            0.684605
~t_1->~chi_2+,b;                             0.0316715          0.0141308
~t_1->~chi_20,W+,b;                          0.00206632         0.000921927
~t_1->~chi_1+,Z0,b;                          0.000537068        0.000239623
~t_1->~chi_1+,h0,b;                          0.000312008        0.000139208
~t_1->~nu_eL,e+,b;                           0.000943163        0.00042081
~t_1->~nu_muL,mu+,b;                         0.000943334        0.000420886
~t_1->~nu_tauL,tau+,b;                       0.000997305        0.000444966
#
# Parent: ~d_R  Mass (GeV): 547.94  Total Width (GeV): 0.291108
#                                            Partial Width/GeV  BR
~d_R->~chi_10,d;                             0.286256           0.983333
~d_R->~chi_20,d;                             0.00271294         0.00931937
~d_R->~chi_30,d;                             0.000360151        0.00123718
```

```
~d_R->~chi_40,d;                          0.00115854          0.00397976
~d_R->~chi_10,Z0,d;                       0.00016364          0.000562128
~d_R->~e_R-,e+,d;                         0.000146074         0.000501788
~d_R->~mu_R-,mu+,d;                       0.000146174         0.000502131
~d_R->~tau_1-,tau+,d;                     0.000164464         0.00056496
#
# Parent: ~u_R  Mass (GeV): 548.177  Total Width (GeV): 1.16473
#                                           Partial Width/GeV   BR
~u_R->~chi_10,u;                          1.14559             0.983565
~u_R->~chi_20,u;                          0.0108586           0.00932282
~u_R->~chi_30,u;                          0.00144265          0.00123861
~u_R->~chi_40,u;                          0.00464329          0.00398658
~u_R->~chi_10,Z0,u;                       0.00036894          0.00031676
~u_R->~e_R-,e+,u;                         0.000585056         0.00050231
~u_R->~mu_R-,mu+,u;                       0.000585456         0.000502653
~u_R->~tau_1-,tau+,u;                     0.000658659         0.000565503
#
# Parent: ~s_R  Mass (GeV): 547.936  Total Width (GeV): 0.291334
#                                           Partial Width/GeV   BR
~s_R->~chi_10,s;                          0.28626             0.982585
~s_R->~chi_20,s;                          0.00273281          0.00938035
~s_R->~chi_30,s;                          0.000409627         0.00140604
~s_R->~chi_40,s;                          0.00119537          0.0041031
~s_R->~chi_1-,c;                          4.26655e-05         0.000146449
~s_R->~chi_2-,c;                          7.2708e-05          0.00024957
~s_R->~chi_10,Z0,s;                       0.000163636         0.00056168
~s_R->~e_R-,e+,s;                         0.000146072         0.00050139
~s_R->~mu_R-,mu+,s;                       0.000146171         0.000501732
~s_R->~tau_1-,tau+,s;                     0.000164461         0.000564513
#
# Parent: ~c_R  Mass (GeV): 548.165  Total Width (GeV): 1.16501
#                                           Partial Width/GeV   BR
~c_R->~chi_10,c;                          1.14555             0.983289
~c_R->~chi_20,c;                          0.0108706           0.00933091
~c_R->~chi_30,c;                          0.00153668          0.00131902
~c_R->~chi_40,c;                          0.00472072          0.00405207
~c_R->~chi_2+,s;                          0.000142443         0.000122267
~c_R->~chi_10,Z0,c;                       0.000368816         0.000316577
~c_R->~e_R-,e+,c;                         0.000585            0.00050214
~c_R->~mu_R-,mu+,c;                       0.000585399         0.000502482
~c_R->~tau_1-,tau+,c;                     0.000658599         0.000565314
#
# Parent: ~b_2  Mass (GeV): 547.669  Total Width (GeV): 0.81577
#                                           Partial Width/GeV   BR
~b_2->~t_1,W-;                            0.193888            0.237674
~b_2->~chi_10,b;                          0.221612            0.271659
~b_2->~chi_20,b;                          0.0566178           0.0694041
```

```
~b_2->~chi_30,b;                          0.116406          0.142695
~b_2->~chi_40,b;                          0.129793          0.159104
~b_2->~chi_1-,t;                          0.0724826         0.0888518
~b_2->~chi_10,Z0,b;                       0.00013803        0.000169202
~b_2->~chi_20,Z0,b;                       8.61701e-05       0.00010563
~b_2->~chi_1-,Z0,t;                       0.00205341        0.00251714
~b_2->~chi_10,W-,t;                       0.00107678        0.00131995
~b_2->~chi_20,W-,t;                       0.00222917        0.0027326
~b_2->~chi_1+,W-,b;                       0.000358229       0.00043913
~b_2->~e_R-,e+,b;                         0.000112962       0.000138472
~b_2->~mu_R-,mu+,b;                       0.000113039       0.000138567
~b_2->~tau_1-,tau+,b;                     0.000127197       0.000155923
~b_2->~chi_1-,W+,b;                       0.000167241       0.000205011
~b_2->~chi_2-,W+,b;                       0.00309914        0.00379904
~b_2->~chi_1-,h0,t;                       0.00152502        0.00186943
~b_2->~nu_eLbar,e-,t;                     0.000268498       0.000329135
~b_2->~e_L-,nu_ebar,t;                    0.000520299       0.000637801
~b_2->~nu_muLbar,mu-,t;                   0.000268804       0.000329509
~b_2->~mu_L-,nu_mubar,t;                  0.000520204       0.000637684
~b_2->~nu_tauLbar,tau-,t;                 0.000356084       0.000436501
~b_2->~tau_2-,nu_taubar,t;                0.00203701        0.00249704
~b_2->~tau_1-,nu_taubar,t;                0.00991454        0.0121536
#
# Parent: ~t_2  Mass (GeV): 586.318  Total Width (GeV): 9.596
#                                         Partial Width/GeV  BR
~t_2->~t_1,Z0;                            1.41663           0.147627
~t_2->~chi_10,t;                          0.21062           0.0219488
~t_2->~chi_20,t;                          0.634578          0.0661294
~t_2->~chi_30,t;                          0.407323          0.0424471
~t_2->~chi_40,t;                          1.82459           0.190141
~t_2->~t_1,h0;                            1.54398           0.160898
~t_2->~chi_1+,b;                          1.59034           0.165729
~t_2->~chi_2+,b;                          1.88296           0.196223
~t_2->~chi_10,W+,b;                       0.00218682        0.000227889
~t_2->~chi_20,W+,b;                       0.0566992         0.00590863
~t_2->~chi_30,W+,b;                       0.00125959        0.000131261
~t_2->~chi_40,W+,b;                       0.00157203        0.000163821
~t_2->~chi_1-,W+,t;                       0.0037224         0.000387911
~t_2->~b_1,u,dbar;                        0.00160338        0.000167088
~t_2->~b_1,c,sbar;                        0.00160067        0.000166806
~t_2->~chi_1+,Z0,b;                       0.00959643        0.00100004
~t_2->~chi_1+,h0,b;                       0.000969623       0.000101044
~t_2->~nu_eL,e+,b;                        0.00190238        0.000198247
~t_2->~nu_muL,mu+,b;                      0.00190261        0.000198271
~t_2->~nu_tauL,tau+,b;                    0.00197424        0.000205736
#
# Parent: ~e_L-  Mass (GeV): 202.456  Total Width (GeV): 0.217129
```

```
#                                        Partial Width/GeV   BR
~e_L-->~chi_10,e-;                       0.119487            0.550303
~e_L-->~chi_20,e-;                       0.0357026           0.16443
~e_L-->~chi_1-,nu_e;                     0.0619397           0.285266
#
# Parent: ~nu_eL  Mass (GeV): 186.25  Total Width (GeV): 0.157412
#                                        Partial Width/GeV   BR
~nu_eL->~chi_10,nu_e;                    0.149069            0.947
~nu_eL->~chi_20,nu_e;                    0.00221491          0.0140708
~nu_eL->~chi_1+,e-;                      0.00612797          0.0389296
#
# Parent: ~mu_L-  Mass (GeV): 202.472  Total Width (GeV): 0.217278
#                                        Partial Width/GeV   BR
~mu_L-->~chi_10,mu-;                     0.11951             0.550035
~mu_L-->~chi_20,mu-;                     0.0357482           0.164528
~mu_L-->~chi_1-,nu_mu;                   0.0620192           0.285437
#
# Parent: ~nu_muL  Mass (GeV): 186.247  Total Width (GeV): 0.157396
#                                        Partial Width/GeV   BR
~nu_muL->~chi_10,nu_mu;                  0.149063            0.947057
~nu_muL->~chi_20,nu_mu;                  0.00221264          0.0140578
~nu_muL->~chi_1+,mu-;                    0.00612044          0.0388857
#
# Parent: ~tau_1-  Mass (GeV): 134.477  Total Width (GeV): 0.145033
#                                        Partial Width/GeV   BR
~tau_1-->~chi_10,tau-;                   0.145033            1
#
# Parent: ~nu_tauL  Mass (GeV): 185.331  Total Width (GeV): 0.152848
#                                        Partial Width/GeV   BR
~nu_tauL->~chi_10,nu_tau;                0.147228            0.96323
~nu_tauL->~chi_20,nu_tau;                0.0015708           0.0102768
~nu_tauL->~chi_1+,tau-;                  0.00401209          0.0262488
~nu_tauL->~tau_1-,u,dbar;                1.87282e-05         0.000122528
~nu_tauL->~tau_1-,c,sbar;                1.86631e-05         0.000122102
#
# Parent: ~e_R-  Mass (GeV): 144.086  Total Width (GeV): 0.21233
#                                        Partial Width/GeV   BR
~e_R-->~chi_10,e-;                       0.21233             1
#
# Parent: ~mu_R-  Mass (GeV): 144.05  Total Width (GeV): 0.212099
#                                        Partial Width/GeV   BR
~mu_R-->~chi_10,mu-;                     0.212099            1
#
# Parent: ~tau_2-  Mass (GeV): 206.428  Total Width (GeV): 0.248301
#                                        Partial Width/GeV   BR
~tau_2-->~chi_10,tau-;                   0.157886            0.635865
~tau_2-->~chi_20,tau-;                   0.0423298           0.170478
```

```
~tau_2-->~chi_1-,nu_tau;                0.0480851          0.193657
#
# Parent: ~g  Mass (GeV): 604.485  Total Width (GeV): 4.92374
#                                       Partial Width/GeV  BR
~g->~d_L,dbar;                          0.0909972          0.0184813
~g->~u_L,ubar;                          0.121301           0.0246359
~g->~s_L,sbar;                          0.0909969          0.0184813
~g->~c_L,cbar;                          0.121195           0.0246145
~g->~b_1,bbar;                          0.557065           0.113139
~g->~t_1,tbar;                          0.246285           0.05002
~g->~d_R,dbar;                          0.244699           0.0496979
~g->~u_R,ubar;                          0.242752           0.0493024
~g->~s_R,sbar;                          0.244732           0.0497045
~g->~c_R,cbar;                          0.242796           0.0493114
~g->~b_2,bbar;                          0.257781           0.0523548
~g->~d_Lbar,d;                          0.0909972          0.0184813
~g->~u_Lbar,u;                          0.121301           0.0246359
~g->~s_Lbar,s;                          0.0909969          0.0184813
~g->~c_Lbar,c;                          0.121195           0.0246145
~g->~b_1bar,b;                          0.557065           0.113139
~g->~t_1bar,t;                          0.246285           0.05002
~g->~d_Rbar,d;                          0.244699           0.0496979
~g->~u_Rbar,u;                          0.242752           0.0493024
~g->~s_Rbar,s;                          0.244732           0.0497045
~g->~c_Rbar,c;                          0.242796           0.0493114
~g->~b_2bar,b;                          0.257781           0.0523548
~g->~chi_2-,t,bbar;                     0.000551254        0.000111958
~g->~chi_1+,tbar,b;                     0.000716014        0.000145421
~g->~chi_2+,tbar,b;                     0.000551254        0.000111958
~g->~chi_1-,t,bbar;                     0.000716014        0.000145421
#
# Parent: ~chi_20  Mass (GeV): 180.576  Total Width (GeV): 0.0212547
#                                       Partial Width/GeV  BR
~chi_20->~e_R-,e+;                      0.000659992        0.0310515
~chi_20->~e_R+,e-;                      0.000659992        0.0310515
~chi_20->~mu_R-,mu+;                    0.000661677        0.0311308
~chi_20->~mu_R+,mu-;                    0.000661677        0.0311308
~chi_20->~tau_1-,tau+;                  0.00925854         0.435599
~chi_20->~tau_1+,tau-;                  0.00925854         0.435599
~chi_20->~chi_10,d,dbar;                4.78696e-06        0.000225219
~chi_20->~chi_10,u,ubar;                3.58543e-06        0.000168689
~chi_20->~chi_10,s,sbar;                4.78693e-06        0.000225217
~chi_20->~chi_10,c,cbar;                3.57799e-06        0.000168338
~chi_20->~chi_10,b,bbar;                5.05674e-06        0.000237911
~chi_20->~chi_10,e-,e+;                 6.36854e-06        0.000299629
~chi_20->~chi_10,nu_e,nu_ebar;          1.76114e-05        0.000828587
~chi_20->~chi_10,mu-,mu+;               6.36398e-06        0.000299415
```

```
~chi_20->~chi_10,nu_mu,nu_mubar;          1.76167e-05          0.000828837
~chi_20->~chi_10,tau-,tau+;               5.19942e-06          0.000244624
~chi_20->~chi_10,nu_tau,nu_taubar;        1.93629e-05          0.000910993
#
# Parent: ~chi_30  Mass (GeV): 363.907    Total Width (GeV): 2.01012
#                                         Partial Width/GeV    BR
~chi_30->~e_L-,e+;                        0.00120245           0.000598199
~chi_30->~e_L+,e-;                        0.00120245           0.000598199
~chi_30->~e_R-,e+;                        0.00243756           0.00121265
~chi_30->~e_R+,e-;                        0.00243756           0.00121265
~chi_30->~nu_eL,nu_ebar;                  0.00644468           0.00320612
~chi_30->~nu_eLbar,nu_e;                  0.00644468           0.00320612
~chi_30->~mu_L-,mu+;                      0.00123363           0.000613713
~chi_30->~mu_L+,mu-;                      0.00123363           0.000613713
~chi_30->~mu_R-,mu+;                      0.00248477           0.00123613
~chi_30->~mu_R+,mu-;                      0.00248477           0.00123613
~chi_30->~nu_muL,nu_mubar;                0.00644483           0.0032062
~chi_30->~nu_muLbar,nu_mu;                0.00644483           0.0032062
~chi_30->~tau_1-,tau+;                    0.0102832            0.00511572
~chi_30->~tau_1+,tau-;                    0.0102832            0.00511572
~chi_30->~tau_2-,tau+;                    0.0135199            0.00672592
~chi_30->~tau_2+,tau-;                    0.0135199            0.00672592
~chi_30->~nu_tauL,nu_taubar;              0.00648979           0.00322857
~chi_30->~nu_tauLbar,nu_tau;              0.00648979           0.00322857
~chi_30->~chi_10,Z0;                      0.228876             0.113862
~chi_30->~chi_20,Z0;                      0.431301             0.214565
~chi_30->~chi_1-,W+;                      0.591362             0.294193
~chi_30->~chi_1+,W-;                      0.591362             0.294193
~chi_30->~chi_10,h0;                      0.0416117            0.0207011
~chi_30->~chi_20,h0;                      0.0245225            0.0121995
#
# Parent: ~chi_40  Mass (GeV): 381.248    Total Width (GeV): 2.71974
#                                         Partial Width/GeV    BR
~chi_40->~e_L-,e+;                        0.0265988            0.0097799
~chi_40->~e_L+,e-;                        0.0265988            0.0097799
~chi_40->~e_R-,e+;                        0.00997223           0.00366661
~chi_40->~e_R+,e-;                        0.00997223           0.00366661
~chi_40->~nu_eL,nu_ebar;                  0.0684517            0.0251685
~chi_40->~nu_eLbar,nu_e;                  0.0684517            0.0251685
~chi_40->~mu_L-,mu+;                      0.0266246            0.0097894
~chi_40->~mu_L+,mu-;                      0.0266246            0.0097894
~chi_40->~mu_R-,mu+;                      0.0100166            0.00368291
~chi_40->~mu_R+,mu-;                      0.0100166            0.00368291
~chi_40->~nu_muL,nu_mubar;                0.0684531            0.025169
~chi_40->~nu_muLbar,nu_mu;                0.0684531            0.025169
~chi_40->~tau_1-,tau+;                    0.00698504           0.00256828
~chi_40->~tau_1+,tau-;                    0.00698504           0.00256828
```

```
~chi_40->~tau_2-,tau+;                    0.0441713          0.016241
~chi_40->~tau_2+,tau-;                    0.0441713          0.016241
~chi_40->~nu_tauL,nu_taubar;              0.0688748          0.0253241
~chi_40->~nu_tauLbar,nu_tau;              0.0688748          0.0253241
~chi_40->~chi_10,Z0;                      0.0572175          0.0210379
~chi_40->~chi_20,Z0;                      0.0513444          0.0188784
~chi_40->~chi_1-,W+;                      0.695609           0.255763
~chi_40->~chi_1+,W-;                      0.695609           0.255763
~chi_40->~chi_10,h0;                      0.180653           0.0664228
~chi_40->~chi_20,h0;                      0.378163           0.139044
~chi_40->~chi_10,W+,W-;                   0.000846196        0.000311131
#
# Parent: ~chi_1+  Mass (GeV): 180.169  Total Width (GeV): 0.113504
#                                         Partial Width/GeV  BR
~chi_1+->~tau_1+,nu_tau;                  0.112683           0.992766
~chi_1+->~chi_10,W+;                      0.000711215        0.00626597
~chi_1+->~chi_10,nu_e,e+;                 3.76262e-05        0.000331496
~chi_1+->~chi_10,nu_mu,mu+;               3.76274e-05        0.000331506
~chi_1+->~chi_10,nu_tau,tau+;             3.4675e-05         0.000305494
#
# Parent: ~chi_2+  Mass (GeV): 382.332  Total Width (GeV): 4.56081
#                                         Partial Width/GeV  BR
~chi_2+->~nu_eL,e+;                       0.0514269          0.0112758
~chi_2+->~nu_muL,mu+;                     0.0514942          0.0112906
~chi_2+->~nu_tauL,tau+;                   0.0706154          0.0154831
~chi_2+->~e_L+,nu_e;                      0.136879           0.0300119
~chi_2+->~mu_L+,nu_mu;                    0.136862           0.0300082
~chi_2+->~tau_1+,nu_tau;                  2.01598            0.442023
~chi_2+->~tau_2+,nu_tau;                  0.516906           0.113337
~chi_2+->~chi_1+,Z0;                      0.627357           0.137554
~chi_2+->~chi_10,W+;                      0.172786           0.0378849
~chi_2+->~chi_20,W+;                      0.75308            0.16512
~chi_2+->~chi_1+,h0;                      0.0259849          0.00569744
~chi_2+->~chi_1+,b,bbar;                  0.000763643        0.000167436
~chi_2+->~chi_1+,nu_tau,nu_taubar;        0.000673657        0.000147706
#
# Parent: h0  Mass (GeV): 110.761  Total Width (GeV): 0.00603692
#                                         Partial Width/GeV  BR
h0->b,bbar;                               0.00492594         0.815969
h0->g,g;                                  0.000696727        0.115411
h0->tau-,tau+;                            0.000296023        0.0490355
h0->W-,nu_tau,tau+;                       6.35102e-06        0.00105203
h0->W+,nu_taubar,tau-;                    6.351e-06          0.00105203
h0->Z0,d,dbar;                            9.6548e-07         0.000159929
h0->Z0,s,sbar;                            9.6521e-07         0.000159885
h0->W+,ubar,d;                            1.85185e-05        0.00306754
h0->W+,cbar,d;                            9.71473e-07        0.000160922
```

```
h0->W+,s,ubar;                          9.80777e-07          0.000162463
h0->W+,cbar,s;                          1.83285e-05          0.00303607
h0->W+,nu_ebar,e-;                      6.49986e-06          0.00107668
h0->W+,nu_mubar,mu-;                    6.4996e-06           0.00107664
h0->W-,u,dbar;                          1.85185e-05          0.00306754
h0->W-,sbar,u;                          9.80777e-07          0.000162463
h0->W-,c,dbar;                          9.71473e-07          0.000160922
h0->W-,c,sbar;                          1.83285e-05          0.00303607
h0->W-,nu_e,e+;                         6.49986e-06          0.00107668
h0->W-,nu_mu,mu+;                       6.4996e-06           0.00107664
#
# Parent: H0  Mass (GeV): 399.111  Total Width (GeV): 1.65108
#                                       Partial Width/GeV    BR
H0->~e_R-,~e_R+;                        0.000386415          0.000234038
H0->~nu_eL,~nu_eLbar;                   0.000931403          0.000564119
H0->~mu_R-,~mu_R+;                      0.00038631           0.000233975
H0->~nu_muL,~nu_muLbar;                 0.000931504          0.00056418
H0->~tau_1-,~tau_1+;                    0.00478719           0.00289944
H0->~tau_2-,~tau_1+;                    0.00425196           0.00257527
H0->~tau_2+,~tau_1-;                    0.00425196           0.00257527
H0->~nu_tauL,~nu_tauLbar;               0.000961884          0.00058258
H0->~chi_10,~chi_10;                    0.0163311            0.00989117
H0->~chi_1+,~chi_1-;                    0.0360143            0.0218126
H0->~chi_20,~chi_10;                    0.0477795            0.0289384
H0->~chi_20,~chi_20;                    0.0134134            0.00812406
H0->h0,h0;                              0.0100872            0.00610945
H0->b,bbar;                             1.38443              0.838501
H0->t,tbar;                             0.0362769            0.0219717
H0->tau-,tau+;                          0.0826528            0.05006
H0->Z0,Z0;                              0.00159576           0.000966499
H0->W+,W-;                              0.00337624           0.00204487
H0->Z0,b,bbar;                          0.000760118          0.000460378
H0->W-,t,bbar;                          0.000600221          0.000363533
H0->W-,nu_tau,tau+;                     0.000342802          0.000207623
H0->W+,tbar,b;                          0.000302087          0.000182964
H0->W+,nu_taubar,tau-;                  0.00022523           0.00136414
#
# Parent: A0  Mass (GeV): 398.728  Total Width (GeV): 2.08137
#                                       Partial Width/GeV    BR
A0->~tau_2-,~tau_1+;                    0.00620443           0.00298094
A0->~tau_2+,~tau_1-;                    0.00620443           0.00298094
A0->~chi_10,~chi_10;                    0.0250866            0.0120529
A0->~chi_1+,~chi_1-;                    0.24582              0.118105
A0->~chi_20,~chi_10;                    0.109059             0.0523978
A0->~chi_20,~chi_20;                    0.0946477            0.0454738
A0->h0,Z0;                              0.0027737            0.00133263
A0->b,bbar;                             1.38796              0.66685
```

```
A0->t,tbar;                                  0.116144          0.0558018
A0->tau-,tau+;                               0.0828336         0.0397977
A0->Z0,b,bbar;                               0.00301702        0.00144954
A0->W-,t,bbar;                               0.000581149       0.000279215
A0->W-,nu_tau,tau+;                          0.000341401       0.000164027
A0->W+,tbar,b;                               0.000470145       0.000225883
A0->W+,nu_taubar,tau-;                       0.000224475       0.00010785
#
# Parent: H+  Mass (GeV): 407.043  Total Width (GeV): 1.35418
#                                            Partial Width/GeV  BR
H+->~nu_eL,~e_L+;                            0.000785542       0.000580088
H+->~nu_muL,~mu_L+;                          0.000785131       0.000579785
H+->~nu_tauL,~tau_1+;                        0.016163          0.0119356
H+->~chi_1+,~chi_10;                         0.14297           0.105577
H+->~chi_1+,~chi_20;                         0.00109307        0.000807186
H+->h0,W+;                                   0.00311512        0.00230037
H+->t,bbar;                                  1.09972           0.812095
H+->nu_tau,tau+;                             0.084581          0.0624593
H+->Z0,t,bbar;                               0.000395819       0.000292295
H+->Z0,nu_tau,tau+;                          0.000229523       0.000169493
H+->h0,t,bbar;                               0.000310126       0.000229014
H+->W+,b,bbar;                               0.00346686        0.00256012
H+->W+,tau-,tau+;                            0.000561561       0.000414688
```

B.4.2 Minimal Universal Extra Dimensions

The output shown here is a result of running Herwig++ for the MUED model with $R^{-1} = 500\,\text{GeV}$ and $\Lambda R = 20$, the mass spectrum shown in Table 3.2. Again, any decay modes with a branching fraction lower than 1×10^{-4} are not written out.

```
# Parent: KK1_d_L  Mass (GeV): 588.268  Total Width (GeV): 0.181431
#                                       Partial Width/GeV  BR
KK1_d_L->KK1_W-,u;                      0.112386           0.61944
KK1_d_L->KK1_W-,c;                      0.0059445          0.0327645
KK1_d_L->KK1_gamma,d;                   0.00118795         0.00654766
KK1_d_L->KK1_Z0,d;                      0.0600085          0.33075
KK1_d_L->KK1_H-,u;                      0.00190457         0.0104975
#
# Parent: KK1_u_L  Mass (GeV): 588.268  Total Width (GeV): 0.188582
#                                       Partial Width/GeV  BR
KK1_u_L->KK1_W+,d;                      0.112386           0.595951
KK1_u_L->KK1_W+,s;                      0.00595237         0.0315637
KK1_u_L->KK1_gamma,u;                   0.0124368          0.065949
```

```
KK1_u_L->KK1_Z0,u;                          0.0559028          0.296437
KK1_u_L->KK1_H+,d;                          0.00190457         0.0100994
#
# Parent: KK1_s_L  Mass (GeV): 588.268  Total Width (GeV): 0.181213
#                                         Partial Width/GeV  BR
KK1_s_L->KK1_W-,u;                          0.00595238         0.0328475
KK1_s_L->KK1_W-,c;                          0.112159           0.618936
KK1_s_L->KK1_gamma,s;                       0.00118795         0.00655556
KK1_s_L->KK1_Z0,s;                          0.0600083          0.331149
KK1_s_L->KK1_H-,c;                          0.00190494         0.0105122
#
# Parent: KK1_c_L  Mass (GeV): 588.269  Total Width (GeV): 0.18859
#                                         Partial Width/GeV  BR
KK1_c_L->KK1_W+,d;                          0.00594646         0.0315312
KK1_c_L->KK1_W+,s;                          0.112196           0.59492
KK1_c_L->KK1_W+,b;                          0.000201073        0.00106619
KK1_c_L->KK1_gamma,c;                       0.0124357          0.0659405
KK1_c_L->KK1_Z0,c;                          0.0558883          0.296349
KK1_c_L->KK1_H+,s;                          0.00192244         0.0101938
#
# Parent: KK1_b_1  Mass (GeV): 588.283  Total Width (GeV): 0.0612287
#                                         Partial Width/GeV  BR
KK1_b_1->KK1_W-,c;                          0.000201783        0.00329557
KK1_b_1->KK1_gamma,b;                       0.00118683         0.0193835
KK1_b_1->KK1_Z0,b;                          0.05984            0.977321
#
# Parent: KK1_t_1  Mass (GeV): 574.204  Total Width (GeV): 0.299178
#                                         Partial Width/GeV  BR
KK1_t_1->KK1_W+,s;                          0.000108355        0.000362176
KK1_t_1->KK1_W+,b;                          0.0650458          0.217415
KK1_t_1->KK1_H+,b;                          0.234023           0.782222
#
# Parent: KK1_d_R  Mass (GeV): 574.899  Total Width (GeV): 0.0157198
#                                         Partial Width/GeV  BR
KK1_d_R->KK1_gamma,d;                       0.0156783          0.997358
KK1_d_R->KK1_Z0,d;                          4.15239e-05        0.00264151
#
# Parent: KK1_u_R  Mass (GeV): 576.314  Total Width (GeV): 0.0651352
#                                         Partial Width/GeV  BR
KK1_u_R->KK1_gamma,u;                       0.0649574          0.99727
KK1_u_R->KK1_Z0,u;                          0.000177803        0.00272975
#
# Parent: KK1_s_R  Mass (GeV): 574.899  Total Width (GeV): 0.0157198
#                                         Partial Width/GeV  BR
KK1_s_R->KK1_gamma,s;                       0.0156783          0.997358
KK1_s_R->KK1_Z0,s;                          4.15238e-05        0.0026415
#
```

```
# Parent: KK1_c_R  Mass (GeV): 576.315  Total Width (GeV): 0.0651271
#                                       Partial Width/GeV   BR
KK1_c_R->KK1_gamma,c;                   0.0649494           0.997271
KK1_c_R->KK1_Z0,c;                      0.000177724         0.00272888
#
# Parent: KK1_b_2  Mass (GeV): 574.914  Total Width (GeV): 0.0156983
#                                       Partial Width/GeV   BR
KK1_b_2->KK1_gamma,b;                   0.015657            0.997369
KK1_b_2->KK1_Z0,b;                      4.13069e-05         0.0026313
#
# Parent: KK1_t_2  Mass (GeV): 600.428  Total Width (GeV): 1.73415e-06
#                                       Partial Width/GeV   BR
KK1_t_2->KK1_t_1,d,dbar;                1.72013e-07         0.0991921
KK1_t_2->KK1_t_1,u,ubar;                1.33395e-07         0.0769225
KK1_t_2->KK1_t_1,s,sbar;                1.71991e-07         0.0991789
KK1_t_2->KK1_t_1,c,cbar;                1.2939e-07          0.0746131
KK1_t_2->KK1_t_1,b,bbar;                1.28003e-07         0.0738133
KK1_t_2->KK1_t_1,e-,e+;                 3.90212e-08         0.0225017
KK1_t_2->KK1_t_1,nu_e,nu_ebar;          7.76399e-08         0.0447713
KK1_t_2->KK1_t_1,mu-,mu+;               3.90127e-08         0.0224968
KK1_t_2->KK1_t_1,nu_mu,nu_mubar;        7.76399e-08         0.0447713
KK1_t_2->KK1_t_1,tau-,tau+;             3.64907e-08         0.0210425
KK1_t_2->KK1_t_1,nu_tau,nu_taubar;      7.76399e-08         0.0447713
KK1_t_2->KK1_gamma,W+,s;                1.20238e-09         0.0006934
KK1_t_2->KK1_gamma,W+,b;                6.50707e-07         0.375232
#
# Parent: KK1_e_L-  Mass (GeV): 514.784  Total Width (GeV): 0.0019425
#                                       Partial Width/GeV   BR
KK1_e_L-->KK1_gamma,e-;                 0.0019425           1
#
# Parent: KK1_nu_eL  Mass (GeV): 514.784  Total Width (GeV): 9.596e-04
#                                       Partial Width/GeV   BR
KK1_nu_eL->KK1_gamma,nu_e;              0.00095392          0.994058
KK1_nu_eL->KK1_H+,e-;                   5.70204e-06         0.00594196
#
# Parent: KK1_mu_L-  Mass (GeV): 514.784  Total Width (GeV): 0.00194244
#                                       Partial Width/GeV   BR
KK1_mu_L-->KK1_gamma,mu-;               0.00194244          1
#
# Parent: KK1_nu_muL  Mass (GeV): 514.784  Total Width (GeV): 9.596e-04
#                                       Partial Width/GeV   BR
KK1_nu_muL->KK1_gamma,nu_mu;            0.00095392          0.99406
KK1_nu_muL->KK1_H+,mu-;                 5.69974e-06         0.00593958
#
# Parent: KK1_tau_1-  Mass (GeV): 514.787  Total Width (GeV): 0.001927
#                                       Partial Width/GeV   BR
KK1_tau_1-->KK1_gamma,tau-;             0.00192699          1
```

```
#
# Parent: KK1_nu_tauL  Mass (GeV): 514.784  Total Width (GeV): 9.589e-04
#                                    Partial Width/GeV   BR
KK1_nu_tauL->KK1_gamma,nu_tau;       0.00095392          0.994777
KK1_nu_tauL->KK1_H+,tau-;            5.00876e-06         0.00522329
#
# Parent: KK1_e_R-  Mass (GeV): 504.245  Total Width (GeV): 0.0003223
#                                    Partial Width/GeV   BR
KK1_e_R-->KK1_gamma,e-;              0.0003223           1
#
# Parent: KK1_mu_R-  Mass (GeV): 504.245  Total Width (GeV): 0.0003221
#                                    Partial Width/GeV   BR
KK1_mu_R-->KK1_gamma,mu-;            0.00032213          1
#
# Parent: KK1_tau_2-  Mass (GeV): 504.248  Total Width (GeV): 2.707e-04
#                                    Partial Width/GeV   BR
KK1_tau_2-->KK1_gamma,tau-;          0.000270755         1
#
# Parent: KK1_g  Mass (GeV): 626.318  Total Width (GeV): 2.88308
#                                    Partial Width/GeV   BR
KK1_g->KK1_d_Lbar,d;                 0.10588             0.0367245
KK1_g->KK1_d_L,dbar;                 0.10588             0.0367245
KK1_g->KK1_u_Lbar,u;                 0.10588             0.0367245
KK1_g->KK1_u_L,ubar;                 0.10588             0.0367245
KK1_g->KK1_s_Lbar,s;                 0.105879            0.0367244
KK1_g->KK1_s_L,sbar;                 0.105879            0.0367244
KK1_g->KK1_c_Lbar,c;                 0.105818            0.0367032
KK1_g->KK1_c_L,cbar;                 0.105818            0.0367032
KK1_g->KK1_b_1bar,b;                 0.105164            0.0364761
KK1_g->KK1_b_1,bbar;                 0.105164            0.0364761
KK1_g->KK1_d_Rbar,d;                 0.186519            0.0646943
KK1_g->KK1_d_R,dbar;                 0.186519            0.0646943
KK1_g->KK1_u_Rbar,u;                 0.177069            0.0614164
KK1_g->KK1_u_R,ubar;                 0.177069            0.0614164
KK1_g->KK1_s_Rbar,s;                 0.186518            0.0646942
KK1_g->KK1_s_R,sbar;                 0.186518            0.0646942
KK1_g->KK1_c_Rbar,c;                 0.177008            0.0613953
KK1_g->KK1_c_R,cbar;                 0.177008            0.0613953
KK1_g->KK1_b_2bar,b;                 0.185806            0.064447
KK1_g->KK1_b_2,bbar;                 0.185806            0.064447
#
# Parent: KK1_Z0  Mass (GeV): 535.806  Total Width (GeV): 0.079517
#                                    Partial Width/GeV   BR
KK1_Z0->KK1_e_L+,e-;                 0.00585549          0.0736382
KK1_Z0->KK1_e_L-,e+;                 0.00585549          0.0736382
KK1_Z0->KK1_e_R+,e-;                 0.000160928         0.00202382
KK1_Z0->KK1_e_R-,e+;                 0.000160928         0.00202382
```

```
KK1_Z0->KK1_nu_eLbar,nu_e;                0.00724398          0.0910998
KK1_Z0->KK1_nu_eL,nu_ebar;                0.00724398          0.0910998
KK1_Z0->KK1_mu_L+,mu-;                    0.00585542          0.0736373
KK1_Z0->KK1_mu_L-,mu+;                    0.00585542          0.0736373
KK1_Z0->KK1_mu_R+,mu-;                    0.000160927         0.00202381
KK1_Z0->KK1_mu_R-,mu+;                    0.000160927         0.00202381
KK1_Z0->KK1_nu_muLbar,nu_mu;              0.00724398          0.0910998
KK1_Z0->KK1_nu_muL,nu_mubar;              0.00724398          0.0910998
KK1_Z0->KK1_tau_1+,tau-;                  0.00583315          0.0733572
KK1_Z0->KK1_tau_1-,tau+;                  0.00583315          0.0733572
KK1_Z0->KK1_tau_2+,tau-;                  0.000160647         0.00202029
KK1_Z0->KK1_tau_2-,tau+;                  0.000160647         0.00202029
KK1_Z0->KK1_nu_tauLbar,nu_tau;            0.00724398          0.0910998
KK1_Z0->KK1_nu_tauL,nu_taubar;            0.00724398          0.0910998
#
# Parent: KK1_W+  Mass (GeV): 535.494  Total Width (GeV): 0.0768434
#                                         Partial Width/GeV   BR
KK1_W+->KK1_e_L+,nu_e;                    0.0128157           0.166776
KK1_W+->KK1_nu_eL,e+;                     0.0128157           0.166776
KK1_W+->KK1_mu_L+,nu_mu;                  0.0128157           0.166776
KK1_W+->KK1_nu_muL,mu+;                   0.0128155           0.166774
KK1_W+->KK1_tau_1+,nu_tau;                0.0128121           0.166729
KK1_W+->KK1_nu_tauL,tau+;                 0.0127689           0.166168
#
# Parent: h0  Mass (GeV): 115  Total Width (GeV): 0.00473474
#                                         Partial Width/GeV   BR
h0->b,bbar;                               0.00391647          0.827178
h0->c,cbar;                               0.000349457         0.073807
h0->mu-,mu+;                              8.32848e-07         0.000175902
h0->tau-,tau+;                            0.000235238         0.0496835
h0->s,sbar;                               2.01989e-06         0.00042661
h0->Z0,d,dbar;                            2.46506e-06         0.000520633
h0->Z0,u,ubar;                            1.91163e-06         0.000403746
h0->Z0,s,sbar;                            2.46439e-06         0.000520491
h0->Z0,c,cbar;                            1.81285e-06         0.000382884
h0->Z0,b,bbar;                            1.48516e-06         0.000313673
h0->W+,nu_ebar,e-;                        1.21275e-05         0.00256139
h0->W-,nu_e,e+;                           1.21275e-05         0.00256139
h0->W+,nu_mubar,mu-;                      1.21269e-05         0.00256125
h0->W-,nu_mu,mu+;                         1.21269e-05         0.00256125
h0->W+,nu_taubar,tau-;                    1.19012e-05         0.0025136
h0->W-,nu_tau,tau+;                       1.19012e-05         0.0025136
h0->W-,u,dbar;                            3.45519e-05         0.00729754
h0->W-,sbar,u;                            1.82996e-06         0.000386496
h0->W-,c,dbar;                            1.81623e-06         0.000383596
h0->W-,c,sbar;                            3.42667e-05         0.0072373
h0->W+,ubar,d;                            3.45519e-05         0.00729754
```

```
h0->W+,cbar,d;                          1.81623e-06          0.000383596
h0->W+,s,ubar;                          1.82996e-06          0.000386496
h0->W+,cbar,s;                          3.42667e-05          0.0072373
h0->Z0,nu_e,nu_ebar;                    1.11263e-06          0.000234993
h0->Z0,nu_mu,nu_mubar;                  1.11263e-06          0.000234993
h0->Z0,nu_tau,nu_taubar;                1.11263e-06          0.000234993
#
# Parent: KK1_h0  Mass (GeV): 517.647  Total Width (GeV): 2.00019e-09
#                                       Partial Width/GeV    BR
KK1_h0->KK1_A0,d,dbar;                  3.93394e-10          0.196679
KK1_h0->KK1_A0,u,ubar;                  3.05075e-10          0.152523
KK1_h0->KK1_A0,s,sbar;                  3.92114e-10          0.196039
KK1_h0->KK1_A0,c,cbar;                  1.75939e-10          0.0879614
KK1_h0->KK1_A0,e-,e+;                   8.92416e-11          0.0446166
KK1_h0->KK1_A0,nu_e,nu_ebar;            1.77563e-10          0.088773
KK1_h0->KK1_A0,mu-,mu+;                 8.90203e-11          0.0445059
KK1_h0->KK1_A0,nu_mu,nu_mubar;          1.77563e-10          0.088773
KK1_h0->KK1_A0,tau-,tau+;               2.27158e-11          0.0113568
KK1_h0->KK1_A0,nu_tau,nu_taubar;        1.77563e-10          0.088773
#
# Parent: KK1_A0  Mass (GeV): 512.883  Total Width (GeV): 2.96458e-11
#                                       Partial Width/GeV    BR
KK1_A0->KK1_H+,ubar,d;                  8.47825e-12          0.285985
KK1_A0->KK1_H+,s,ubar;                  4.42929e-13          0.0149407
KK1_A0->KK1_H+,nu_ebar,e-;              2.97586e-12          0.10038
KK1_A0->KK1_H+,nu_mubar,mu-;            2.92587e-12          0.0986941
KK1_A0->KK1_H-,u,dbar;                  8.47825e-12          0.285985
KK1_A0->KK1_H-,sbar,u;                  4.42929e-13          0.0149407
KK1_A0->KK1_H-,nu_e,e+;                 2.97586e-12          0.10038
KK1_A0->KK1_H-,nu_mu,mu+;               2.92587e-12          0.0986941
#
# Parent: KK1_H+  Mass (GeV): 511.076  Total Width (GeV): 7.53157e-07
#                                       Partial Width/GeV    BR
KK1_H+->KK1_mu_R+,nu_mu;                2.65448e-09          0.00352447
KK1_H+->KK1_tau_2+,nu_tau;              7.50176e-07          0.996041
KK1_H+->KK1_gamma,nu_e,e+;              1.09798e-10          0.000145784
KK1_H+->KK1_gamma,nu_mu,mu+;            1.10505e-10          0.000146723
KK1_H+->KK1_gamma,nu_tau,tau+;          1.06934e-10          0.000141981
```

Many of the decay modes above have small branching fractions due to the approximate degeneracy of the MUED mass spectrum, even when radiative corrections have been taken into account. Furthermore, particles such as the $t_1'^{\circ}$ do not have any two-body decay modes at this parameter point and so the three-body decays are a necessary addition if the model is to be used in an event generator.

Appendix C

Technical Details

The general method for simulating BSM physics, described in Chapter 3, is implemented in the Herwig++ event generator. Herwig++ is a new event generator, written in C++, which builds on the experience and knowledge gained from its predecessor HERWIG [29]. The code structure of the BSM physics modules is designed so that the addition of new models is a relatively simple task. The details of this structure will be briefly described here, however for a more detailed description of the program, see Ref. [28]. In the following descriptions we use the term "interface" to refer to a method by which a parameter of a particular class can be altered.

C.1 Code Structure

The ModelGenerator class is responsible for setting up the new MatrixElement objects, which inherit from the GeneralHardME class, and DecayMode objects for a new physics model. Helper classes aid in the creation of these objects, they are:

Class Name	Hard Process
MEff2ff	Fermion fermion to fermion fermion.
MEff2ss	Fermion fermion to scalar scalar.
MEff2vs	Fermion fermion to vector scalar.
MEff2vv	Fermion fermion to vector vector.
MEfv2fs	Fermion vector to fermion scalar.
MEfv2vf	Fermion vector to vector fermion.
MEvv2ff	Vector vector to fermion fermion.
MEvv2ss	Vector vector to scalar scalar.
MEvv2vv	Vector vector to vector vector.

Table C.1: The general hard process matrix elements, based on spin structures, implemented in Herwig++.

HardProcessConstructor the HardProcessConstructor is responsible for creating the diagrams for the requested processes and constructing the appropriate GeneralHardME object(s);

ResonantProcessConstructor the ResonantProcessConstructor is of a similar design to the HardProcessConstructor but it only constructs the resonant diagrams for a process;

DecayConstructor the DecayConstructor stores a collection of objects that inherit from the NBodyDecayConstructor class. Each of these is responsible for constructing all of the decay modes for the $1 \to N$ decays.

The matrix element classes all inherit from the GeneralHardME class and implement the matrix element for a particular spin configuration. The classes inheriting from the GeneralHardME class and the spin structures they implement are given in Table C.1.

All of the decayer classes inherit from either the GeneralTwoBodyDecayer or the GeneralThreeBodyDecayer class and each is responsible for calculating the value

Class Name	Decay
FFSDecayer	Fermion to fermion scalar decay.
FFVDecayer	Fermion to fermion vector decay.
FFVCurrentDecayer	Fermion to fermion vector decay with the vector off-shell and decaying via a weak current from Ref. [28].
FtoFFFDecayer	Fermion to three fermion decay.
FtoFVVDecayer	Fermion to fermion and two vector decay.
SFFDecayer	Scalar to fermion fermion decay.
SSSDecayer	Scalar to two scalar decay.
SSVDecayer	Scalar to scalar vector decay.
SVVDecayer	Scalar to two vector decay.
SVVLoopDecayer	Scalar to two vector decay via a loop.
StoSFFDecayer	Scalar to scalar and two fermion decay.
StoFFVDecayer	Scalar to two fermion and vector decay.
VFFDecayer	Vector to two fermion decay.
VSSDecayer	Vector to two scalar decay.
VVVDecayer	Vector to two vector decay.
VtoFFVDecayer	Vector to two fermion and vector decay.
TFFDecayer	Tensor to two fermion decay.
TSSDecayer	Tensor to two scalar decay
TVVDecayer	Tensor to two vector decay.

Table C.2: The general decay classes based on spin structures implemented in Herwig++.

of the matrix element for that particular set of spins. There is also a GeneralTwoBodyCurrentDecayer class for decay modes created with the WeakCurrentDecayConstructor class. The Decayer classes implemented in Herwig++ and the types of decay they implement are given in Table C.2.

The specification of the particles involved in the hard process is achieved through the **Incoming** and **Outgoing** interfaces of the HardProcessConstructor. Both interfaces are lists of ParticleData objects. The switch **IncludeEW** can be set to **No** to include only the strong coupling diagrams.

In order to pass spin correlations through the decay stage, DecayIntegrator objects must be created. This is achieved by populating a list held in the ModelGenerator class, which can be accessed through the **DecayParticles** interface. The particles in this list will have spin correlation information passed along when their decays are generated. If a decay table is read in for a SUSY model then the **CreateDecayModes** interface should be set to **No** so that only the decay modes listed in the externally generated decay table are created[1]. For all other models the possible decay modes are also created from the particles in the **DecayParticles** list.

In addition to the code that handles the calculation of the matrix elements for the decays and scattering cross sections, each model requires a number of classes to implement the model.

The Standard Model is implemented in the StandardModel class, which inherits from the StandardModelBase class of ThePEG and implements access to the helicity Vertex classes and some additional couplings, such as the running mass, used by Herwig++. The Vertex classes that implement the Standard Model interactions are given in Table C.3.

The structure of the implementation of the MSSM in Herwig++ is designed to allow extended SUSY models to be added in the future. Therefore the SusyBase class, which inherits from the StandardModel class, is designed to read in the SLHA files specifying the SUSY spectrum. The details of the MSSM are implemented in the MSSM class, which inherits from the SusyBase class. The Vertex classes for the MSSM are given in Table C.4. A spectrum file in SLHA format [64, 65] must be supplied or the MSSM model cannot be used.

[1]If a decay table is being used with a SUSY model then the DecayParticles list must still be populated so that the decays will have spin correlation information included.

Class	Interaction
SMFFGVertex	Interaction of the gluon with the SM fermions
SMFFPVertex	Interaction of the photon with the SM fermions
SMFFWVertex	Interaction of the $W^{\pm}$ boson with the SM fermions
SMFFZVertex	Interaction of the Z^0 boson with the SM fermions
SMFFHVertex	Interaction of the Higgs boson with the SM fermions
SMGGGVertex	Triple gluon vertex
SMGGGGVertex	Four gluon vertex
SMWWWVertex	Triple electroweak gauge boson vertex
SMWWWWVertex	Four electroweak gauge boson vertex
SMWWHVertex	Interaction of the Higgs boson with the electroweak gauge bosons
SMHGGVertex	Higgs boson coupling to two gluons via quark loops
SMHPPVertex	Higgs boson coupling to two photons via fermion and boson loops

Table C.3: Herwig++ Vertex classes for the Standard Model.

Class	Interaction
SSNFSVertex	Neutralino with a SM fermion and a sfermion
SSCFSVertex	Chargino with a SM fermion and a sfermion
SSGFSVertex	Gluino with a quark and squark
SSNNZVertex	A pair of neutralinos with a Z^0 boson
SSCCZVertex	A pair of charginos with a Z^0 boson
SSCNWVertex	Chargino with a neutralino and a $W^{\pm}$ boson
SSGSGSGVertex	SM gluon with a pair of gluinos
SSGSSVertex	SM gluon with a pair of squarks
SSWSSVertex	SM gauge boson with a pair of sfermions
SSFFHVertex	A pair of SM fermions with a Higgs boson
SSWHHVertex	SM electroweak gauge bosons with a pair of Higgs bosons
SSWWHVertex	A pair of gauge bosons with a Higgs boson
SSGOGOHVertex	A pair of gauginos with a Higgs boson
SSHSFSFVertex	A Higgs boson with a pair of sfermions
SSHHHVertex	Triple Higgs boson self coupling
SSHGGVertex	A Higgs boson with a pair of gluons via quark and squark loops
SSGGSQSQVertex	A pair of gluons with a pair of squarks

Table C.4: Herwig++ Vertex classes for the MSSM.

Class	Interaction
RSModelFFGRVertex	Coupling of the graviton to SM fermions
RSModelSSGRVertex	Coupling of the graviton to the Higgs boson
RSModelFFVGRVertex	Coupling of the graviton to two SM fermions and a gauge boson
RSModelVVGRVertex	Coupling of the graviton to two gauge bosons
RSModelVVVGRVertex	Coupling of the graviton to three gauge bosons

Table C.5: Herwig++ Vertex classes for the Randall-Sundrum model.

Class	Interaction
UEDF1F1P0Vertex	SM photon with a pair of KK-1 fermions
UEDF1F1W0Vertex	SM $W^{\pm}$ boson with a pair of KK-1 fermions
UEDF1F1Z0Vertex	SM Z^0 boson with a pair of KK-1 fermions
UEDF1F1G0Vertex	SM gluon with a pair of KK-1 fermions
UEDF1F0W1Vertex	KK-1 fermion with an EW KK-1 boson and a SM fermion
UEDF1F0G1Vertex	KK-1 fermion with a KK-1 gluon and a SM fermion
UEDF1F0H1Vertex	KK-1 fermion with a KK-1 Higgs boson and a SM fermion
UEDP0H1H1Vertex	SM photon with a pair of KK-1 charged Higgs boson
UEDW0W1W1Vertex	A pair of KK-1 gauge bosons with a SM $W^{\pm}$ or Z^0 boson
UEDG1G1G0Vertex	A pair of KK-1 gluons with a SM gluon
UEDG0G0G1G1Vertex	A pair of SM gluons with a pair of KK-1 gluons
UEDW0A1H1Vertex	SM $W^{\pm}$ boson with a KK-1 charged Higgs boson and a KK-1 pseudoscalar Higgs boson
UEDZ0H1H1Vertex	SM Z^0 boson with a pair of KK-1 charged Higgs boson
UEDZ0A1h1Vertex	SM Z^0 boson with a KK-1 pseudoscalar Higgs boson and a KK-1 scalar Higgs boson

Table C.6: Herwig++ Vertex classes for the MUED model.

The RSModel class inherits from the StandardModel class and implements the calculations needed for the Randall-Sundrum model. We have only implemented the vertices that are phenomenologically relevant and therefore some four-point vertices that are not important for resonance graviton production are not included. The Vertex classes implemented for the Randall-Sundrum model are given in Table C.5.

Class	Interaction
LHTPFFPVertex	Interaction of an SM photon or a heavy T-odd photon with a pair of fermions
LHTPFFGVertex	Interaction of an SM gluon with a pair of fermions
LHTPFFWVertex	Interaction of an SM $W^{\pm}$ boson or a T-odd $W_H^{\pm}$ boson with a pair of fermions
LHTPFFZVertex	Interaction of an SM Z^0 boson or a T-odd Z_H^0 boson with a pair of fermions
LHTPFFHVertex	Interaction of a Higgs boson with a pair of fermions
LHTPWWWVertex	Triple electroweak gauge boson vertex for both SM and T-odd particles
LHTPWWWVertex	Quartic electroweak gauge boson vertex for both SM and T-odd particles
LHTPWWHVertex	Interaction of two electroweak gauge bosons, SM and T-odd, with a Higgs field
LHTPWHHVertex	Interaction of an electroweak gauge boson, SM and T-odd, with a pair of Higgs bosons
LHTPHHHVertex	Triple Higgs boson vertex

Table C.7: Herwig++ Vertex classes for the Littlest Higgs model with T-parity.

Two parameters can be controlled in the Randall-Sundrum model; the cutoff Λ_π and the mass of the graviton. The default mass of the graviton is 500 GeV and this can be changed via the **NominalMass** interface of its ParticleData object. The cutoff is set via the **Lambda_pi** interface of the RSModel object and has a default value of 10 TeV.

The Minimal Universal Extra Dimensions model is implemented in the UEDBase class, which inherits from the StandardModel class and implements the calculation of the parameters of the model. The Vertex classes for the MUED model are given in Table C.6.

There are three parameters that can be set to control the UED model: the inverse of the radius of compactification R^{-1}; the cutoff scale Λ; and the mass of

the Higgs boson at the boundary of the compactified dimension $\bar{m}_h$. These are controlled through the interfaces:

- **InverseRadius** - the value of R^{-1}, the default value is 500 GeV;
- **LambdaR** - the dimensionless number ΛR, the default value is 20;
- **HiggsBoundaryMass** - the value of the Higgs boson mass at the boundary, the default value is 0 GeV.

The Littlest Higgs model with T-parity is implemented in the LHTPModel class, which inherits from the StandardModel class and implements the calculation of the parameters for the model. The Vertex classes for the LHT are given in Table C.7.

There are three parameters that can be set to control the LHT: the scale of the non-linear sigma model f; the top quark mixing angle $\sin\alpha$; and a Yukawa like parameter κ which controls the mass of the fermions odd under the action of T-parity. These are controlled through the interfaces:

- **f** - the value of f, the default value is 10 TeV;
- **SinAlpha** - the value of $\sin\alpha$, the default value is $1/\sqrt{2}$;
- **Kappa** - the value of κ, the default is 1.

Appendix D

Feynman Rules

D.1 Minimal Supersymmetric Standard Model

We give the Feynman rules for the CP, R-parity and flavour conserving MSSM following the conventions in Ref. [85–87]. The sfermion mixing matrices are denoted by $Q^k_{\alpha\beta}$ and $L^k_{\alpha\beta}$ for the squarks and leptons respectively where k is the generation number, α the left/right eigenstate and β the mass eigenstate. N_{ij}, U_{ij} and V_{ij} are the neutralino and chargino mixing matrices respectively.

D.1.1 Gauge Boson Interactions

A Standard Model gauge boson interacts with a pair of sfermions, a gauge boson and a Higgs boson, a pair of Higgs bosons and a pair of gauginos through the three-point perturbative vertices defined in Figs. D.1–D.4 and Tables D.1–D.2. There is also a quartic coupling between a pair of gluons and a pair of squarks, defined in Fig. D.5.

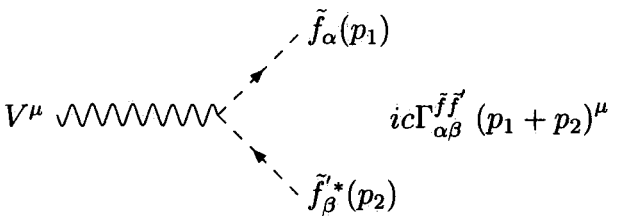

Figure D.1: Feynman rule for the interaction of a gauge boson with a pair of sfermions. The definition of Γ for the various types of gauge boson and sfermion is given in Table D.1. The momenta are to be taken as in the direction of the arrows.

V^μ	$\tilde{f}\tilde{f}'$	c	$\Gamma^{\tilde{f}\tilde{f}'}_{\alpha\beta}$
γ	$\tilde{q}\tilde{q}'$	$-ee_q$	$\delta^{\tilde{q}\tilde{q}'}_{\alpha\beta}$
γ	$\tilde{l}\tilde{l}'$	e	$\delta^{\tilde{l}\tilde{l}'}_{\alpha\beta}$
g	$\tilde{q}\tilde{q}'$	$-gt^a$	$\delta^{\tilde{q}\tilde{q}'}_{\alpha\beta}$
Z^0	$\tilde{u}_\alpha\tilde{u}_\beta$	$\frac{g}{\cos\theta_W}$	$\frac{1}{2}\left(-Q^{2i}_{1\alpha}Q^{2i}_{1\beta}+2e_u\sin^2\theta_W\delta_{\alpha\beta}\right)$
Z^0	$\tilde{d}_\alpha\tilde{d}_\beta$	$\frac{g}{\cos\theta_W}$	$\frac{1}{2}\left(Q^{2i-1}_{1\alpha}Q^{2i-1}_{1\beta}+2e_d\sin^2\theta_W\delta_{\alpha\beta}\right)$
Z^0	$\tilde{l}_\alpha\tilde{l}_\beta$	$\frac{g}{\cos\theta_W}$	$\frac{1}{2}\left(L^{2i-1}_{1\alpha}L^{2i-1}_{1\beta}-2\sin^2\theta_W\delta_{\alpha\beta}\right)$
Z^0	$\tilde{\nu}_\alpha\tilde{\nu}_\beta$	$\frac{g}{\cos\theta_W}$	$-\frac{1}{2}\delta_{11}$
W^-	$\tilde{q}_\alpha\tilde{q}'_\beta$	$-\frac{g}{\sqrt{2}}$	$Q^{2i}_{1\alpha}Q^{2i-1}_{1\beta}$
W^-	$\tilde{\nu}\tilde{l}_\beta$	$-\frac{g}{\sqrt{2}}$	$L^{2i-1}_{1\beta}$

Table D.1: Couplings for the gauge bosons and sfermions.

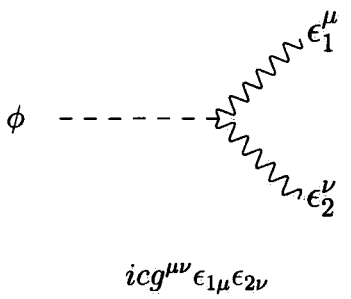

ϕ	$\epsilon_1^\mu\epsilon_2^\nu$	c
h^0	Z^0Z^0	$g\frac{m_W\sin(\beta-\alpha)}{\cos\theta_W}$
	W^+W^-	$gm_W\sin(\beta-\alpha)$
H^0	Z^0Z^0	$g\frac{m_W\cos(\beta-\alpha)}{\cos\theta_W}$
	W^+W^-	$gm_W\cos(\beta-\alpha)$

Figure D.2: Feynman rule for the interaction of a Higgs boson with a pair of gauge bosons. The coupling constant c for the various types of Higgs and gauge boson are given in the adjacent table.

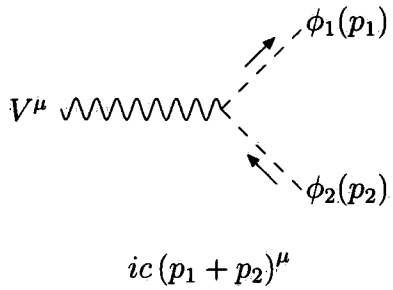

V^μ	$\phi_1\phi_2$	c
γ	H^+H^-	e
Z^0	h^0A^0	$-ie\dfrac{\cos(\beta-\alpha)}{\sin 2\theta_W}$
	H^0A^0	$ie\dfrac{\sin(\beta-\alpha)}{\sin 2\theta_W}$
	H^+H^-	$e\dfrac{\cos 2\theta_W}{\sin 2\theta_W}$
W^+	h^0H^+	$=e\dfrac{\cos(\beta-\alpha)}{2\sin\theta_W}$
	H^0H^+	$e\dfrac{\sin(\beta-\alpha)}{2\sin\theta_W}$
	A^0H^+	$ie\dfrac{1}{2\sin\theta_W}$

Figure D.3: Feynman rule for the interaction of a gauge boson with a pair of Higgs bosons where the momenta are to be taken as in the direction of the arrows. The coupling constant c for the various types of gauge and Higgs boson are given in the adjacent table.

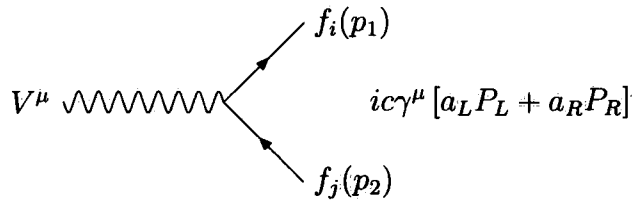

Figure D.4: Feynman rule for the interaction of a gauge boson and a pair of gauginos. The couplings are defined in Table D.2.

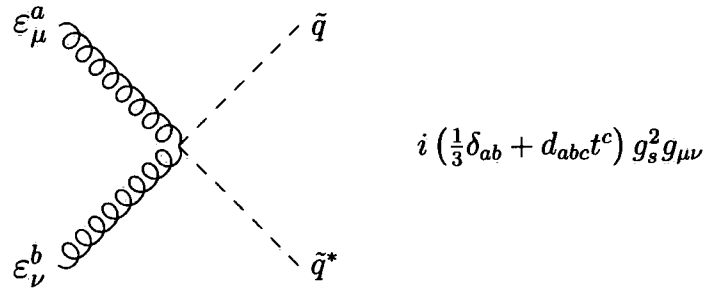

Figure D.5: Feynman rule for the coupling of two gluons to a pair of squarks in the MSSM.

V^μ	ff'	c	a_L	a_R
γ	$\tilde{\chi}_i^+\tilde{\chi}_j^-$	$-e$	1	1
W^+	$\tilde{\chi}_i^0\tilde{\chi}_j^+$	g	$-\frac{1}{\sqrt{2}}N_{i4}V_{j2}^* + N_{i2}V_{j1}^*$	$\frac{1}{\sqrt{2}}N_{i3}^*U_{j2} + N_{i2}^*U_{j1}$
Z^0	$\tilde{\chi}_i^0\tilde{\chi}_j^0$	$\frac{g}{\cos\theta_W}$	$-\frac{1}{2}N_{i3}N_{j3}^* + \frac{1}{2}N_{i4}N_{j4}^*$	$-a_L^*$
Z^0	$\tilde{\chi}_i^-\tilde{\chi}_j^+$	$\frac{g}{\cos\theta_W}$	$-V_{i1}V_{j1}^* - \frac{1}{2}V_{i2}V_{j2}^*$ $+\delta_{ij}\sin^2\theta_W$	$-U_{i1}^*U_{j1} - \frac{1}{2}U_{i2}^*U_{j2}$ $+\delta_{ij}\sin^2\theta_W$
g_a	$\tilde{g}_b\tilde{g}_c$	$\{if_{abc}\}\, g_s$	1	1

Table D.2: Couplings for a gauge boson and a pair of electroweak gauginos. All momenta are to be taken as outgoing.

D.1.2 Fermion-Sfermion Interactions

In the MSSM a sfermion has interactions with a Standard Model fermion and all of the gauginos through the rules defined in Figs. D.6–D.7 and Table D.3. The primed matrices used in the neutralino rules are related to the unprimed ones via

$$N'_{i1} = N_{i1}\cos\theta_W + N_{i2}\sin\theta_W, \tag{D.1a}$$

$$N'_{i2} = N_{i2}\cos\theta_W - N_{i1}\sin\theta_W, \tag{D.1b}$$

$$N'_{i3} = N_{i3}, \tag{D.1c}$$

$$N'_{i4} = N_{i4}. \tag{D.1d}$$

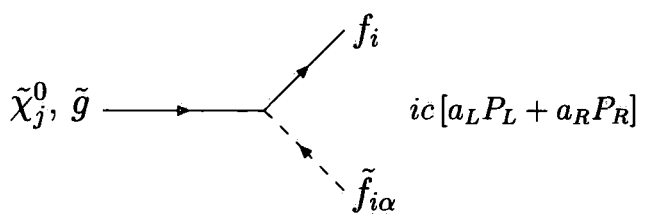

Figure D.6: Feynman rule for the coupling of an electrically neutral gaugino to a Standard Model fermion and a sfermion. Table D.3 gives the definitions of a_L and a_R.

$f_i\tilde{f}_{i\alpha}$	c	
$u_i\tilde{u}_{i\alpha}$	$-\sqrt{2}$	a_L: $\frac{gm_{u_i}N^*_{j4}}{2M_W\sin\beta}Q^{2i}_{1\alpha} - Q^{2i}_{2\alpha}\left(ee_uN'^*_{j1} - \frac{ge_u\sin^2\theta_W N'^*_{j2}}{\cos\theta_W}\right)$ a_R: $\frac{gm_{u_i}N_{j4}}{2M_W\sin\beta}Q^{2i}_{2\alpha} + Q^{2i}_{1\alpha}\left(ee_uN'_{j1} + \frac{g(\frac{1}{2}-e_u\sin^2\theta_W)N'_{j2}}{\cos\theta_W}\right)$
$d_i\tilde{d}_{i\alpha}$	$-\sqrt{2}$	a_L: $\frac{gm_{d_i}N^*_{j3}}{2M_W\cos\beta}Q^{2i-1}_{1\alpha} - Q^{2i-1}_{2\alpha}\left(ee_dN'^*_{j1} - \frac{ge_d\sin^2\theta_W N'^*_{j2}}{\cos\theta_W}\right)$ a_R: $\frac{gm_{d_i}N_{j3}}{2M_W\cos\beta}Q^{2i-1}_{2\alpha} + Q^{2i-1}_{1\alpha}\left(ee_dN'_{j1} - \frac{g(\frac{1}{2}+e_d\sin^2\theta_W)N'_{j2}}{\cos\theta_W}\right)$
$l_i\tilde{l}_{i\alpha}$	$-\sqrt{2}$	a_L: $\frac{gm_{l_i}N^*_{j3}}{2M_W\cos\beta}L^{2i-1}_{1\alpha} + L^{2i=1}_{2\alpha}\left(eN'^*_{j1} - \frac{g\sin^2\theta_W}{\cos\theta_W}N'^*_{j2}\right)$ a_R: $\frac{gm_{l_i}N_{j3}}{2M_W\cos\beta}L^{2i-1}_{2\alpha} - L^{2i-1}_{1\alpha}\left(eN'_{j1} + \frac{g(\frac{1}{2}-\sin^2\theta_W)}{\cos\theta_W}N'_{j2}\right)$
$\nu_i\tilde{\nu}_i$	$-\sqrt{2}$	a_L: 0 $\quad a_R$: $\frac{gN'_{j2}}{2\cos\theta_W}$
$q_i^b\tilde{q}^c_{i\alpha}$	$\{t^a_{bc}\}\,(-g_s\sqrt{2})$	a_L: $-Q^k_{2\alpha}$ $\quad a_R$: $Q^k_{1\alpha}$

Table D.3: Neutralino and gluino couplings. In the case of the gluino $k = 2i$ for up-type quarks and $k = 2i - 1$ for down-type quarks.

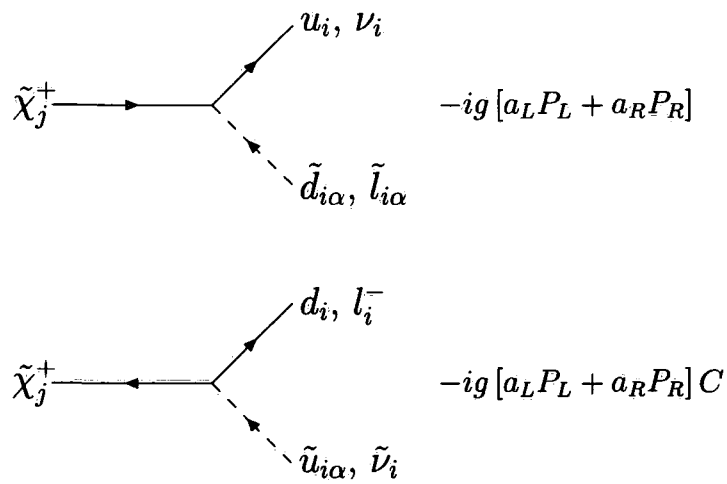

$f_i\tilde{f}'_{i\alpha}$	a_L	a_R
$u_i\tilde{d}_{i\alpha}$	$-\frac{m_{u_i}V^*_{j2}}{\sqrt{2}M_W\sin\beta}Q^{2i-1}_{1\alpha}$	$U_{j1}Q^{2i-1}_{1\alpha} - \frac{m_{d_i}U_{j2}}{\sqrt{2}M_W\cos\beta}Q^{2i-1}_{2\alpha}$
$d_i\tilde{u}_{i\alpha}$	$-\frac{m_{d_i}U^*_{j2}}{\sqrt{2}M_W\cos\beta}Q^{2i}_{1\alpha}$	$V_{j1}Q^{2i}_{1\alpha} - \frac{m_{u_i}V_{j2}}{\sqrt{2}M_W\sin\beta}Q^{2i}_{2\alpha}$
$\nu_i\tilde{l}_{i\alpha}$	0	$U_{j1}L^{2i-1}_{1\alpha} - \frac{m_{l_i}U_{j2}}{\sqrt{2}M_W\cos\beta}L^{2i-1}_{2\alpha}$
$l_i\tilde{\nu}_{i\alpha}$	$-\frac{m_{l_i}U^*_{j2}}{\sqrt{2}M_W\cos\beta}$	V_{j1}

Figure D.7: Feynman rule of the coupling of a chargino with a Standard Model fermion and a sfermion. C is the charge conjugation matrix.

D.1.3 Higgs-Fermion Interactions

A Higgs boson interacts with a pair of Standard Model fermions through the rules defined in Fig. D.8 where $\sin\alpha$ is the Higgs mixing angle, $\tan\beta$ is the ratio of the Higgs vacuum expectation values.

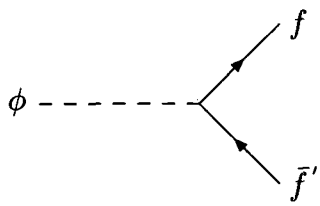

$$i\frac{g}{\sqrt{2}M_W}c\left[a_L P_L + a_R P_R\right]$$

ϕ	$f\bar{f}'$	c	a_L	a_R
h^0	$t\bar{t}$	$-\frac{m_f\cos\alpha}{\sqrt{2}\sin\beta}$	1	1
	$b\bar{b}$ $\tau\bar{\tau}$	$\frac{m_f\sin\alpha}{\sqrt{2}\cos\beta}$		
H^0	$t\bar{t}$	$-\frac{m_f\sin\alpha}{\sqrt{2}\sin\beta}$		
	$b\bar{b}$ $\tau\bar{\tau}$	$-\frac{m_f\cos\alpha}{\sqrt{2}\cos\beta}$		
H^+	$f_u\bar{f}_d$	$-\frac{1}{\sqrt{2}}$	$\frac{m_u}{\tan\beta}$	$m_d\tan\beta$
A^0	$t\bar{t}$	$\frac{im_f}{\sqrt{2}\tan\beta}$	1	-1
	$b\bar{b}$ $\tau\bar{\tau}$	$im_f\tan\beta$		

Figure D.8: Feynman rule for the interaction of a Higgs boson with a pair of Standard Model fermions.

There is also an interaction with a pair of gauginos through the rules defined in Fig. D.9 and Table D.9 where $Q_{ij} = V_{i1}U_{j2}/\sqrt{2}$, $S_{ij} = V_{i2}U_{j1}/\sqrt{2}$. The double primed matrices Q'' and S'' are a combination of neutralino mixing matrices where

$$Q''_{ij} = \frac{1}{2}\left[N_{i3}(N_{j2} - N_{j1}\tan\theta_W) + N_{j3}(N_{i2} - N_{i1}\tan\theta_W)\right], \quad \text{(D.2a)}$$

$$S''_{ij} = \frac{1}{2}\left[N_{i4}(N_{j2} - N_{j1}\tan\theta_W) + N_{j4}(N_{i2} - N_{i1}\tan\theta_W)\right]. \quad \text{(D.2b)}$$

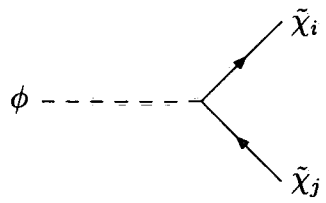

$$i\frac{e}{\sin\theta_W}\left[a_L P_L + a_R P_R\right]$$

Figure D.9: Feynman rule for the interaction of a Higgs boson and a pair of gauginos. The couplings are defined in Table D.4.

ϕ	$\tilde{\chi}_i\tilde{\chi}_j$	a_L	a_R
h^0	$\tilde{\chi}_i^0\tilde{\chi}_j^0$	$Q''^*_{ji}\sin\alpha + S''^*_{ji}\cos\alpha$	$Q''_{ij}\sin\alpha + S''_{ij}\cos\alpha$
	$\tilde{\chi}_i^+\tilde{\chi}_j^-$	$Q^*_{ji}\sin\alpha - S^*_{ji}\cos\alpha$	$Q_{ij}\sin\alpha = S_{ij}\cos\alpha$
H^0	$\tilde{\chi}_i^0\tilde{\chi}_j^0$	$-Q''^*_{ji}\cos\alpha + S''^*_{ji}\sin\alpha$	$-Q''_{ij}\cos\alpha + S''_{ij}\sin\alpha$
	$\tilde{\chi}_i^+\tilde{\chi}_j^-$	$-Q^*_{ji}\cos\alpha - S^*_{ji}\sin\alpha$	$-Q_{ij}\cos\alpha - S_{ij}\sin\alpha$
A^0	$\tilde{\chi}_i^0\tilde{\chi}_j^0$	$i\left(Q''^*_{ji}\sin\beta - S''^*_{ji}\cos\beta\right)$	$-i\left(Q''_{ij}\sin\beta - S''_{ij}\cos\beta\right)$
	$\tilde{\chi}_i^+\tilde{\chi}_j^-$	$i\left(Q^*_{ji}\sin\beta + S^*_{ji}\cos\beta\right)$	$-i\left(Q''_{ij}\sin\beta + S''_{ij}\cos\beta\right)$
H^+	$\tilde{\chi}_i^0\tilde{\chi}_j^+$	$-\left[(N_{i2} + N_{i1}\tan\theta_W)\frac{V_{j2}}{\sqrt{2}} + N_{i4}V_{j1}\right]\cos\beta$	$-\left[(N_{i2} + N_{i1}\tan\theta_W)\frac{U_{j2}}{\sqrt{2}} + N_{i3}U_{j1}\right]\sin\beta$
H^-	$\tilde{\chi}_i^0\tilde{\chi}_j^-$	$-\left[(N_{i2} + N_{i1}\tan\theta_W)\frac{U_{j2}}{\sqrt{2}} + N_{i3}U_{j1}\right]^*\sin\beta$	$-\left[(N_{i2} + N_{i1}\tan\theta_W)\frac{V_{j2}}{\sqrt{2}} + N_{i4}V_{j1}\right]^*\cos\beta$

Table D.4: Couplings for a Higgs boson and a pair of gauginos in the MSSM.

D.1.4 Higgs-Sfermion Interactions

The couplings between a Higgs boson and a pair of sfermions differ greatly depending on the type of Higgs boson. The Feynman rule for the interaction of three scalar particles is given in Fig. D.10 and the definitions of the couplings for each type of Higgs particle are given in Tables D.5–D.8.

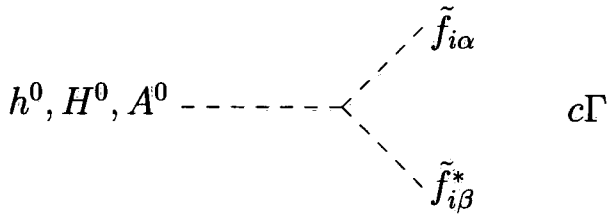

Figure D.10: Feynman rule for the coupling of a higgs with a pair of sfermions. The definition of Γ for the three neutral Higgs' are given in Tables D.5–D.8.

$\tilde{f}_{i\alpha}\tilde{f}^*_{i\beta}$	Γ
$\tilde{u}_{i\alpha}\tilde{u}^*_{i\beta}$	$\frac{M_Z \sin(\alpha+\beta)}{\cos\theta_W}\left[Q^{2i}_{1\alpha}Q^{2i}_{1\beta}(\frac{1}{2} - e_u \sin^2\theta_W) + e_u \sin^2\theta_W Q^{2i}_{2\alpha}Q^{2i}_{2\beta}\right]$ $-\frac{m^2_{u_i}\cos\alpha}{M_W \sin\beta}\left[Q^{2i}_{1\alpha}Q^{2i}_{1\beta} + Q^{2i}_{2\alpha}Q^{2i}_{2\beta}\right]$ $-\frac{m_{u_i}}{2M_W \sin\beta}(A_{u_i}\cos\alpha + \mu\sin\alpha)\left[Q^{2i}_{2\alpha}Q^{2i}_{1\beta} + Q^{2i}_{1\alpha}Q^{2i}_{2\beta}\right]$
$\tilde{d}_{i\alpha}\tilde{d}^*_{i\beta}$	$-\frac{M_Z \sin(\alpha+\beta)}{\cos\theta_W}\left[Q^{2i-1}_{1\alpha}Q^{2i-1}_{1\beta}(\frac{1}{2} + e_d \sin^2\theta_W) - e_d \sin^2\theta_W Q^{2i-1}_{2\alpha}Q^{2i-1}_{2\beta}\right]$ $+\frac{m^2_{d_i}\sin\alpha}{M_W \cos\beta}\left[Q^{2i-1}_{1\alpha}Q^{2i-1}_{1\beta} + Q^{2i-1}_{2\alpha}Q^{2i-1}_{2\beta}\right]$ $+\frac{m_{d_i}}{2M_W \cos\beta}(A_{d_i}\sin\alpha + \mu\cos\alpha)\left[Q^{2i-1}_{2\alpha}Q^{2i-1}_{1\beta} + Q^{2i=1}_{1\alpha}Q^{2i-1}_{2\beta}\right]$
$\tilde{l}_{i\alpha}\tilde{l}^*_{i\beta}$	$-\frac{M_Z \sin(\alpha+\beta)}{\cos\theta_W}\left[L^{2i-1}_{1\alpha}L^{2i-1}_{1\beta}(\frac{1}{2} - \sin^2\theta_W) + \sin^2\theta_W L^{2i-1}_{2\alpha}L^{2i-1}_{2\beta}\right]$ $+\frac{m^2_{l_i}\sin\alpha}{M_W \cos\beta}\left[L^{2i-1}_{1\alpha}L^{2i-1}_{1\beta} + L^{2i-1}_{2\alpha}L^{2i-1}_{2\beta}\right]$ $+\frac{m_{l_i}}{2M_W \cos\beta}(A_{e_i}\sin\alpha + \mu\cos\alpha)\left[L^{2i-1}_{2\alpha}L^{2i-1}_{1\beta} + L^{2i-1}_{1\alpha}L^{2i-1}_{2\beta}\right]$
$\tilde{\nu}_{i\alpha}\tilde{\nu}^*_{i\beta}$	$\frac{M_Z \sin(\alpha+\beta)}{2\cos\theta_W}$

Table D.5: Couplings for the light CP-even Higgs boson h^0 with a pair of sfermions where i is the generation index and $c = ig$.

$\tilde{f}_{i\alpha}\tilde{f}^*_{i\beta}$	Γ
$\tilde{u}_{i\alpha}\tilde{u}^*_{i\beta}$	$\frac{m_{u_i}}{2M_W}(A_{u_i}\cot\beta + \mu)\,\delta_{\alpha\neq\beta}$
$\tilde{d}_{i\alpha}\tilde{d}^*_{i\beta}$	$\frac{m_{d_i}}{2M_W}(A_{d_i}\tan\beta + \mu)\,\delta_{\alpha\neq\beta}$
$\tilde{l}_{i\alpha}\tilde{l}^*_{i\beta}$	$\frac{m_{l_i}}{2M_W}(A_{e_i}\tan\beta + \mu)\,\delta_{\alpha\neq\beta}$

Table D.6: Couplings for the CP-odd Higgs boson A^0 with a pair of sfermions where $c = g$.

$\tilde{f}_{i\alpha}\tilde{f}^*_{i\beta}$	Γ
$\tilde{u}_{i\alpha}\tilde{u}^*_{i\beta}$	$-\frac{M_Z\cos(\alpha+\beta)}{\cos\theta_W}\left[Q^{2i}_{1\alpha}Q^{2i}_{1\beta}(\frac{1}{2}-e_u\sin^2\theta_W)+e_u\sin^2\theta_W Q^{2i}_{2\alpha}Q^{2i}_{2\beta}\right]$ $-\frac{m^2_{u_i}\sin\alpha}{M_W\sin\beta}\left[Q^{2i}_{1\alpha}Q^{2i}_{1\beta}+Q^{2i}_{2\alpha}Q^{2i}_{2\beta}\right]$ $-\frac{m_{u_i}}{2M_W\sin\beta}(A_{u_i}\sin\alpha-\mu\cos\alpha)\left[Q^{2i}_{2\alpha}Q^{2i}_{1\beta}+Q^{2i}_{1\alpha}Q^{2i}_{2\beta}\right]$
$\tilde{d}_{i\alpha}\tilde{d}^*_{i\beta}$	$\frac{M_Z\cos(\alpha+\beta)}{\cos\theta_W}\left[Q^{2i-1}_{1\alpha}Q^{2i-1}_{1\beta}(\frac{1}{2}+e_d\sin^2\theta_W)-e_d\sin^2\theta_W Q^{2i-1}_{2\alpha}Q^{2i-1}_{2\beta}\right]$ $-\frac{m^2_{d_i}\cos\alpha}{M_W\cos\beta}\left[Q^{2i-1}_{1\alpha}Q^{2i-1}_{1\beta}+Q^{2i-1}_{2\alpha}Q^{2i-1}_{2\beta}\right]$ $+\frac{m_{d_i}}{2M_W\cos\beta}(\mu\sin\alpha-A_{d_i}\cos\alpha)\left[Q^{2i-1}_{2\alpha}Q^{2i-1}_{1\beta}+Q^{2i-1}_{1\alpha}Q^{2i-1}_{2\beta}\right]$
$\tilde{l}_{i\alpha}\tilde{l}^*_{i\beta}$	$\frac{M_Z\cos(\alpha+\beta)}{\cos\theta_W}\left[L^{2i-1}_{1\alpha}L^{2i-1}_{1\beta}(\frac{1}{2}-\sin^2\theta_W)+\sin^2\theta_W L^{2i-1}_{2\alpha}L^{2i-1}_{2\beta}\right]$ $-\frac{m^2_{l_i}\cos\alpha}{M_W\cos\beta}\left[L^{2i-1}_{1\alpha}L^{2i-1}_{1\beta}+L^{2i-1}_{2\alpha}L^{2i-1}_{2\beta}\right]$ $+\frac{m_{l_i}}{2M_W\cos\beta}(\mu\sin\alpha-A_{e_i}\cos\alpha)\left[L^{2i-1}_{2\alpha}L^{2i-1}_{1\beta}+L^{2i-1}_{1\alpha}L^{2i-1}_{2\beta}\right]$
$\tilde{\nu}_{i\alpha}\tilde{\nu}^*_{i\beta}$	$-\frac{M_Z\cos(\alpha+\beta)}{2\cos\theta_W}$

Table D.7: Couplings for the light CP-even Higgs boson H^0 with a pair of sfermions where i is the generation index where $c = ig$.

$\tilde{f}_{i\alpha}\tilde{f}^*_{i\beta}$	Γ
$\tilde{u}_{i\alpha}\tilde{d}^*_{i\beta}$	$\frac{1}{\sqrt{2}M_W}\left[Q^{2i}_{1\alpha}Q^{2i-1}_{1\beta}(m^2_{d_i}\tan\beta+m^2_{u_i}\cot\beta-M^2_W\sin 2\beta)\right.$ $+Q^{2i}_{2\alpha}Q^{2i-1}_{2\beta}m_{u_i}m_{d_i}(\cot\beta+\tan\beta)$ $\left.+Q^{2i}_{1\alpha}Q^{2i-1}_{2\beta}m_{d_i}(A_{d_i}\tan\beta+\mu)+Q^{2i}_{2\alpha}Q^{2i-1}_{1\beta}m_{u_i}(A_{u_i}\cot\beta+\mu)\right]$
$\tilde{\nu}_i\tilde{l}^*_{i\beta}$	$\frac{1}{\sqrt{2}}\left[L^{2i-1}_{1\beta}(m^2_{l_i}\tan\beta-M^2_W\sin 2\beta)+L^{2i-1}_{1\beta}(m_{l_i}(A_{l_i}\tan\beta+\mu)\right]$

Table D.8: Couplings for the charged Higgs boson H^+ with a pair of sfermions where i is the generation index and $c = ig$.

D.2 Minimal Universal Extra Dimensions

Here we present the Feynman rules for the MUED model, considering the level-1 KK-modes only, where we follow the conventions in Refs. [22,88] As in the main body of this thesis $f^\bullet$ denotes a fermion whose zero mode is Standard Model doublet and f° denotes a partner whose zero mode is a Standard Model singlet. The fermion mixing angle, defined in Chapter 1, is denoted α_f.

The level-1 "Weinberg" mixing angle θ_1 for the electroweak vector bosons is defined by

$$\cos^2\theta_1 = \frac{1+\delta_{W_1}+\frac{1}{4}g^2v^2-m_{\gamma_1}^2}{R^2(m_{Z_1}^2-m_{\gamma_1}^2)}, \tag{D.3}$$

where δ_{W_1} is defined in Appendix A, g is the $SU(2)$ coupling constant, v is the vacuum expectation value of the Standard Model Higgs field, R is the radius of the compactified dimension, m_{γ_1} is the mass of the level-1 KK photon and m_{Z_1} is the mass of the level-1 KK Z boson.

D.2.1 FFV Interactions

The inclusion of KK-parity limits the form of the interactions so that all of the vertices have an even number of KK particles associated with them. For a gauge boson interacting with a pair of fermions, the rule for which is shown in Fig. D.11, there are two types of vertex, a Standard Model gauge boson with a pair of KK-fermions, Table D.9, or a KK-1 gauge boson with a Standard Model fermion and a KK-fermion, Table D.10.

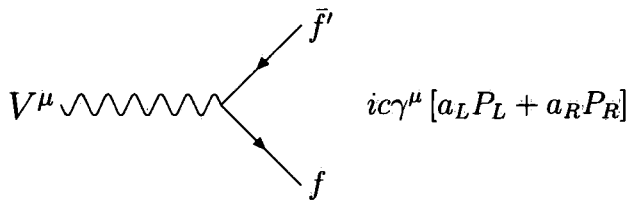

Figure D.11: Feynman rule for a gauge boson with a pair of Dirac fermions.

V^μ	$f\bar{f}'$	c	a_L	a_R
γ	$f_1\bar{f}_1$	$-Q_f e$	1	1
g^a	$q_{1b}\bar{q}_{1c}$	$-t^a_{bc} g_s$	1	1
Z^0	$f_1^\bullet \bar{f}_1^\bullet$	$\frac{e}{\sin\theta_W \cos\theta_W}$	$I_{3f}\cos^2\alpha_f - Q_f \sin^2\theta_W$	a_L
	$f_1^\circ \bar{f}_1^\circ$		$I_{3f}\sin^2\alpha_f - Q_f \sin^2\theta_W$	a_L
	$f_1^\circ \bar{f}_1^\bullet$		$-I_{3f}\sin\alpha_f \cos\alpha_f$	$-a_L$
$W^\pm$	$f_{1d}^\bullet \bar{f}_{1u}^\bullet$	$\frac{e}{\sqrt{2}\sin\theta_W}$	$\cos\alpha_{f_u}\cos\alpha_{f_d}$	a_L
	$f_{1d}^\circ \bar{f}_{1u}^\circ$		$\sin\alpha_{f_u}\sin\alpha_{f_d}$	a_L
	$f_{1d}^\bullet \bar{f}_{1u}^\circ$		$\sin\alpha_{f_u}\cos\alpha_{f_d}$	$-a_L$
	$f_{1d}^\circ \bar{f}_{1u}^\bullet$		$\cos\alpha_{f_u}\sin\alpha_{f_d}$	$-a_L$

Table D.9: Couplings for a Standard Model gauge boson V^μ with a pair of KK-fermions $f\bar{f}'$, where I_{3f} and Q_f are the hypercharge and electric charge of fermion f respectively.

D.2.2 Gauge Boson Self-Interactions

The three-point interactions of the gauge bosons amongst themselves can be summarised by the rule shown in Fig. D.12, with the couplings for the various possible combinations of vector boson shown in Table D.11. We also include here the quartic coupling between a pair of Standard Model gluons and a pair of KK-1 gluons, Fig. D.13, which is necessary to achieve a gauge invariant answer for the matrix element of the process $gg \to g_1 g_1$.

V^μ	$f\bar{f}_1'$	c	a_L	a_R
γ_1	$f\bar{f}_1^\bullet$	$-\frac{e}{\cos\theta_W}$	$Q_f\cos\theta_1 - \frac{I_{3f}\sin(\theta_W-\theta_1)}{\sin\theta_W}$	0
γ_1	$f\bar{f}_1^\circ$		0	$Q_f\cos\theta_1$
g_1^a	$q_{1b}^\bullet\bar{q}_c$	$-t_{bc}^a g_s$	1	0
g_1^a	$q_{1b}^\circ\bar{q}_c$	$-t_{bc}^a g_s$	0	1
Z_1^0	$f\bar{f}_1^\bullet$	$\frac{e}{\cos\theta_W}$	$Q_f\sin\theta_1 - \frac{I_{3f}\cos(\theta_W=\theta_1)}{\sin\theta_W}$	0
Z_1^0	$f\bar{f}_1^\circ$		0	$Q_f\sin\theta_1$

Table D.10: Couplings for a KK-1 gauge boson V^μ with a Standard Model fermion f and a KK-fermion f_1, where I_{3f} and Q_f are the hypercharge and electric charge of fermion f respectively and $\sin\theta_1$ is the level-1 gauge boson mixing angle.

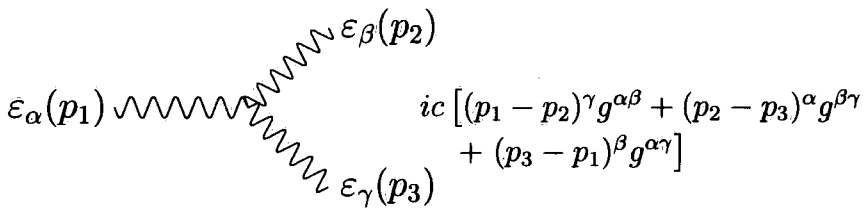

Figure D.12: The Feynman rule for a triple vector boson vertex where the momenta are all incoming.

D.2.3 Higgs Interactions

The five Higgs bosons in the MUED model can interact with a pair of fermions in a variety of ways. The general rule is given in Fig. D.14 and the couplings for the specfic interactions of each of the Higgs particles are given in Tables D.12–D.14. There are also interactions with the vector bosons with either a single gauge boson and a pair of Higgs particles, the rule for which is identical to that given in

$\varepsilon_\alpha\varepsilon_\beta\varepsilon_\gamma$	c
$g\,g_1 g_1$	$if^{abc}g_S$
$\gamma W_1^+ W_1^-$	$-e$
$Z^0 W_1^+ W_1^-$	$-\frac{e\cos\theta_W}{\sin\theta_W}$
$W^\pm W_1^\mp \gamma$	$\mp\frac{e\sin\theta_1}{\sin\theta_W}$
$W^\pm W_1^\mp Z^0$	$\mp\frac{e\cos\theta_1}{\sin\theta_W}$

Table D.11: Couplings for the triple vector boson vertices where f^{abc} are the anti-symmetric structure constants of $SU(3)$.

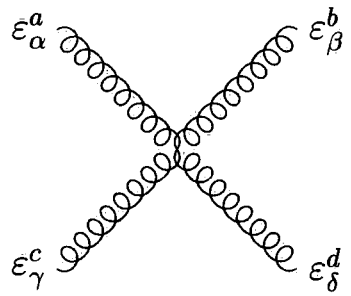

$$-ig_S^2\left[f^{xac}f^{xbd}\left(g^{\alpha\beta}g^{\gamma\delta}-g^{\alpha\delta}g^{\beta\gamma}\right)+f^{xad}f^{xbc}\left(g^{\alpha\beta}g^{\gamma\delta}-g^{\alpha\gamma}g^{\beta\delta}\right)+f^{xab}f^{xcd}\left(g^{\alpha\gamma}g^{\beta\delta}-g^{\alpha\delta}g^{\beta\gamma}\right)\right]$$

Figure D.13: Feynman rule for a pair of Standard Model gluons interacting with a pair of level-1 KK-gluons where f^{abc} are the anti-symmetric structure constants of $SU(3)$.

Fig. D.3, or a pair of gauge bosons and a single Higgs boson, identical to Fig. D.2.

The specific couplings for the MUED model are defined in Tables D.15 and D.16.

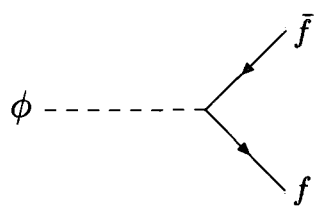

$$ic\left[a_L P_L + a_R P_R\right]$$

Figure D.14: Feynman rule for the interaction of a scalar particle with a pair of Dirac fermions.

(a) $c = \dfrac{em_f \cos\alpha_f \sin\alpha_f}{2\sin\theta_W m_w}$

$f\bar{f}'$	a_L	a_R
$f_1^\bullet \bar{f}_1^\bullet$	-1	-1
$f_1^\circ \bar{f}_1^\circ$	1	1
$f_1^\bullet \bar{f}_1^\circ$	-1	1
$f_1^\circ \bar{f}_1^\bullet$	1	-1

(b) $c = \dfrac{em_f}{2\sin\theta_W m_w}$

$f\bar{f}'$	a_L	a_R
$f\bar{f}_1^\bullet$	$(\sin\alpha + \cos\alpha)$	a_L
$f\bar{f}_1^\circ$	$(\sin\alpha - \cos\alpha)$	a_L

Table D.12: Couplings of a pair of fermions with (a) the light CP-even Higgs boson h^0 and (b) the heavy CP-even Higgs boson H_1^0.

$f\bar{f}'$	a_L	a_R
$f\bar{f}_1^\bullet$	$m_Z \cos\alpha_f (I_{3f} - Q_f \sin^2\theta_W) - \dfrac{m_f \sin\alpha_f}{Rm_W}$	$-m_Z \sin\alpha_f Q_f \sin^2\theta_W + \dfrac{m_f \cos\alpha_f}{Rm_W}$
$f\bar{f}_1^\circ$	$m_Z \sin\alpha_f (I_{3f} - Q_f \sin^2\theta_W) + \dfrac{m_f \cos\alpha_f}{Rm_W}$	$-m_Z \cos\alpha_f Q_f \sin^2\theta_W - \dfrac{m_f \cos\alpha_f}{Rm_W}$

Table D.13: Couplings for the CP-odd Higgs boson A_1^0 with a pair of fermions where I_{3f} is the third component of the hypercharge, Q_f denotes the electric charge and $c = \dfrac{gR}{\cos\theta_W \sqrt{1+m_Z^2 R^2}}$.

$f\bar{f}'$	a_L	a_R
$d\bar{u}_1^\bullet$	$m_W \cos\alpha_u - \dfrac{m_u \sin\alpha_u}{Rm_W}$	$\dfrac{m_u \cos\alpha_u}{Rm_W}$
$d\bar{u}_1^\circ$	$m_W \sin\alpha_u + \dfrac{m_u \cos\alpha_u}{Rm_W}$	$-\dfrac{m_u \sin\alpha_u}{Rm_W}$
$u\bar{d}_1^\bullet$	$m_W \cos\alpha_d - \dfrac{m_d \sin\alpha_d}{Rm_W}$	$\dfrac{m_d \cos\alpha_d}{Rm_W}$
$u\bar{d}_1^\circ$	$m_W \sin\alpha_d + \dfrac{m_d \cos\alpha_u}{Rm_W}$	$-\dfrac{m_u \sin\alpha_u}{Rm_W}$

Table D.14: Couplings for the charged Higgs boson $H_1^\pm$ with a pair of fermions where $c = \dfrac{gR}{2\sqrt{1+m_W^2 R^2}}$. The lepton couplings can be obtained by replacing the quark fields with their lepton partners of the same hypercharge.

V^μ	$\phi_1\phi_2$	c
γ	H^+H^-	e
Z^0	$H_1^0A_1^0$	$\frac{gm_Z}{\cos\theta_W\sqrt{1+m_Z^2R^2}}$
	H^+H^-	$\frac{g}{1+m_W^2R^2}\left(\cos^2\theta_W m_W^2R^2 - \frac{\cos^2\theta_W-\sin^2\theta_W}{2\cos\theta_W}\right)$
$W^\pm$	$H_1^\mp A_1^0$	$\pm\frac{g(m_W^2R^2+1/2)}{\sqrt{(1+m_W^2R^2)(1+m_Z^2R^2)}}$
	$H_1^0H_1^\mp$	$\frac{gm_W}{\sqrt{1+m_W^2R^2}}$

Table D.15: Couplings for a single gauge boson and a pair of Higgs bosons in the MUED model.

ϕ	$\epsilon_\mu\epsilon_\nu$	c
A_1^0	$W_1^\pm W^\mp$	$\mp(-1)^\beta\frac{g\cos\theta_W m_Z}{\sqrt{1+m_Z^2R^2}}$
$H_1^\mp$	$W_1^\pm Z^0$	$\pm\frac{gm_Z}{\sqrt{1+m_W^2R^2}}\left(\sin^2\theta_W+(-1)^\beta\cos^2\theta_W\right)$
	$Z_1W^\pm$	$\pm\frac{gm_Z}{\sqrt{1+m_W^2R^2}}\left(\sin^2\theta_W-(-1)^\beta\cos^2\theta_W\right)$
	$W_1^\pm\gamma$	$\pm\frac{gm_Z\sin\theta_W\cos\theta_W}{\sqrt{1+m_W^2R^2}}\left((-1)^\beta-1\right)$
	$\gamma_1W^\pm$	$\mp\frac{gm_Z\sin\theta_W\cos\theta_W}{\sqrt{1+m_W^2R^2}}\left((-1)^\beta+1\right)$

Table D.16: Couplings for a single Higgs boson and a pair of gauge bosons in the MUED model.

D.3 Littlest Higgs Model with T-parity

The form of the interactions in this model, *i.e.* the Feynman rules, are the same as in the Minimal Universal Extra Dimensions model since the particles involved possess the same spin. Therefore, we will only give the form of the couplings for the specific interactions in the Littles Higgs model with T-parity. In the heavy electroweak sector the W_H^3 and B_H gauge bosons mix to form the mass eigenstates Z_H and γ_H through [89]

$$\begin{pmatrix} Z_H \\ \gamma_H \end{pmatrix} = \begin{pmatrix} \cos\theta_H & \sin\theta_H \\ -\sin\theta_H & \cos\theta_H \end{pmatrix} \begin{pmatrix} W_H^3 \\ B_H \end{pmatrix}, \tag{D.4}$$

with

$$\sin\theta_H \approx \frac{5gg'}{4(5g^2 - g'^2)} \frac{v^2}{f^2}, \tag{D.5}$$

where g is the $SU(2)$ coupling, g' is the $U(1)_Y$ coupling, $v = 246\,\text{GeV}$ is the vacuum expectation value of the Higgs field and f is the scale of the non-linear sigma model. The only free parameter here is f, which sets the scale for the heavy electroweak sector.

The top quark sector is more complicated in Little Higgs models since there are additional partners due to the large Yukawa coupling of the SM top quark. The mixing angles appearing in the coupings are defined as [90]

$$\sin\alpha = \frac{\lambda_1}{\sqrt{\lambda_1^2 + \lambda_2^2}}, \tag{D.6a}$$

$$\sin\beta = \frac{\lambda_1^2}{\sqrt{\lambda_1^2 + \lambda_2^2}} \frac{v}{f}, \tag{D.6b}$$

$\varepsilon_\alpha\varepsilon_\beta\varepsilon_\gamma$	C
$\gamma W_H^\pm W_H^\mp$	$\mp e$
$Z^0 W_1^\pm W_1^\mp$	$\mp\frac{e\cos\theta_W}{\sin\theta_W}$
$W^\pm W_1^\mp \gamma$	$\pm\frac{e\sin\theta_H}{\sin\theta_W}$
$W^\pm W_1^\mp Z^0$	$\mp\frac{e}{\sin\theta_W}$

Table D.17: Couplings for the triple vector boson vertices.

where $\lambda_{1,2}$ are related to the SM top quark mass m_t through

$$m_t = \frac{\lambda_1\lambda_2 v}{\sqrt{\lambda_1^2+\lambda_2^2}}. \tag{D.7}$$

The Feynman rules are calculated in Refs. [89, 91] and those appropriate to the work here are given in Tables D.17–D.20.

(a)

$\epsilon_\mu\epsilon_\nu$	C
W^+W^-	$\frac{e^2v(1-\frac{v^2}{3f^2})}{\sin^2\theta_W}$
Z^0Z^0	$\frac{e^2v(1-\frac{v^2}{3f^2})}{\sin^2\theta_W\cos^2\theta_W}$
$W_H^+W_H^-$	$-\frac{e^2v}{2\sin^2\theta_W}$
Z_HZ_H	$-\frac{e^2v}{2\sin^2\theta_W}$
$\gamma_H\gamma_H$	$-\frac{e^2v}{2\cos^2\theta_W}$
γ_HZ_H	$-\frac{e^2v\sin\theta_W}{2\cos\theta_W}$

(b)

ϕ	$\epsilon_\mu\epsilon_\nu$	C
H^0	$Z^0Z_H^0$	$-\frac{e^2v^2}{2\sqrt{2}\sin^2\theta_W\cos\theta_W f}$
	$Z^0\gamma_H$	$\frac{e^2v^2}{2\sqrt{2}\sin\theta_W\cos^2\theta_W f}$
H^+	$Z^0W_H^+$	$\frac{e^2v^2(1+2\sin^2\theta_W)}{12\sin^2\theta_W\cos\theta_W f}$
	$W^+\gamma_H$	$-\frac{e^2v}{4\sin\theta_W\cos\theta_W}$
	W^+Z_H	$\frac{5e^2v^2}{12\sin^2\theta_W f}$
	γW_H^+	$-\frac{e^2v^2}{6\sin\theta_W f}$

Table D.18: Higgs boson couplings to a pair of gauge bosons in the LHT.

V^μ	$f\bar{f}'$	c	a_L	a_R
Z^0	$f_-\bar{f}_-$	$-\frac{g}{4\cos\theta_W}$	$(I_{3f} - Q_f \sin^2\theta_W)$	$-Q_f \sin^2\theta_W$
	$T_-\bar{T}_-$	$-\frac{2g}{3\cos\theta_W}$	1	1
	$T_+\bar{T}_+$	$-\frac{g}{\cos\theta_W}$	$\frac{\sin^2\beta}{2} - \frac{2\sin^2\theta_W}{3}$	$-\frac{2}{3}$
	$\bar{T}_+ t$	$-\frac{g}{2\cos\theta_W}$	$\sin\beta\cos\beta$	0
$W^\pm$	$b\bar{t}$	$-\frac{g}{\sqrt{2}}$	$V_{tb}\cos\beta$	0
	$b\bar{T}_+$		$V_{tb}\sin\beta$	0
	$b_-\bar{t}_-$		1	1

Table D.19: Couplings for the Standard Model $W^\pm$ and Z^0 bosons to the T-odd fermions where I_{3f} denotes the third component of isopin and Q_f is the electric charge. The couplings for the photon and gluon are identical to those in the Standard Model.

V^μ	$f\bar{f}_1'$	c	a_L	a_R
γ_H	$u\bar{u}_-$	e	$\frac{1}{10}\left(\frac{\cos\theta_H}{\cos\theta_W} - \frac{5\sin\theta_H}{\sin\theta_W}\right)$	0
	$d\bar{d}_-$		$\frac{1}{10}\left(\frac{\cos\theta_H}{\cos\theta_W} + \frac{5\sin\theta_H}{\sin\theta_W}\right)$	0
	$T_+\bar{T}_-$	$-\frac{2}{5}\frac{e\cos\theta_H}{\cos\theta_W}$	$\cos\beta$	$\cos\alpha$
	$t\bar{T}_-$		$\sin\beta$	$\sin\alpha$
Z_H	$u\bar{u}_-$	$-e$	$\frac{1}{10}\left(\frac{\sin\theta_H}{\cos\theta_W} - \frac{5\cos\theta_H}{\sin\theta_W}\right)$	0
	$d\bar{d}_-$		$\frac{1}{10}\left(\frac{\sin\theta_H}{\cos\theta_W} + \frac{5\cos\theta_H}{\sin\theta_W}\right)$	0
	$T_+\bar{T}_-$	$-\frac{2}{5}\frac{e\sin\theta_H}{\cos\theta_W}$	$\cos\beta$	$\cos\alpha$
	$t\bar{T}_-$		$\sin\beta$	$\sin\alpha$

Table D.20: Couplings for the heavy γ_H and Z_H bosons to a T-odd fermion and a Standard Model fermion. The $W_H^\pm$ does not couple to either of the T_-, T_+ fermions and the couplings to the T-odd fermions are the same as in the Standard Model.

Bibliography

[1] I. J. R. Aitchison and A. J. G. Hey, *Gauge Theories in Particle Physics. A Practical Introduction*, (Bristol, UK: Hilger, 1982).

[2] P. W. Higgs, *Broken symmetries, massless particles and gauge fields*, *Phys. Lett.* **12** (1964) 132–133.

[3] P. W. Higgs, *Broken symmetries and the masses of gauge bosons*, *Phys. Rev. Lett.* **13** (1964) 508–509.

[4] P. W. Higgs, *Spontaneous symmetry breakdown without massless bosons*, *Phys. Rev.* **145** (1966) 1156–1163.

[5] F. Englert and R. Brout, *Broken symmetry and the mass of gauge vector mesons*, *Phys. Rev. Lett.* **13** (1964) 321–322.

[6] S. L. Glashow, *Partial symmetries of weak interactions*, *Nucl. Phys.* **22** (1961) 579–588.

[7] S. Weinberg, *A model of leptons*, *Phys. Rev. Lett.* **19** (1967) 1264–1266.

[8] A. Salam, *Weak and electromagnetic interactions*, in *Elementary Particle Theory*, ed. by N. Svaratholm, 1968.

[9] R. K. Ellis, W. J. Stirling, and B. R. Webber, *QCD and Collider Physics*, (Cambridge, UK: Univ. Pr., 1996).

[10] S. P. Martin, *A Supersymmetry primer*, hep-ph/9709356.

[11] S. R. Coleman and J. Mandula, *All possible symmetries of the S-matrix*, *Phys. Rev.* **159** (1967) 1251–1256.

[12] Y. A. Golfand and E. P. Likhtman, *Extension of the algebra of Poincare group generators and violation of P invariance*, *JETP Lett.* **13** (1971) 323–326.

[13] H. E. Haber, *The status of the minimal supersymmetric standard model and beyond*, *Nucl. Phys. Proc. Suppl.* **62** (1998) 469–484, [hep-ph/9709450].

[14] T. Kaluza, *On the problem of unity in physics*, *Sitzungsber. Preuss. Akad. Wiss. Berlin (Math. Phys.)* **1921** (1921) 966–972.

[15] O. Klein, *Quantum theory and five-dimensional theory of relativity*, *Z. Phys.* **37** (1926) 895–906.

[16] I. Antoniadis, *A possible new dimension at a few TeV*, *Phys. Lett.* **B246** (1990) 377–384.

[17] N. Arkani-Hamed, S. Dimopoulos, and G. R. Dvali, *The hierarchy problem and new dimensions at a millimeter*, *Phys. Lett.* **B429** (1998) 263–272, [hep-ph/9803315].

[18] N. Arkani-Hamed, S. Dimopoulos, and G. R. Dvali, *Phenomenology, astrophysics and cosmology of theories with sub-millimeter dimensions and TeV scale quantum gravity*, *Phys. Rev.* **D59** (1999) 086004, [hep-ph/9807344].

[19] I. Antoniadis, N. Arkani-Hamed, S. Dimopoulos, and G. R. Dvali, *New dimensions at a millimeter to a Fermi and superstrings at a TeV*, *Phys. Lett.* **B436** (1998) 257–263, [hep-ph/9804398].

[20] L. Randall and R. Sundrum, *A large mass hierarchy from a small extra dimension*, *Phys. Rev. Lett.* **83** (1999) 3370–3373, [hep-ph/9905221].

[21] T. Appelquist, H.-C. Cheng, and B. A. Dobrescu, *Bounds on universal extra dimensions*, *Phys. Rev.* **D64** (2001) 035002, [hep-ph/0012100].

[22] D. Hooper and S. Profumo, *Dark matter and collider phenomenology of universal extra dimensions*, *Phys. Rept.* **453** (2007) 29–115, [hep-ph/0701197].

[23] T. Flacke, D. Hooper, and J. March-Russell, *Improved bounds on universal extra dimensions and consequences for LKP dark matter*, *Phys. Rev.* **D73** (2006) 095002, [hep-ph/0509352].

[24] H.-C. Cheng and I. Low, *TeV symmetry and the little hierarchy problem*, *JHEP* **09** (2003) 051, [hep-ph/0308199].

[25] H.-C. Cheng and I. Low, *Little hierarchy, little Higgses, and a little symmetry*, *JHEP* **08** (2004) 061, [hep-ph/0405243].

[26] I. Low, *T-parity and the littlest Higgs*, *JHEP* **10** (2004) 067, [hep-ph/0409025].

[27] F. James, *A Review of pseudorandom number generators*, *Comput. Phys. Commun.* **60** (1990) 329–344.

[28] M. Bahr *et. al.*, *Herwig++ physics and manual*, arXiv:0803.0883.

[29] G. Corcella *et. al.*, *HERWIG 6: An event generator for hadron emission reactions with interfering gluons (including supersymmetric processes)*, *JHEP* **01** (2001) 010, [hep-ph/0011363].

[30] S. Moretti, K. Odagiri, P. Richardson, M. H. Seymour, and B. R. Webber, *Implementation of supersymmetric processes in the HERWIG event generator*, *JHEP* **04** (2002) 028, [hep-ph/0204123].

[31] T. Sjostrand, S. Mrenna, and P. Skands, *PYTHIA 6.4 physics and manual*, *JHEP* **05** (2006) 026, [hep-ph/0603175].

[32] T. Sjostrand, S. Mrenna, and P. Skands, *A brief introduction to PYTHIA 8.1*, *Comput. Phys. Commun.* **178** (2008) 852–867, [arXiv:0710.3820].

[33] T. Gleisberg *et. al.*, *SHERPA 1.α, A proof-of-concept version*, *JHEP* **02** (2004) 056, [hep-ph/0311263].

[34] F. Maltoni and T. Stelzer, *MadEvent: Automatic event generation with MadGraph*, *JHEP* **02** (2003) 027, [hep-ph/0208156].

[35] A. Pukhov *et. al.*, *CompHEP: A package for evaluation of Feynman diagrams and integration over multi-particle phase space. User's manual for version 33*, hep-ph/9908288.

[36] A. Pukhov, *CalcHEP 3.2: MSSM, structure functions, event generation, batchs, and generation of matrix elements for other packages*, hep-ph/0412191.

[37] W. Kilian, T. Ohl, and J. Reuter, *WHIZARD: Simulating multi-particle processes at LHC and ILC*, arXiv:0708.4233.

[38] M. Moretti, T. Ohl, and J. Reuter, *O'Mega: An optimizing matrix element generator*, hep-ph/0102195.

[39] F. Krauss, R. Kuhn, and G. Soff, *AMEGIC++ 1.0: A matrix element generator in C++*, *JHEP* **02** (2002) 044, [hep-ph/0109036].

[40] **GEANT4** Collaboration, S. Agostinelli *et. al.*, *GEANT4: A simulation toolkit*, *Nucl. Instrum. Meth.* **A506** (2003) 250–303.

[41] E. Richter-Was, *AcerDET: A particle level fast simulation and reconstruction package for phenomenological studies on high p_T physics at LHC*, hep-ph/0207355.

[42] The homepage for the PGS package can be found at, http://www.physics.ucdavis.edu/~conway/research/software/pgs/pgs4-general.htm.

[43] G. R. Farrar and P. Fayet, *Phenomenology of the production, decay, and detection of new hadronic states associated with supersymmetry*, *Phys. Lett.* **B76** (1978) 575–579.

[44] H. Lehmann, K. Symanzik, and W. Zimmermann, *On the formulation of quantized field theories*, *Nuovo Cim.* **1** (1955) 205–225.

[45] M. E. Peskin and D. V. Schroeder, *An Introduction to Quantum Field Theory*, (Reading, USA: Addison-Wesley, 1995).

[46] R. Kleiss, W. J. Stirling, and S. D. Ellis, *A new Monte Carlo treatment of multiparticle phase space at high-energies*, *Comput. Phys. Commun.* **40** (1986) 359.

[47] R. Kleiss and W. J. Stirling, *Massive multiplicities and Monte Carlo*, *Nucl. Phys.* **B385** (1992) 413–432.

[48] P. Richardson, *Spin correlations in Monte Carlo simulations*, *JHEP* **11** (2001) 029, [hep-ph/0110108].

[49] I. G. Knowles, *Spin correlations in parton-parton scattering*, *Nucl. Phys.* **B310** (1988) 571.

[50] J. C. Collins, *Spin correlations in Monte Carlo event generators*, *Nucl. Phys.* **B304** (1988) 794.

[51] I. G. Knowles, *A linear algorithm for calculating spin correlations in hadronic collisions*, *Comput. Phys. Commun.* **58** (1990) 271–284.

[52] H. Murayama, I. Watanabe, and K. Hagiwara, *HELAS: HELicity Amplitude Subroutines for Feynman diagram evaluations*, KEK-91-11.

[53] J. Hakkinen and H. Kharraziha, *Colour: A computer program for QCD colour factor calculations*, *Comput. Phys. Commun.* **100** (1997) 311–321, [hep-ph/9603229].

[54] K. Odagiri, *Color connection structure of supersymmetric QCD ($2 \to 2$) processes*, *JHEP* **10** (1998) 006, [hep-ph/9806531].

[55] J. M. Smillie and B. R. Webber, *Distinguishing spins in supersymmetric and universal extra dimension models at the Large Hadron Collider*, *JHEP* **10** (2005) 069, [hep-ph/0507170].

[56] A. Denner, H. Eck, O. Hahn, and J. Kublbeck, *Compact Feynman rules for Majorana fermions*, *Phys. Lett.* **B291** (1992) 278–280.

[57] A. Denner, H. Eck, O. Hahn, and J. Kublbeck, *Feynman rules for fermion-number-violating interactions*, *Nucl. Phys.* **B387** (1992) 467–484.

[58] B. C. Allanach, K. Odagiri, M. A. Parker, and B. R. Webber, *Searching for narrow graviton resonances with the ATLAS detector at the Large Hadron Collider*, *JHEP* **09** (2000) 019, [hep-ph/0006114].

[59] B. C. Allanach *et. al.*, *Exploring small extra dimensions at the Large Hadron Collider*, *JHEP* **12** (2002) 039, [hep-ph/0211205].

[60] F. E. Paige, S. D. Protopopescu, H. Baer, and X. Tata, *ISAJET 7.69: A Monte Carlo event generator for pp, $\bar{p}p$, and e^+e^- reactions*, hep-ph/0312045.

[61] B. C. Allanach, *SOFTSUSY: A C++ program for calculating supersymmetric spectra*, *Comput. Phys. Commun.* **143** (2002) 305–331, [hep-ph/0104145].

[62] W. Porod, *SPheno, a program for calculating supersymmetric spectra, SUSY particle decays and SUSY particle production at e+ e- colliders*, *Comput. Phys. Commun.* **153** (2003) 275–315, [hep-ph/0301101].

[63] A. Djouadi, J.-L. Kneur, and G. Moultaka, *SuSpect: A FORTRAN code for the supersymmetric and Higgs particle spectrum in the MSSM*, *Comput. Phys. Commun.* **176** (2007) 426–455, [hep-ph/0211331].

[64] P. Skands *et. al.*, *SUSY Les Houches accord: Interfacing SUSY spectrum calculators, decay packages, and event generators*, *JHEP* **07** (2004) 036, [hep-ph/0311123].

[65] B. Allanach *et. al.*, *SUSY Les Houches Accord 2*, arXiv:0801.0045.

[66] **Particle Data Group** Collaboration, W. M. Yao *et. al.*, *Review of particle physics*, *J. Phys.* **G33** (2006) 1–1232.

[67] B. C. Allanach *et. al.*, *The Snowmass points and slopes: Benchmarks for SUSY searches*, hep-ph/0202233.

[68] B. C. Allanach, C. G. Lester, M. A. Parker, and B. R. Webber, *Measuring sparticle masses in non-universal string inspired models at the LHC*, *JHEP* **09** (2000) 004, [hep-ph/0007009].

[69] B. K. Bullock, K. Hagiwara, and A. D. Martin, *τ polarization as a signal of charged Higgs bosons*, *Phys. Rev. Lett.* **67** (1991) 3055–3057.

[70] S. Jadach, Z. Was, R. Decker, and J. H. Kuhn, *The tau decay library TAUOLA: Version 2.4*, *Comput. Phys. Commun.* **76** (1993) 361–380.

[71] S. Y. Choi, K. Hagiwara, Y. G. Kim, K. Mawatari, and P. M. Zerwas, *τ polarization in SUSY cascade decays*, *Phys. Lett.* **B648** (2007) 207–212, [hep-ph/0612237].

[72] D. Berdine, N. Kauer, and D. Rainwater, *Breakdown of the narrow width approximation for new physics*, *Phys. Rev. Lett.* **99** (2007) 111601, [hep-ph/0703058].

[73] N. Kauer, *Narrow-width approximation limitations*, *Phys. Lett.* **B649** (2007) 413–416, [hep-ph/0703077].

[74] N. Kauer, *A threshold-improved narrow-width approximation for BSM physics*, *JHEP* **04** (2008) 055, [arXiv:0708.1161].

[75] M. H. Seymour, *The Higgs boson line shape and perturbative unitarity*, *Phys. Lett.* **B354** (1995) 409–414, [hep-ph/9505211].

[76] J. D. Jackson, *Remarks on the phenomenological analysis of resonances*, *Nuovo Cim.* **34** (1964) 1644–1666.

[77] U. Baur, J. A. M. Vermaseren, and D. Zeppenfeld, *Electroweak vector boson production in high-energy e-p collisions*, *Nucl. Phys.* **B375** (1992) 3–44.

[78] Y. Kurihara, D. Perret-Gallix, and Y. Shimizu, *$e^+e^- \to e^-\bar{\nu}_e u\bar{d}$ from LEP to linear collider energies*, *Phys. Lett.* **B349** (1995) 367–374, [hep-ph/9412215].

[79] E. N. Argyres *et. al.*, *Stable calculations for unstable particles: restoring gauge invariance*, *Phys. Lett.* **B358** (1995) 339–346, [hep-ph/9507216].

[80] A. J. Barr, *Using lepton charge asymmetry to investigate the spin of supersymmetric particles at the LHC*, *Phys. Lett.* **B596** (2004) 205–212, [hep-ph/0405052].

[81] J. M. Smillie, *Spin correlations in decay chains involving W bosons*, *Eur. Phys. J.* **C51** (2007) 933–943, [hep-ph/0609296].

[82] H.-C. Cheng, K. T. Matchev, and M. Schmaltz, *Radiative corrections to Kaluza-Klein masses*, *Phys. Rev.* **D66** (2002) 036005, [hep-ph/0204342].

[83] H. E. Haber, *Spin formalism and applications to new physics searches*, hep-ph/9405376.

[84] T. Han, J. D. Lykken, and R.-J. Zhang, *On Kaluza-Klein states from large extra dimensions*, *Phys. Rev.* **D59** (1999) 105006, [hep-ph/9811350].

[85] H. E. Haber and G. L. Kane, *The search for supersymmetry: probing physics beyond the Standard Model*, *Phys. Rept.* **117** (1985) 75–263.

[86] J. F. Gunion and H. E. Haber, *Higgs bosons in supersymmetric models 1*, *Nucl. Phys.* **B272** (1986) 1.

[87] J. F. Gunion, H. E. Haber, G. L. Kane, and S. Dawson, *The Higgs Hunter's Guide*, (Redwood City, USA: Addison-Wesley, 1990).

[88] F. Burnell and G. D. Kribs, *The abundance of Kaluza-Klein dark matter with coannihilation*, *Phys. Rev.* **D73** (2006) 015001, [hep-ph/0509118].

[89] J. Hubisz and P. Meade, *Phenomenology of the littlest Higgs with T-parity*, *Phys. Rev.* **D71** (2005) 035016, [hep-ph/0411264].

[90] J. Hubisz, P. Meade, A. Noble, and M. Perelstein, *Electroweak precision constraints on the littlest Higgs model with T-parity*, *JHEP* **01** (2006) 135, [hep-ph/0506042].

[91] A. Belyaev, C.-R. Chen, K. Tobe, and C. P. Yuan, *Phenomenology of littlest Higgs model with T-parity: including effects of T-odd fermions*, *Phys. Rev.* **D74** (2006) 115020, [hep-ph/0609179].